Influence of classical anisotropy fields on the properties of Heisenberg antiferromagnets within unified molecular field theory

David C. Johnston

Ames Laboratory and Department of Physics and Astronomy, Iowa State University, Ames, Iowa 50011, USA

A comprehensive study of the influence of classical anisotropy fields on the magnetic properties of Heisenberg antiferromagnets within unified molecular field theory versus temperature T, magnetic field H, and anisotropy field parameter h_{A1} is presented for systems comprised of identical crystallographically-equivalent local moments. The anisotropy field for collinear z-axis antiferromagnetic (AFM) ordering is constructed so that it is aligned in the direction of each ordered and/or field-induced thermal-average moment with a magnitude proportional to the moment, whereas that for XY anisotropy is defined to be in the direction of the projection of the moment onto the xy plane, again with a magnitude proportional to the moment. Properties studied include the zero-field Néel temperature T_N, ordered moment, heat capacity, and anisotropic magnetic susceptibility of the AFM phase versus T with moments aligned either along the z axis or in the xy plane. Also determined are the high-field magnetization perpendicular to the axis or plane of collinear or planar noncollinear AFM ordering, the high-field magnetization along the z axis of a collinear z-axis AFM, spin-flop (SF), and paramagnetic (PM) phases, and the free energies of these phases versus T, H, and h_{A1}. Phase diagrams at $T = 0$ in the H_z-h_{A1} plane and at $T > 0$ in the H_z-T plane are constructed for spins $S = 1/2$. For $h_{A1} = 0$, the SF phase is stable at low field and the PM phase at high field with no AFM phase present. As h_{A1} increases, the phase diagram contains the AFM, SF, and PM phases. Further increases in h_{A1} lead to the disappearance of the SF phase and the appearance of a tricritical point on the AFM-PM transition curve. Applications of the theory to extract h_{A1} from experimental low-field magnetic susceptibility data and high-field magnetization versus field isotherms for single crystals of AFMs are discussed.

I. INTRODUCTION

Collinear and planar noncollinear Heisenberg antiferromagnets (AFMs) always have at least a small amount of some type of magnetocrystalline anisotropy present that establishes the axis or plane, respectively, along which the ordered magnetic moments are aligned with respect to the crystal axes. These include single-ion anisotropy, spin exchange anistropy in spin space, and anisotropy due to classical magnetic dipole interactions. These anisotropies are known to change the AFM ordering (Néel) temperature T_N as well as the magnetic and thermal properties of the spin system [1,2]. Recently, we carried out comprehensive studies of the influence of dipolar and uniaxial quantum DS_z^2 magnetocrystalline anisotropies on the thermal and magnetic properties of Heisenberg AFMs containing identical crystallographically equivalent spins [3,4], where the Heisenberg interactions are treated within unified molecular-field theory (MFT) [5–7]. In this MFT, the properties of collinear and planar noncollinear AFMs are calculated on the same footing and the theory is expressed in terms of directly measurable quantities instead of exchange interactions or molecular-field coupling constants [5,6]. The theory for DS_z^2 anisotropy applies only to spins $S \geqslant 1$, a serious limitation, since the magnetic properties of $S = 1/2$ systems are of great interest.

A generic classical anisotropy field H_A has been used sporadically in the past to study the effects of anisotropy. In particular, this field can give rise to an energy gap in the spin-wave spectrum $\sim \sqrt{2H_A H_{exch}}$, where H_{exch} is the exchange field, and can affect macroscopic properties such as yielding an anisotropy in the external field-induced magnetization [8]. For collinear AFMs, a field applied along the easy axis can give rise to a spin-flop transition, where the ordered moments flop to an orientation roughly perpendicular to the easy axis, given by Eq. (140) below [9], which again involves H_A.

However, a complete formulation of the classical anisotropy field and comprehensive study of its influence on the thermal and static magnetic properties of Heisenberg AFMs are lacking. Here we report results from such investigations. An important advantage of this type of anisotropy is that such uniaxial and planar (XY) anisotropies apply to systems with $S = 1/2$ in addition to $S \geqslant 1$. Another is that the anisotropy parameter in a system is much more easily derived from experimental magnetic data on single crystals compared to that for single-ion anisotropy. The Heisenberg exchange interactions are treated within the unified MFT, again assuming identical crystallographically equivalent spins.

Results from the unified MFT of Heisenberg AFMs that are needed to develop the theory incorporating classical anisotropy fields are summarized in the Appendix. A summary of notation and thermodynamics expressions used in the paper are given in Sec. II. We use two forms of anisotropy field depending on whether the anisotropy field induces collinear AFM ordering along the z axis or collinear or planar noncollinear AFM ordering in the xy plane. A detailed discussion of these is presented in Sec. III.

Calculations of the AFM ordering (Néel) temperature T_N and ordered moment versus temperature T in the presence of both the exchange and anisotropy fields in zero applied field H are given in Sec. IV for arbitrary antiferromagnets containing identical crystallographically equivalent spins. Laws of corresponding states for these properties and others are the same for all AFMs and ferromagnets (FMs) when

expressed in terms of the universal reduced parameters of the unified MFT. Expressions for the magnetic internal energy, heat capacity, entropy, and free energy of the AFM phase in zero field for both uniaxial and planar anisotropy are also derived and plotted in Sec. IV. The anisotropic magnetic susceptibilities χ arising from the classical anisotropy field are derived for the paramagnetic (PM) phase in Sec. V and for the AFM phase in Sec. VI, and the perpendicular high-field magnetizations for the PM and AFM states are calculated in Sec. VII.

The high-field magnetization parallel to the easy axis of a collinear AFM is of special interest. This is derived for the PM phase together with its free energy F_{mag} versus H in Sec. VIII B. The spin-flop (SF) phase is treated in Sec. VIII C, in which are presented the ordered moment versus T in $H = 0$, the thermal-average moment μ_{iz} versus H using two different approaches, the spin-flop critical field h_{cSF} at which the SF phase exhibits a second-order transition to the PM phase with increasing H, the zero-field internal energy U_{mag} versus T, and the (Helmholtz) free energy F_{mag} versus T and H. The more involved calculations of the magnetic properties of the AFM phase in high longitudinal fields are given separately in Sec. IX, including the z-axis sublattice, average and staggered moments, and F_{mag} versus T, H, and anisotropy parameter h_{A1}.

Phase diagrams are constructed in Sec. X. We start with the determination of the low-temperature properties of the AFM, SF, and PM phases and their dependencies on the parameters of the MFT in Sec. X A. The H_z versus h_{A1} phase diagrams at $T = 0$ are then constructed. In addition, μ_z versus H_z plots are provided for various values of h_{A1} to compare with experimental data at $T \ll T_{\mathrm{N}}$. In this section, $T = 0$ phase diagrams in the $H_\perp$-h_{A1} plane for fields $H_\perp$ perpendicular to the easy z axis of a collinear AFM or easy plane of a planar noncollinear AFM are presented.

We then move on to construct phase diagrams in the H_z-T plane in Sec. X B from free energy minimization with respect to the SF and z-axis collinear AFM phases (the PM phases are high-field extensions of these phases beyond their respective critical fields). Representative phase diagrams are presented for spins $S = 1/2$ for six values of h_{A1}. For $h_{\mathrm{A1}} = 0$, the only stable phases with increasing H_z are the SF and higher-field PM phases, as expected. With increasing h_{A1}, the AFM phase appears at low fields for $T \leqslant T_{\mathrm{N}}$ followed by the SF and PM phases with increasing field. Further increasing h_{A1} results in the gradual disappearance of the SF phase and appearance of a tricritical point on the AFM-PM phase boundary. When h_{A1} is sufficiently large, the SF phase disappears, leaving only the AFM and PM phases in the phase diagram with both first- and second-order transitions between them along the transition curve with a tricritical point separating the two regions. At $T = 0$, the AFM to PM transition is a 180° spin-flip transition of the moment initially opposite in direction to the field to being parallel to the field, whereas at finite T the transition is a "gradual" spin flip where the magnitude of the initially oppositely directed moment smoothly decreases to zero and then that moment increases with field in the direction of the field, eventually becoming the same in a second-order transition to the PM phase as that of the moment that was initially in the direction of the field.

A summary is given in Sec. XI. We discuss in depth how h_{A1} and another parameter f_J can be derived from experimental data using our formulas for different magnetic properties. Also discussed are the relationships between the formulas for T_{N} and the Weiss temperature θ_{p} in the Curie-Weiss law for the present classical anisotropy field treatment with those with $D S_z^2$ anisotropy [4] and arrive at a proportional relationship between h_{A1} and D for small values of D. In general, magnetic anisotropy data are much easier to analyze in terms of the present classical anisotropy field than in terms of $D S_z^2$ anisotropy.

II. NOTATION AND THERMODYNAMICS

A. Notation summary

Henceforth we designate two parameters changed by the presence of the anisotropy field by removing the subscript J to indicate that these values contain the contribution of the anisotropy field in zero applied field:

$$T_{\mathrm{N}J} \to T_{\mathrm{N}}, \quad \theta_{\mathrm{p}J} \to \theta_{\mathrm{p}}. \tag{1a}$$

The $T_{\mathrm{N}J}$, $\theta_{\mathrm{p}J}$, and f_J parameters retain their meanings in terms of the Heisenberg exchange constants and magnetic structure as given in Eqs. (A6a), (A6b), and (A7), respectively. We normalize energies, fields, and temperatures by $T_{\mathrm{N}J}$ in this paper, as given in the following summary and definitions of parameters:

$$\bar{\mu}_\alpha = \frac{\mu_\alpha}{\mu_{\mathrm{sat}}} = \frac{\mu_\alpha}{g S \mu_{\mathrm{B}}}, \tag{1b}$$

$$h_\alpha \equiv \frac{g \mu_{\mathrm{B}} H_\alpha}{k_{\mathrm{B}} T_{\mathrm{N}J}}, \tag{1c}$$

$$T_{\mathrm{A1}} \equiv \frac{g \mu_{\mathrm{B}} H_{\mathrm{A1}}}{k_{\mathrm{B}}}, \tag{1d}$$

$$h_{\mathrm{A1}} \equiv \frac{T_{\mathrm{A1}}}{T_{\mathrm{N}J}} = \frac{g \mu_{\mathrm{B}} H_{\mathrm{A1}}}{k_{\mathrm{B}} T_{\mathrm{N}J}} \geqslant 0, \tag{1e}$$

$$f_J \equiv \frac{\theta_{\mathrm{p}J}}{T_{\mathrm{N}J}}, \tag{1f}$$

$$t \equiv \frac{T}{T_{\mathrm{N}J}}, \tag{1g}$$

$$T_{\mathrm{N}} = T_{\mathrm{N}J} + T_{\mathrm{A1}} \tag{1h}$$

$$\frac{T_{\mathrm{N}}}{T_{\mathrm{N}J}} = 1 + \frac{T_{\mathrm{A1}}}{T_{\mathrm{N}J}} = 1 + h_{\mathrm{A1}}, \tag{1i}$$

$$t_{\mathrm{A}} \equiv \frac{T}{T_{\mathrm{N}}} = \frac{t}{1 + h_{\mathrm{A1}}}. \tag{1j}$$

The magnetic susceptibility per spin χ_α in the α principal-axis direction is rigorously defined in the absence of a ferromagnetic component to the magnetization as

$$\chi_\alpha = \lim_{H_\alpha \to 0} \mu_\alpha(H_\alpha)/H_\alpha. \tag{2}$$

We define two reduced magnetic susceptibilities in the α principal-axis direction. The first is

$$\chi_\alpha^* \equiv \left. \frac{\bar{\mu}_\alpha}{h_\alpha} \right|_{h_\alpha \to 0}. \tag{3a}$$

The second is

$$\bar{\chi}_\alpha \equiv \frac{\chi_\alpha T_{\mathrm{N}J}}{C_1} = \left(\frac{3}{S+1}\right)\chi_\alpha^*, \tag{3b}$$

where the single-spin Curie constant C_1 is given in Eq. (A1b).

B. Thermodynamics

In this section, we give thermodynamics expressions needed in this paper assuming that the ordered and/or induced moment of a representative spin $\vec{\mu}_i$ versus field and temperature has already been determined within the unified MFT as outlined in the Appendix in the case of zero applied and anisotropy fields.

The magnetic internal energy U_{mag} of spin i for a local magnetic induction $\mathbf{B}_i$ in the α principal-axis direction is

$$U_{\mathrm{mag}i} = -\mu_{i\alpha} B_{i\alpha}, \tag{4}$$

where here $B_{i\alpha}$ is written in general as

$$B_{i\alpha} = \tfrac{1}{2}(H_{\mathrm{exch}i\alpha} + H_{\mathrm{A}i\alpha}) + H_\alpha, \tag{5}$$

and $H_{\mathrm{A}i\alpha}$ is the local anisotropy field seen by spin i discussed later. We have seen that the exchange field seen by a spin is proportional to $\mu_{i\alpha}$. This is also true for the anisotropy field by assumption in Sec. III below. Thus the parts of $U_{\mathrm{mag}i}$ associated with these fields are both proportional to $\mu_{i\alpha}^2$, indicating that they both ultimately arise from interactions between pairs of spins, hence the prefactor of $1/2$ in the first term of Eq. (5) as discussed in regard to Eq. (A16) where only the exchange field was present. We write the sum of the exchange and anisotropy fields as

$$H_{\mathrm{exch}i\alpha} + H_{\mathrm{A}i\alpha} = a\mu_{i\alpha}, \tag{6}$$

where the constant a contains the parameters associated with these fields. Then Eq. (5) becomes

$$B_{i\alpha} = a\mu_{i\alpha} + H_\alpha. \tag{7}$$

1. Properties in zero applied field

When $H_\alpha = 0$, Eqs. (4) and (5) yield the internal energy per spin as

$$U_{\mathrm{mag}}(H_\alpha = 0, T) = -\frac{a}{2}\mu_\alpha^2(T). \tag{8}$$

We always assume that the spins are identical and crystallographically equivalent, so the subscript i is suppressed when $H_\alpha = 0$. Then the magnetic heat capacity per spin C_{mag} is

$$C_{\mathrm{mag}}(H_\alpha = 0, T) = \frac{dU_{\mathrm{mag}}(H_\alpha = 0, T)}{dT} = -a\mu_\alpha \frac{d\mu_\alpha}{dT}. \tag{9}$$

The magnetic entropy $S_{\mathrm{mag}}(H_\alpha = 0, T)$ per spin is then obtained as

$$S_{\mathrm{mag}}(H_\alpha = 0, T) = S_{\mathrm{mag}}(H_\alpha = 0, T = 0) + \int_0^T \frac{C_{\mathrm{mag}}(H_\alpha = 0, T)}{T} dT, \tag{10}$$

and the (Helmholtz) free energy $F_{\mathrm{mag}}(H_\alpha = 0, T)$ as

$$F_{\mathrm{mag}}(H_\alpha = 0, T) = U_{\mathrm{mag}}(H_\alpha = 0, T) - T S_{\mathrm{mag}}(H_\alpha = 0, T). \tag{11}$$

2. Properties at nonzero temperature and nonzero applied field

It is most convenient in this paper to calculate the thermodynamic state functions in the H_α-T plane by choosing the path from $(H_\alpha = 0, T = 0)$ to $(H_\alpha = 0, T)$ as in the previous section and then at constant T from $(H_\alpha = 0, T)$ to (H_α, T). The differential of the free energy for the second part of the path at constant T, $dF_{\mathrm{mag}} = -S_{\mathrm{mag}}dT - \mu_\alpha dH_\alpha$ with $dT = 0$, yields

$$dF_{\mathrm{mag}}(H_\alpha, T) = -\mu_\alpha dH_\alpha. \tag{12}$$

Then using Eq. (11) one obtains

$$F_{\mathrm{mag}}(H_\alpha, T) = F_{\mathrm{mag}}(H_\alpha = 0, T) - \int_0^{H_\alpha} \mu_\alpha(H_\alpha, T) dH_\alpha, \tag{13}$$

where $F_{\mathrm{mag}}(H_\alpha = 0, T)$ is found as described above.

The variation of the magnetic entropy with field at constant temperature is found from the Maxwell relation

$$(dS_{\mathrm{mag}})_T = \left(\frac{\partial \mu_\alpha(H_\alpha, T)}{\partial T}\right)_{H_\alpha} dH_\alpha. \tag{14}$$

Then using Eq. (10) one obtains

$$S_{\mathrm{mag}}(H_\alpha, T) = S_{\mathrm{mag}}(H_\alpha = 0, T) + \int_0^{H_\alpha} \left(\frac{\partial \mu_\alpha(H_\alpha, T)}{\partial T}\right)_{H_\alpha} dH_\alpha. \tag{15}$$

An increment of internal energy is

$$dU_{\mathrm{mag}} = T dS_{\mathrm{mag}} - \mu_\alpha dH_\alpha. \tag{16}$$

Using Eq. (14) for dS_{mag} at fixed T gives

$$(dU_{\mathrm{mag}})_T = \left[T\left(\frac{\partial \mu_\alpha(H_\alpha, T)}{\partial T}\right)_{H_\alpha} - \mu_\alpha\right]dH_\alpha, \tag{17}$$

and hence

$$U_{\mathrm{mag}}(H_\alpha, T) = U_{\mathrm{mag}}(H_\alpha = 0, T) + \int_0^{H_\alpha} \left[T\left(\frac{\partial \mu_\alpha(H_\alpha, T)}{\partial T}\right)_{H_\alpha} - \mu_\alpha\right]dH_\alpha. \tag{18}$$

In the free-energy expression (13), the integral of $(\partial \mu_\alpha(H_\alpha, T)/\partial T)_{H_\alpha}$ over H_α in S_{mag} and U_{mag} is not present because it canceled out in the definition $F_{\mathrm{mag}} = U_{\mathrm{mag}} - T S_{\mathrm{mag}}$.

3. Expressions in reduced variables

In order to formulate laws of corresponding states for the thermodynamic properties, we normalize all energies by $k_\mathrm{B} T_{\mathrm{N}J}$, where $T_{\mathrm{N}J}$ is the Néel temperature in zero field arising from exchange interactions alone as discussed in the Appendix. We also define the following dimensionless reduced variables:

$$b_\alpha = \frac{g\mu_\mathrm{B} B_\alpha}{k_\mathrm{B} T_{\mathrm{N}J}}, \tag{19a}$$

$$A = \frac{a}{k_\mathrm{B} T_{\mathrm{N}J}}, \tag{19b}$$

$$b_\alpha = A\bar{\mu}_\alpha + h_\alpha. \tag{19c}$$

Then also using Eqs. (1), the expressions in the above two subsections become

$$\frac{U_{\text{mag}}(h_\alpha = 0,t)}{k_B T_{NJ}} = -\frac{AS}{2}\bar{\mu}_\alpha^2(h_\alpha = 0,t), \tag{20a}$$

$$\frac{C_{\text{mag}}(h_\alpha = 0,t)}{k_B} = -AS\bar{\mu}_\alpha(t)\frac{d\bar{\mu}_\alpha(h_\alpha = 0,t)}{dt}, \tag{20b}$$

$$\frac{S_{\text{mag}}(h_\alpha = 0,t)}{k_B} = \frac{S_{\text{mag}}(h_\alpha = 0,t=0)}{k_B}$$
$$+ \int_0^t \frac{C_{\text{mag}}(h_\alpha = 0,t)/k_B}{t}dt, \tag{20c}$$

$$\frac{F_{\text{mag}}(h_\alpha = 0,t)}{k_B T_{NJ}} = \frac{F_{\text{mag}}(h_\alpha = 0,t)}{k_B T_{NJ}} - t\frac{S_{\text{mag}}(h_\alpha = 0,t)}{k_B}. \tag{20d}$$

$$\frac{F_{\text{mag}}(h_\alpha,t)}{k_B T_{NJ}} = \frac{F_{\text{mag}}(h_\alpha = 0,t)}{k_B T_{NJ}}$$
$$- S\int_0^{h_\alpha} \bar{\mu}_\alpha(h_\alpha,t)dh_\alpha, \tag{20e}$$

$$\frac{S_{\text{mag}}(h_\alpha,t)}{k_B} = \frac{S_{\text{mag}}(h_\alpha = 0,t)}{k_B}$$
$$+ S\int_0^{h_\alpha} \left(\frac{\partial\bar{\mu}_\alpha(h_\alpha,t)}{\partial t}\right)_{h_\alpha} dh_\alpha, \tag{20f}$$

$$\frac{U_{\text{mag}}(h_\alpha,t)}{k_B T_{NJ}} = \frac{U_{\text{mag}}(h_\alpha = 0,t)}{k_B T_{NJ}}$$
$$+ S\int_0^{h_\alpha} \left[t\left(\frac{\partial\bar{\mu}_\alpha(h_\alpha,t)}{\partial t}\right)_{h_\alpha}\right.$$
$$\left. - \bar{\mu}_\alpha(h_\alpha,t)\right]dh_\alpha. \tag{20g}$$

III. AFM ORDERING IN A CLASSICAL ANISOTROPY FIELD

The lowest-order uniaxial anisotropy free energy F_{Ai} per spin associated with a uniaxial or planar anisotropy symmetry as in Figs. 1 and 2, respectively, for an ordered and/or magnetic field-induced thermal-average magnetic moment $\vec{\mu}_i$ is written as [2]

$$F_{Ai} = K_{1i}\sin^2\theta_i, \tag{21}$$

where θ_i is the polar angle between $\vec{\mu}_i$ and the uniaxial z axis. Here, we assume that this relation is valid for the entire angular region $0 \leqslant \theta \leqslant \pi$. The z axis for F_{Ai} from which θ_i is defined is assumed to be a uniaxial axis of the lattice, and hence the anisotropy is fundamentally magnetocrystalline in origin. This generic model is assumed to apply to spin systems with any spin angular momentum quantum number S (in units of $\hbar$, which is Planck's constant divided by 2π) and can therefore treat systems with $S = 1/2$ for which a magnetocrystalline DS_z^2 term in the Hamiltonian gives no anisotropy. The anisotropy constant K_1 is in general different for different moments $\vec{\mu}_i$ because of their different magnitudes as discussed below, hence the subscripts i in Eq. (21). If K_{1i} is positive and $\mathbf{H} = 0$, then the lowest free energy of a
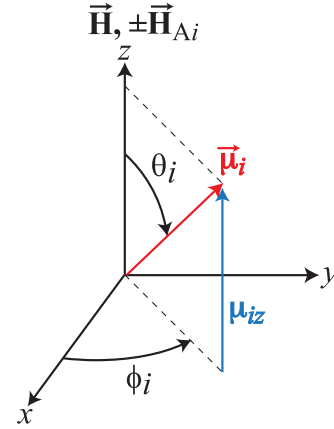

FIG. 1. The orientation of a representative magnetic moment $\vec{\mu}_i$ described by spherical coordinates θ_i and ϕ_i in an applied magnetic field $\mathbf{H} = H_z\,\hat{\mathbf{k}}$ and a generic classical anisotropy field $\mathbf{H}_{Ai}$ directed along the $\pm z$ axis. For such an anisotropy field, collinear AFM ordering along the z axis is favored if $H_z = 0$.

system occurs with $\sin\theta_i = 0$ for all $\vec{\mu}_i$, for which the ordered moments are collinear and aligned parallel or antiparallel to the uniaxial z axis, whereas if K_{1i} is negative the lowest free energy occurs when $\sin\theta_i = 90°$ for all $\vec{\mu}_i$, resulting in collinear or coplanar ordering in the xy plane. Using Eq. (21), the magnitude τ_{Ai} of the torque on each $\vec{\mu}_i$ by its anisotropy field $\mathbf{H}_{Ai}$ (see below) has the same form for all moments and is given by

$$\tau_{Ai} = \left|\frac{\partial F_{Ai}}{\partial\theta}\right| = 2|K_{1i}\sin\theta_i\cos\theta_i|. \tag{22}$$

A. Collinear ordering along the z axis: Uniaxial anisotropy

For collinear AFM ordering along the z axis in $H = 0$ with uniaxial anisotropy, one has $\theta_i = 0$ or $180°$ in Fig. 1. The anisotropy field $\mathbf{H}_{Ai}$ along the z axis in such a collinear AFM
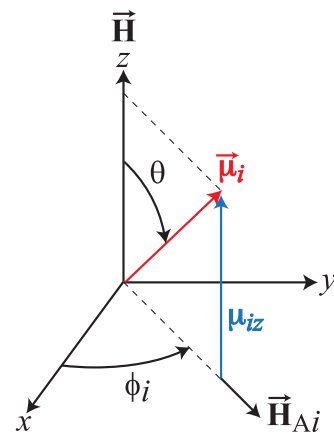

FIG. 2. The orientation of a representative magnetic moment $\vec{\mu}_i$ in an applied magnetic field $\mathbf{H} = H_z\,\hat{\mathbf{k}}$ and an anisotropy field $\mathbf{H}_{Ai}$ in the xy plane that is directed along the projection of $\vec{\mu}_i$ onto the xy plane as shown. For such an anisotropy field, collinear or planar noncollinear AFM ordering within the xy plane is favored if $H_z = 0$. The azimuthal angle ϕ_i is in general different for different moments but the value for each moment is not affected by $\mathbf{H}$.
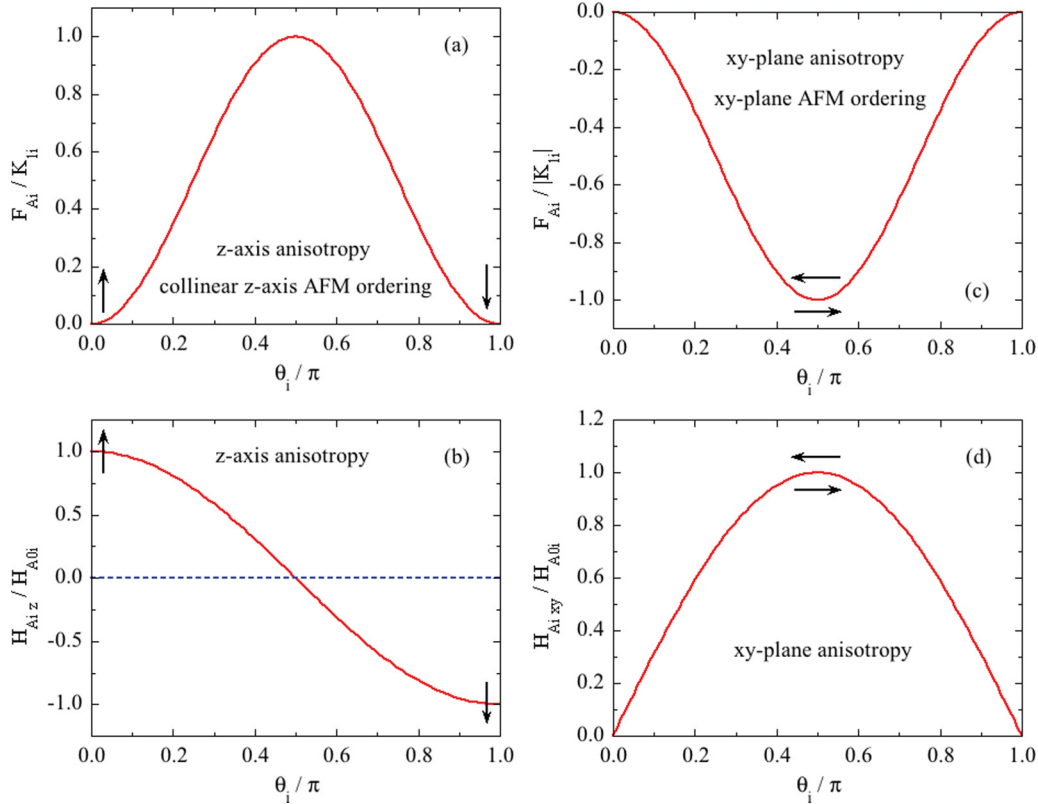
FIG. 3. Comparisons of the free energy and anisotropy fields, respectively, for (a) and (b) axial z-axis anisotropy and ordering and (c) and (d) xy-plane anisotropy and ordering. The anisotropy free energy per spin F_{Ai} normalized by $|K_{1i}|$ is given in Eq. (21), where $K_{1i} > 0$ for axial anisotropy and $K_{1i} < 0$ for planar anisotropy. The anisotropy fields H_{Ai} for axial and planar anisotropies are given in Eqs. (23) and (27), respectively.

is defined to be in the same direction $\pm\hat{\mathbf{k}}$ as that of the ordered moment $\vec{\mu}_i$, which can be written as

$$\mathbf{H}_{Ai} = H_{A0i} \cos\theta_i \, \hat{\mathbf{k}}, \qquad (23a)$$

$$H_{Aiz} = H_{A0i} \cos\theta_i, \qquad (23b)$$

where $H_{A0i} \geqslant 0$ is the amplitude of the anisotropy field for axial anisotropy. For uniaxial ordering $K_{1i} > 0$ in Eq. (21), so that the minimum free energy $F_{Ai} = 0$ occurs for collinear AFM ordering with the moments oriented along the z axis as shown in Fig. 3(a). If the moments all rotate with increasing field into a "spin-flop" phase to give $\theta_i \lesssim 90°$ for each spin, then from Eq. (21) and Fig. 3(a) the anisotropy free energy of each moment increases to $\approx K_{1i}$.

Using Eq. (A27a) for a representative moment $\vec{\mu}_i$, the torque due to the anisotropy field on the moment tilted by an angle θ with respect to the z axis is

$$\vec{\tau}_{Ai} = \vec{\mu}_i \times \mathbf{H}_{Ai} = \mu_i H_{A0i} \sin\theta_i \cos\theta_i [\sin\phi_i \, \hat{\mathbf{i}} - \cos\phi_i \, \hat{\mathbf{j}}],$$
$$(24a)$$

with magnitude

$$\tau_{Ai} = |\mu_i H_{A0i} \sin\theta_i \cos\theta_i|, \qquad (24b)$$

where μ_i is the magnitude of the (thermal-average) $\vec{\mu}_i$ and θ_i is the polar angle in Fig. 1. Comparing Eqs. (24b) and (22)

gives the anisotropy constant for moment i as

$$K_{1i} = \frac{\mu_i H_{A0i}}{2} > 0, \qquad (25)$$

where K_{1i} is positive for uniaxial collinear ordering in zero field as discussed above. As noted above, K_1 can depend on the specific moment i if the magnitude μ_i is not the same for all moments.

The maximum magnitude of $\mathbf{H}_{Ai}$ from Eqs. (23) occurs at $\theta_i = 0$ or $180°$, at which the anisotropy free energy in Eq. (21) is minimum (zero) as shown in Fig. 3(a). A plot of H_{Aiz}/H_{A0i} versus θ_i from Eq. (23b) is shown in Fig. 3(b), which by comparison with Fig. 3(a) demonstrates that the maximum magnitude of the anisotropy field occurs at the ordering angles for collinear AFM ordering, for which the free energy is minimum.

B. Collinear or planar noncollinear ordering in the xy plane: Planar anisotropy

When planar (XY) anisotropy is present, the ordered AFM structure in $H = 0$ can be either a collinear structure or a planar noncollinear structure with the ordered moments aligned in the xy plane for both structures. In either case, the polar angle for the orientations of all ordered moments for $H = 0$ is $\theta_i = 90°$ in Fig. 2. In order that these magnetic structures have a lower magnetic free energy than for collinear AFM ordering along

the z axis requires that

$$K_{1i} < 0 \tag{26}$$

in Eq. (21), as shown in Fig. 3(c).

From Fig. 2, $\mathbf{H}_{\mathrm{A}i}$ *is directed along the projection of* $\vec{\mu}_i$ *onto the* xy *plane instead of along the* z *axis as described in Eq. (23a) for uniaxial anisotropy.* Therefore, instead of Eq. (23a), we now write $\mathbf{H}_{\mathrm{A}i}$ in spherical coordinates as

$$\mathbf{H}_{\mathrm{A}i} = H_{\mathrm{A}0i}\sin\theta_i(\cos\phi_i\,\hat{\mathbf{i}} + \sin\phi_i\,\hat{\mathbf{j}}), \tag{27a}$$

$$H_{\mathrm{A}i\,xy} \equiv H_{\mathrm{A}0i}\sin\theta_i, \tag{27b}$$

where $H_{\mathrm{A}0i}$ is the magnitude of $\mathbf{H}_{\mathrm{A}i}$ when $\theta_i = 90°$. The torque exerted by $\mathbf{H}_{\mathrm{A}i}$ on $\vec{\mu}_i$ is obtained from Eqs. (27a) and (A27) as

$$\vec{\tau}_{\mathrm{A}i} = \vec{\mu}_i \times \mathbf{H}_{\mathrm{A}i} = -\mu_i H_{\mathrm{A}0i}\sin\theta_i\cos\theta_i(\sin\phi_i\,\hat{\mathbf{i}} - \cos\phi_i\,\hat{\mathbf{j}}), \tag{28}$$

with magnitude

$$\tau_{\mathrm{A}i} = |\mu_i H_{\mathrm{A}0i}\sin\theta_i\cos\theta_i|. \tag{29}$$

This is the same expression as in Eq. (24b) for collinear AFM ordering along the z axis, but here the zero-torque condition applies to $\theta_i = \pi/2$ instead of 0 or π as appropriate for z-axis collinear ordering.

Comparing Eqs. (29) and (22) and using (26) gives

$$K_{1i} = -\frac{\mu_i H_{\mathrm{A}0i}}{2} < 0, \tag{30}$$

which is the same as in Eq. (25) for axial anisotropy except for the sign. A plot of $H_{\mathrm{A}i\,xy}/H_{\mathrm{A}0i}$ versus θ_i from Eq. (27b) is shown in Fig. 3(d), which by comparison with Fig. 3(c) demonstrates that the anisotropy field is maximum at the ordering angle $\theta_i = \pi/2$ for planar AFM ordering for which the free energy is minimum.

C. Fundamental anisotropy field $H_{\mathrm{A}1}$

In the present treatment of either uniaxial or planar anisotropy, we write the anisotropy field amplitude $H_{\mathrm{A}0i} \geqslant 0$ in Eqs. (23) and (27) as

$$H_{\mathrm{A}0i}(T) = \frac{3H_{\mathrm{A}1}}{S+1}\bar{\mu}_i(T) = \frac{3H_{\mathrm{A}1}}{g\mu_{\mathrm{B}}S(S+1)}\mu_i(T), \tag{31a}$$

where the subsidiary anisotropy field

$$H_{\mathrm{A}1} \geqslant 0 \tag{31b}$$

does not depend on the moment $\vec{\mu}_i$ or on T and is therefore a more fundamental anisotropy field than $H_{\mathrm{A}0i}$. The reason for including the factor $3/(S+1)$ in Eq. (31a) is explained in Sec. IV below. The reduced ordered moment $\bar{\mu}_i \equiv \mu_i/\mu_{\mathrm{sat}}$ can be numerically calculated for all moments in $H = 0$ using Eqs. (37) below but the value can be different for different moments if $H \neq 0$. Inserting Eq. (31a) into (25) or (30) gives

$$|K_{1i}| = \frac{3g\mu_{\mathrm{B}}SH_{\mathrm{A}1}}{2(S+1)}\bar{\mu}_i^2(T) = \frac{3H_{\mathrm{A}1}}{2g\mu_{\mathrm{B}}S(S+1)}\mu_i^2(T), \tag{32}$$

where we used Eq. (1b). Since $\bar{\mu}_i(T = T_{\mathrm{N}}) = 0$ if $H = 0$ where T_{N} is the Néel temperature in the presence of both exchange and anisotropy fields (see below), one has $K_{1i}(T \to T_{\mathrm{N}}^-) = 0$ if $H = 0$ [10]. However, for $H > 0$, a field-induced thermal-averaged moment μ_i arises in the paramagnetic state at $T \geqslant T_{\mathrm{N}}$, and this anisotropy therefore influences both the AFM and PM (FM-aligned) states.

IV. NÉEL TEMPERATURE, ORDERED MOMENT, INTERNAL ENERGY, HEAT CAPACITY, ENTROPY, AND FREE ENERGY OF THE ANTIFERROMAGNETIC PHASE IN ZERO APPLIED FIELD

The definition of the anisotropy field $\mathbf{H}_{\mathrm{A}i}$ in Eq. (23a) for collinear AFM ordering along the z axis ($\theta_i = 0$ or $180°$) and in Eq. (27a) for ordering in the xy plane shows that for $H = 0$, $\mathbf{H}_{\mathrm{A}i}$ is parallel to each ordered magnetic moment $\vec{\mu}_i$ in the ordered state below T_{N}, just as the exchange field $\mathbf{H}_{\mathrm{exch}\,i}$ is. Since the local exchange and anisotropy fields are both in the same direction as that of the respective ordered moment in the AFM state in $H = 0$, they reinforce each other, and also have the same values for each moment because all moments are identical and crystallographically equivalent by assumption.

For $H = 0$, the parameters μ_0, $\bar{\mu}_0$, K_1, and $H_{\mathrm{A}0}$ do not depend on the spin i and hence we drop the subscript i when discussing these quantities for $H = 0$. Here the parameters μ_0 and $\bar{\mu}_0$ respectively refer to the ordered moment and reduced ordered moment in $H = 0$ but in the presence of both the exchange and anisotropy fields as appropriate.

From Eqs. (A9) for the exchange field in $H = 0$ together with Eq. (A1b), one obtains

$$\frac{g\mu_{\mathrm{B}}H_{\mathrm{exch}0}}{k_{\mathrm{B}}T} = \frac{3T_{\mathrm{N}J}}{(S+1)T}\bar{\mu}_0. \tag{33}$$

Using Eq. (31a), a similar expression for the anisotropy field is

$$\frac{g\mu_{\mathrm{B}}H_{\mathrm{A}0}}{k_{\mathrm{B}}T} = \frac{3g\mu_{\mathrm{B}}H_{\mathrm{A}1}}{(S+1)k_{\mathrm{B}}T}\bar{\mu}_0 = \frac{3T_{\mathrm{A}1}}{(S+1)T}\bar{\mu}_0, \tag{34}$$

where the anisotropy temperature $T_{\mathrm{A}1}$ (not a real temperature) is defined in terms of $H_{\mathrm{A}1}$ in Eq. (1d). For $H = 0$, the magnetic induction obtained by MFT that is seen by each moment is $B = H_{\mathrm{exch}0} + H_{\mathrm{A}0}$. Using Eqs. (33) and (34), $\bar{\mu}_0$ is governed by the Brillouin function $B_S(y)$ according to Eqs. (A10) as

$$\bar{\mu}_0 = B_S(y_0), \quad y_0 = \frac{3}{S+1}(T_{\mathrm{N}J} + T_{\mathrm{A}1})\frac{\bar{\mu}_0}{T}. \tag{35}$$

The ordering temperature occurs as $\bar{\mu}_0 \to 0$. Using the first-order Taylor series expansion term of the Brillouin function in Eq. (A11b), Eq. (35) gives the Néel temperature $T = T_{\mathrm{N}}$ in the presence of both the exchange and anisotropy fields as

$$T_{\mathrm{N}} = T_{\mathrm{N}J} + T_{\mathrm{A}1} = T_{\mathrm{N}J}(1 + h_{\mathrm{A}1}), \tag{36}$$

where $h_{\mathrm{A}1}$ is defined in terms of $T_{\mathrm{A}1}$ and $H_{\mathrm{A}1}$ in Eqs. (1e) and (1i). Thus the presence of the reinforcing anisotropy field $h_{\mathrm{A}1} > 0$ increases the Néel temperature, as expected. From Eq. (36), the fractional increase in the Néel temperature due to the anisotropy field, $\frac{T_{\mathrm{N}}}{T_{\mathrm{N}J}} - 1$, is equal to $h_{\mathrm{A}1}$, an appealing physical interpretation of $h_{\mathrm{A}1}$. This behavior is comparable to the influence of a DS_z^2 anisotropy on T_{N} at small D where T_{N} is

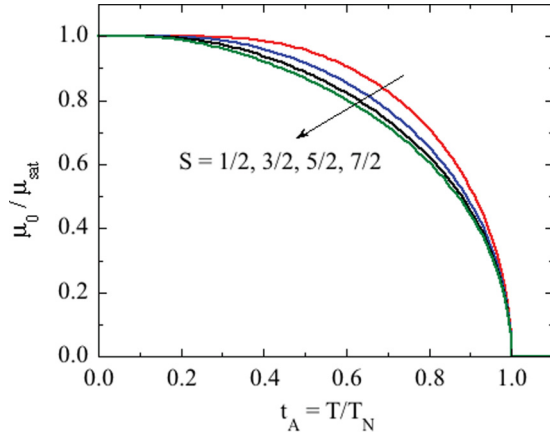FIG. 4. Reduced ordered moment $\bar{\mu}_0$ vs reduced temperature t_A in zero applied field but in the presence of an anisotopy field. These behaviors are valid within MFT for both uniaxial and planar anisotropies for any type of magnetic ordering of identical crystallographically equivalent spins.

proportional to D, but is very different from the behavior of T_N versus D at larger D where T_N varies nonlinearly with D [4]. However, for the classical anisotropy treated in this paper both the ordering temperature T_N and the Weiss temperature θ_p (see below) vary linearly with h_{A1} in the same way for arbitrary values of h_{A1}.

To determine the zero-field ordered moment versus temperature for $T \leqslant T_N$, we use Eqs. (1j) and (36) and then Eqs. (35) become

$$\bar{\mu}_0 = B_S(y_0), \tag{37a}$$

$$y_0 = \frac{3\bar{\mu}_0}{(S+1)t_A}. \tag{37b}$$

These equations, which are used to numerically calculate $\bar{\mu}_0(t_A)$, have the same form as Eqs. (A14) for $H = H_{A1} = 0$, except with $t_A \equiv T/T_N$ in Eq. (1j) replacing $t \equiv T/T_{NJ}$ as shown in Fig. 4 [11]. *Hence the reason we introduced the factor of $3/(S+1)$ in the definition of the anisotropy field H_{A0i} in Eq. (31a) was to require Eqs. (37) to have the same form as Eqs. (A14).*

To determine $\bar{\mu}_0$ in terms of $t = T/T_{NJ}$ instead of $t_A = T/T_N$, one can use Eqs. (1j) and (37) to obtain

$$\bar{\mu}_0 = B_S \left[\frac{3\bar{\mu}_0(1+h_{A1})}{(S+1)t} \right]. \tag{38}$$

Setting $h_{A1} = 0$, one recovers Eqs. (A14) for the case of zero anisotropy.

In zero field, all spins have the same internal energy per spin U_i according to Eq. (5), which has two contributions for either z-axis or xy-plane ordering given by

$$U_i = U_{\text{exch0}} + U_{Ai} \tag{39a}$$

$$U_{\text{exch}i} = -\tfrac{1}{2}\mu H_{\text{exch0}}, \tag{39b}$$

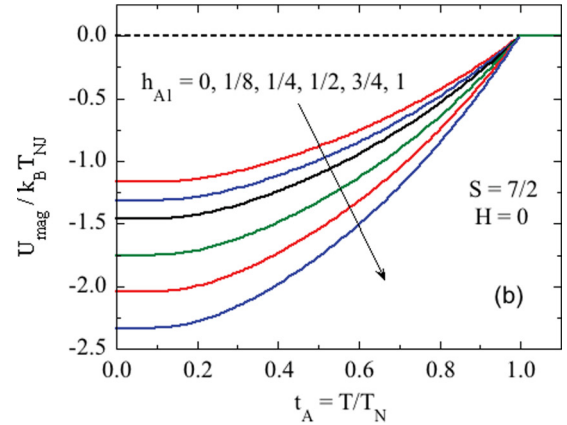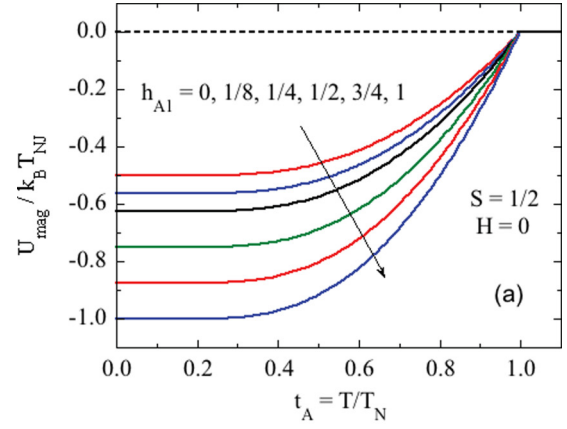$$U_{Ai} = -\tfrac{1}{2}\mu H_{A0i}. \tag{39c}$$

FIG. 5. Magnetic internal energy per spin U_{mag} normalized by $k_B T_{NJ}$ of the AFM phase vs reduced temperature t_A in zero applied field in the presence of a reduced anisotopy fields $h_{A1} = 0$ to 1 for spins (a) $S = 1/2$ and (b) $S = 7/2$ obtained using Eqs. (37) and (40c).

Normalizing the energies by $k_B T_{NJ}$, Eqs. (A17), (1), (23b) or (27b), and (31a) yield

$$\frac{U_{\text{exch0}}}{k_B T_{NJ}} = -\frac{3S}{2(S+1)}\bar{\mu}_0^2, \tag{40a}$$

$$\frac{U_{Ai}}{k_B T_{NJ}} = -\frac{3S}{2(S+1)}h_{A1}\bar{\mu}_0^2, \tag{40b}$$

$$\frac{U_i}{k_B T_{NJ}} = -\frac{3S}{2(S+1)}(1+h_{A1})\bar{\mu}_0^2. \tag{40c}$$

Shown in Fig. 5 are plots of $U_i/k_B T_{NJ}$ versus reduced temperature t_A for a range of reduced anisotropy parameters $h_{A1} = 0$ to 1 and for spins $S = 1/2$ and $S = 7/2$ obtained using Eqs. (37) and (40c). One sees that the zero-temperature internal energy decreases (becomes more stable) with increasing h_{A1} as expected. Also, the internal energy goes to zero when the ordered moment goes to zero with increasing temperature.
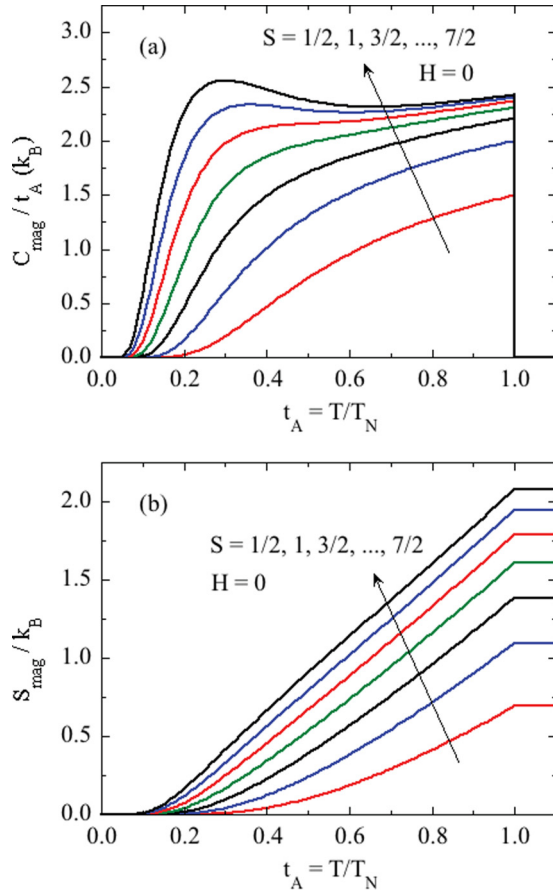
FIG. 6. Magnetic heat capacity per spin C_{mag} of the AFM phase vs reduced temperature t_A in zero applied field for any reduced anisotropy field $h_{A1} \geqslant 0$ and spins $S = 1/2$ to $7/2$ in half-integer increments. The hump that develops with increasing S at a temperature $\sim t_A/4$ is intrinsic to molecular-field theory. (b) Magnetic entropy per spin S_{mag}/k_B vs t_A for the same parameters as in (a).

The magnetic heat capacity per spin is

$$
\begin{aligned}
\frac{C_{mag}}{k_B} &= \frac{d(U_i/k_B T_{NJ})}{dt} \\
&= -\left(\frac{3S}{S+1}\right)(1 + h_{A1})\bar{\mu}_0(t_A)\frac{d\bar{\mu}_0(t_A)}{dt}, \\
&= -\left(\frac{3S}{S+1}\right)\bar{\mu}_0(t_A)\frac{d\bar{\mu}_0(t_A)}{dt_A},
\end{aligned}
\tag{41}
$$

where we used Eq. (1j) to obtain the third equality, $\bar{\mu}_0(t_A)$ is obtained by solving Eqs. (37), and $d\bar{\mu}_0(t_A)/dt_A$ is obtained from Eq. (A11c) where $y = y_0$ is given in Eq. (37b). Equation (41) for C_{mag} is identical in form to the equation for C_{mag} with $h_{A1} = 0$ and with t replacing t_A [11]. The presence of h_{A1} in Eq. (41) is therefore equivalent to the replacements $T_{NJ} \to T_N$ and $t \to t_A$ in the equation for $h_{A1} = 0$. Plots of C_{mag}/t_A versus t_A are shown for $S = 1/2$ to $S = 7/2$ in Fig. 6(a). One sees that with increasing S, on approaching T_N from below C_{mag}/t_A approaches a constant value for increasing S given by

$$
\frac{C_{mag}(t_A \to 1, S \to \infty)}{k_B} = 5/2,
\tag{42}
$$

consistent with the exact expression for finite S [6]:

$$
\frac{C_{mag}(t_A \to 1)}{k_B} = \frac{5S(S+1)}{1 + 2S(S+1)}.
\tag{43}
$$

The broad hump that develops in $C_{mag}/k_B t_A$ at $t_A \sim 1/4$ for large S is intrinsic to the MFT [6], and is therefore prominently observed in the AFM state of compounds containing spin-only Eu^{+2} and Gd^{+3} ions with large spin $S = 7/2$ [6]. It arises from a practical point of view in order that the statistical mechanics value for the magnetic entropy per spin at T_N, given by

$$
S_{mag}(t_A = 1)/k_B = \ln(2S + 1),
\tag{44}
$$

continues to increase with increasing S, since as just stated the $C_{mag}(t_A \sim 1)$ is bounded with increasing S and hence the increasing entropy must arise by increasing C_{mag} at lower and lower temperatures with increasing S.

The S_{mag}/k_B versus t_A for $h_{A1} > 0$ is obtained using

$$
\frac{S_{mag}(t_A)}{k_B} = \int_0^{t_A} \frac{C_{mag}(t_A)/k_B}{t_A} dt_A,
\tag{45}
$$

where $S_{mag}(t_A = 0) = 0$ because the energy levels are nondegenerate at $t_A = 0$ due to the presence of nonzero H_{exch} and H_A, and $C_{mag}(t_A)/k_B$ is obtained as described above. The S_{mag} is plotted versus t_A for $S = 1/2$ to $S = 7/2$ in Fig. 6(b), where the high-T limit in Eq. (44) is indeed obtained for each value of S for $T \geqslant T_N$.

The reduced Helmholtz free energy per spin versus reduced temperature t_A is given in general by

$$
\frac{F_{mag}}{k_B T_{NJ}} = \frac{U_{mag}}{k_B T_{NJ}} - t_A \frac{S_{mag}}{k_B}.
\tag{46}
$$

Shown in Fig. 7 are plots of $F_{mag}/k_B T_{NJ}$ for $H = 0$ versus t_A with h_{A1} values from 0 to 1 for spins $S = 1/2$ and $7/2$ obtained from the data in Figs. 5 and 6. One sees that F_{mag} varies monotonically with t_A, but that the sign of the slope depends on the value of h_{A1}. Another important feature is that F_{mag} is independent of h_{A1} for $t_A \geqslant 1$ because $U_{mag} = 0$ in that temperature range and S_{mag} versus t_A is independent of h_{A1} for a given value of the spin S because the influence of h_{A1} is already included via its effect on T_N in the definition $t_A \equiv T/T_N$.

V. MAGNETIC SUSCEPTIBILITY OF THE PARAMAGNETIC PHASE

In the paramagnetic (PM) phase at $T \geqslant T_N$, there is no ordered or induced moment in the absence of a field $\mathbf{H}$ applied along a principal-axis direction. When $H_\alpha > 0$, the field-induced thermal-average moment of each spin points in the direction of $\mathbf{H}$. From Eq. (A21a), the magnitude of the exchange field seen by each moment is

$$
H_{exch\alpha} = \frac{3k_B \theta_{pJ}}{g\mu_B(S+1)} \bar{\mu}_\alpha,
\tag{47}
$$

where θ_{pJ} is the Weiss temperature due to the exchange interactions alone, which is defined in terms of the exchange constants in the spin system in Eq. (A6b), and $\bar{\mu}_\alpha = \mu_\alpha/\mu_{sat} = \mu_\alpha/gS\mu_B$ is the normalized thermal-average moment induced by H_α in the α direction.
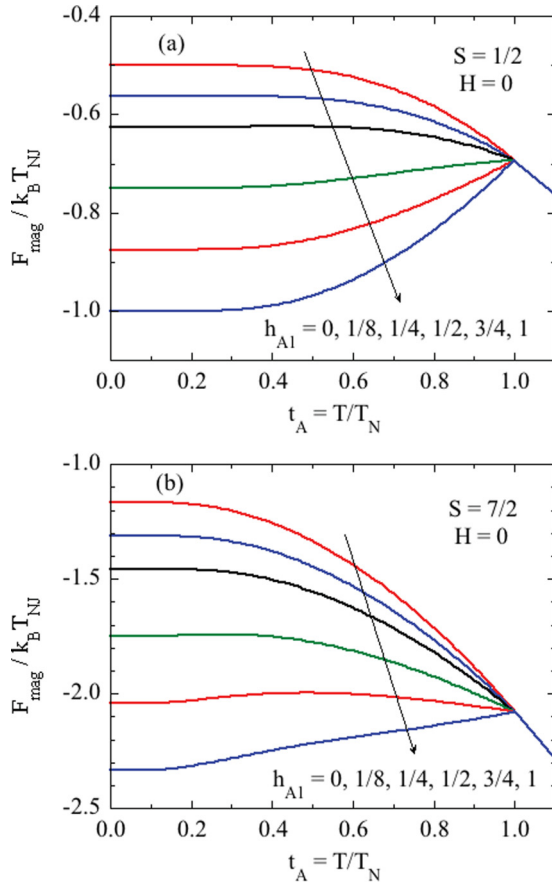
FIG. 7. Reduced magnetic free energy per spin $F_{\mathrm{mag}}/k_{\mathrm{B}}T_{\mathrm{N}J}$ of the AFM phase vs reduced temperature t_{A} in zero applied field for anisotopy fields $h_{\mathrm{A}1}$ as listed and spins (a) $S = 1/2$ and (b) $S = 7/2$, obtained using Eq. (46) and the data in Figs. 5 and 6.

A. Anisotropic paramagnetic susceptibility with a uniaxial anisotropy field along the z axis

1. $\mathbf{H} \perp z$

Here, we consider a uniaxial anisotropy field $\mathbf{H}_{\mathrm{A}i}$ along the z axis as in Eq. (23a) and Fig. 1 with the induced moments in the PM state with $T \geqslant T_{\mathrm{N}}$ aligned perpendicular to the z axis due to an infinitesimal $\mathbf{H}$ applied in the xy plane. According to Eqs. (24) with $\theta_i = 90°$, the torque of $\mathbf{H}_{\mathrm{A}i}$ on $\vec{\mu}_i$ is zero. Hence the anisotropy field has no influence on $\mu_\perp$, where the $\hat{\perp}$ direction is perpendicular to the easy axis or plane for AFM ordering. Therefore the low-field susceptibility $\chi_\perp$ follows the Curie-Weiss law given by Eq. (A23b) for exchange interactions alone as

$$\chi_{\perp\mathrm{PM}}(T \geqslant T_{\mathrm{N}}) \equiv \chi_{xy}(T \geqslant T_{\mathrm{N}}) = \frac{C_1}{T - \theta_{\mathrm{p}J}}. \quad (48\mathrm{a})$$

The xy-plane susceptibility at T_{N} is thus

$$\chi_{\perp\mathrm{PM}}(T_{\mathrm{N}}) = \frac{C_1}{T_{\mathrm{N}} - \theta_{\mathrm{p}J}} = \frac{C_1}{T_{\mathrm{N}J} + T_{\mathrm{A}1} - \theta_{\mathrm{p}J}}, \quad (48\mathrm{b})$$

where we used Eq. (36) for T_{N} to obtain the second equality. The presence of the infinitesimal $H_\perp$ does not measurably affect T_{N}. The reduced susceptibilities defined in Eqs. (3) are

$$\bar{\chi}_{\perp\mathrm{PM}}(T \geqslant T_{\mathrm{N}}) \equiv \frac{\chi_{\perp\mathrm{PM}}T_{\mathrm{N}J}}{C_1} = \frac{1}{t - f_J} = \frac{1}{t_{\mathrm{A}}(1 + h_{\mathrm{A}1}) - f_J}, \quad (49\mathrm{a})$$

$$\bar{\chi}_{\perp\mathrm{PM}}(T = T_{\mathrm{N}}) = \frac{1}{1 + h_{\mathrm{A}1} - f_J}, \quad (49\mathrm{b})$$

$$\chi^*_{\perp\mathrm{PM}}(T \geqslant T_{\mathrm{N}}) \equiv \frac{\bar{\mu}_\perp}{h_\perp} = \left(\frac{S+1}{3}\right)\bar{\chi}_{\perp\mathrm{PM}}(T \geqslant T_{\mathrm{N}})$$

$$= \frac{S+1}{3(t - f_J)} = \frac{S+1}{3[t_{\mathrm{A}}(1 + h_{\mathrm{A}1}) - f_J]}, \quad (49\mathrm{c})$$

$$\chi^*_{\perp\mathrm{PM}}(T = T_{\mathrm{N}}) = \frac{S+1}{3(1 + h_{\mathrm{A}1} - f_J)}. \quad (49\mathrm{d})$$

2. $\mathbf{H} \parallel z$

If $\mathbf{H}$ is along the z axis, then an anisotropy field in the direction of $\mathbf{H}$ and of the induced moment is present with magnitude $H_{\mathrm{A}0}$ given by Eq. (31a). The normalized induced moment in the z direction ($\bar{\mu}_\parallel$) is given by Eqs. (A10), (A21b), (31a), and (1d) as

$$\bar{\mu}_{\parallel\mathrm{PM}} = B_S\left[\frac{g\mu_{\mathrm{B}}}{k_{\mathrm{B}}T}(H_{\mathrm{exch}} + H_{\mathrm{A}0} + H_z)\right]$$

$$= B_S\left[\frac{3}{S+1}(\theta_{\mathrm{p}J} + T_{\mathrm{A}1})\frac{\bar{\mu}_\parallel}{T} + \frac{g\mu_{\mathrm{B}}H_z}{k_{\mathrm{B}}T}\right]. \quad (50)$$

Using the first-order term in the Taylor series expansion of the Brillouin function in Eq. (A11b) one obtains the Curie-Weiss law

$$\chi_{\parallel\mathrm{PM}}(T \geqslant T_{\mathrm{N}}) = \frac{\mu_\parallel}{H_z} = \frac{C_1}{T - \theta_{\mathrm{p}}}, \quad (51\mathrm{a})$$

$$\chi_{\parallel\mathrm{PM}}(T_{\mathrm{N}}) = \frac{C_1}{T_{\mathrm{N}} - \theta_{\mathrm{p}}} \quad (51\mathrm{b})$$

$$= \frac{C_1}{T_{\mathrm{N}J}(1 + h_{\mathrm{A}1}) - \theta_{\mathrm{p}}}, \quad (51\mathrm{c})$$

where the Weiss temperature in the presence of the anisotropy is

$$\theta_{\mathrm{p}} = \theta_{\mathrm{p}J} + T_{\mathrm{A}1} = \theta_{\mathrm{p}J} + \theta_{\mathrm{p}A} = \theta_{\mathrm{p}J} + h_{\mathrm{A}1}T_{\mathrm{N}J}, \quad (51\mathrm{d})$$

$$\theta_{\mathrm{p}A} = T_{\mathrm{A}1} = h_{\mathrm{A}1}T_{\mathrm{N}J}. \quad (51\mathrm{e})$$

Equations (51) yield the reduced forms (3) as

$$\bar{\chi}_{\parallel\mathrm{PM}}(T \geqslant T_{\mathrm{N}}) = \frac{1}{(1 + h_{\mathrm{A}1})t_{\mathrm{A}} - f_J - h_{\mathrm{A}1}}, \quad (52\mathrm{a})$$

$$\bar{\chi}_{\parallel\mathrm{PM}}(T = T_{\mathrm{N}}) = \frac{1}{1 - f_J}, \quad (52\mathrm{b})$$

$$\chi^*_{\parallel\mathrm{PM}}(T \geqslant T_{\mathrm{N}}) = \frac{S+1}{3[(1 + h_{\mathrm{A}1})t_{\mathrm{A}} - f_J - h_{\mathrm{A}1}]}, \quad (52\mathrm{c})$$

$$\chi^*_{\parallel\mathrm{PM}}(T = T_{\mathrm{N}}) = \frac{S+1}{3(1 - f_J)}. \quad (52\mathrm{d})$$

Thus the Weiss temperatures from the exchange interactions and from the anisotropy are additive. This additivity also occurs for anisotropy arising from the magnetic dipole interaction

[3] and from the uniaxial DS_z^2 single-ion anisotropy at small D [4]. From Eqs. (51a) and (51d), one sees that the z-axis anisotropy field in the direction of **H** increases $\chi_{\parallel PM}$ at fixed T, as expected since the anisotropy field increases the magnitude of the local magnetic induction seen by each induced moment.

In addition, one finds that T_N in Eq. (36) and θ_p in Eq. (51d) for **H** directed along the z axis are both shifted towards positive values by the same amount due to the anisotropy field, and therefore

$$T_N - \theta_p = T_{NJ} - \theta_{pJ} \quad (\mathbf{H} \parallel \text{easy axis}). \quad (53)$$

By comparing Eqs. (48a) and (51a), the Weiss temperatures are seen to be different for $\chi_{\perp PM}$ and $\chi_{\parallel PM}$ and hence Eq. (53) applies for $\mathbf{H} \parallel z$ but not for $\mathbf{H} \perp z$. From the definition for f_J in Eq. (A7) together with Eq. (53), Eq. (51b) can alternatively be written as

$$\chi_{\parallel}(T_N) = \frac{C_1}{T_{NJ} - \theta_{pJ}} = \frac{C_1}{T_{NJ}(1 - f_J)}, \quad (54)$$

as is also apparent from Eq. (52b).

Since $T_N > T_{NJ}$, one sees by comparison of Eqs. (49b) and (52b) that $\chi_{\parallel}(T_N) > \chi_{\perp}(T_N)$ if the g values for fields in the two directions are the same.

B. Anisotropic paramagnetic susceptibility with XY planar anisotropy

If the anisotropy field is in the xy plane as in Fig. 2, one cannot identify a unique easy-axis direction. Hence we specify the anisotropic susceptibilities as χ_z and χ_{xy} instead of $\chi_{\perp}$ and $\chi_{\parallel}$, respectively. In the presence of an applied field in some direction in the xy plane, the induced moments in the PM state are aligned in the same direction.

Following the same steps as in the previous section, we find that $\chi_z(T \geqslant T_N)$ is the same as $\chi_{\perp}(T \geqslant T_N)$ in Eqs. (48), i.e.,

$$\chi_z(T \geqslant T_N) = \frac{C_1}{T - \theta_{pJ}}, \quad (55a)$$

$$\chi_z(T_N) = \frac{C_1}{T_N - \theta_{pJ}} = \frac{C_1}{T_{NJ} + T_{A1} - \theta_{pJ}}, \quad (55b)$$

where T_{A1} is defined in Eq. (1d).

Similarly, $\chi_{xy}(T \geqslant T_N)$ is the same as $\chi_{\parallel}(T \geqslant T_N)$ in Eq. (51a):

$$\chi_{xy}(T \geqslant T_N) = \frac{C_1}{T - \theta_p} = \frac{C_1}{T - T_{A1} - \theta_{pJ}}, \quad (55c)$$

Therefore at the Néel temperature, using Eq. (53) one obtains

$$\chi_{xy}(T_N) = \frac{C_1}{T_N - \theta_p} = \frac{C_1}{T_{NJ} - \theta_{pJ}}. \quad (56)$$

Thus in the paramagnetic state with $T \geqslant T_N$, if one has z-axis uniaxial anisotropy then $\chi_z > \chi_{xy}$, whereas for xy planar anisotropy one has $\chi_{xy} > \chi_z$. These relationships are expected, since a uniaxial anisotropy field helps to align the moments along the z axis, whereas an xy planar anisotropy field helps to align the moments in the xy plane.
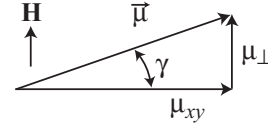

FIG. 8. Figure showing the influence of an infinitesimal magnetic field **H** along the $\perp$ axis on each spin in the xy plane. The **H** induces a tilting of each ordered magnetic moment $\vec{\mu}$ towards the magnetic field direction by an infinitesimal angle γ, which results in an induced $\perp$-axis component $\mu_{\perp}$ of $\vec{\mu}$. The angle γ in the figure is greatly exaggerated for clarity. To first order in γ and H, the magnitude of the ordered moment is unaffected by the presence of **H**.

VI. ANISOTROPIC MAGNETIC SUSCEPTIBILITY OF THE ANTIFERROMAGNETIC PHASE

A. Perpendicular susceptibility

To calculate $\chi_{\perp AFM}(T \leqslant T_N)$ in the presence of $\mathbf{H}_A$, we assume here the presence of a planar XY anisotropy as in Fig. 2 with the ordered moments aligned in the xy plane for $H = 0$. The expression for $\chi_{\perp AFM}$ in Eq. (61) below is valid for both collinear and planar noncollinear AFM structures. We calculate the infinitesimal angle γ in Fig. 8 for which the total torque on a representative moment $\vec{\mu}_i$ is zero, and from that $\chi_{\perp AFM}(T \leqslant T_N)$ is obtained.

From Fig. 8, one finds that the ordered moment magnitude μ_0 in $H_{\perp} = 0$ does not change to first order in $H_{\perp}$ and the radian angle γ. Thus using spherical coordinates, the magnetic moment $\vec{\mu}_i$ to first order in γ is

$$\vec{\mu}_i = \mu_0(\cos\phi_i \,\hat{\mathbf{i}} + \sin\phi_i \,\hat{\mathbf{j}} + \gamma \,\hat{\perp}), \quad (57)$$

where ϕ_i is the angle between $\vec{\mu}_i$ and the positive x axis in $H = 0$. The torque contribution due to the exchange field is obtained writing $\theta = \frac{\pi}{2} - \gamma$ and thus $\sin\theta\cos\theta = \gamma$ in Eq. (A28) and then using Eqs. (A1b) and (1b) yield

$$\vec{\mu}_i \times \mathbf{H}_{\text{exch}\,i} = -\frac{\gamma\mu_0^2}{C_1}(\sin\phi_i \,\hat{\mathbf{i}} - \cos\phi_i \,\hat{\mathbf{j}})(T_{NJ} - \theta_{pJ})$$

$$= -\frac{\gamma\mu_0^2}{\chi_{\perp J}}(\sin\phi_i \,\hat{\mathbf{i}} - \cos\phi_i \,\hat{\mathbf{j}}), \quad (58)$$

where Eq. (A33b) was used to obtain the second equality. The contribution of the applied magnetic field to the torque to first order in $H_{\perp}$ is

$$\vec{\mu}_i \times \mathbf{H} = \mu_0 H_{\perp}(\sin\phi_i \,\hat{\mathbf{i}} - \cos\phi_i \,\hat{\mathbf{j}}). \quad (59)$$

The torque on $\vec{\mu}_i$ exerted by $\mathbf{H}_{Ai}$ to first order in $\gamma = 90° - \theta$ is given by Eq. (28) as

$$\vec{\mu}_i \times \mathbf{H}_{Ai} = -\gamma\mu_0 H_{A0}(\sin\phi_i \,\hat{\mathbf{i}} - \cos\phi_i \,\hat{\mathbf{j}}). \quad (60)$$

Then setting the sum of the three torques to zero, solving for $\gamma\mu_0 = \mu_{\perp}$ and using Eqs. (A1b), (A23c), (31a), and (36), one obtains the perpendicular susceptibility $\chi_{\perp AFM} = \mu_{\perp}/H_{\perp}$ in the AFM state as

$$\chi_{\perp AFM}(T \leqslant T_N) = \frac{C_1}{T_N - \theta_{pJ}} = \frac{C_1}{T_{NJ} + T_{A1} - \theta_{pJ}}, \quad (61)$$

which agrees with Eq. (48b) for the PM state at T_N. Thus $\chi_{\perp AFM}$ is independent of T below T_N with the value $\chi_{\perp PM}(T_N)$. From Eq. (61), one sees that $\chi_{\perp AFM}(T \leqslant T_N)$ is reduced compared

to the pure Heisenberg case in which T_{A1} would be zero, since that anisotropy field resists the tilting of the moments out of the xy plane by $H_\perp$. The same T independence of $\chi_\perp$ for $T \leqslant T_N$ was found for AFM ordering in the presence of magnetic dipole interactions with or without the presence of exchange interactions [3]. In contrast, when quantum uniaxial DS_z^2 anisotropy is present in a Heisenberg spin system, $\chi_\perp$ decreases with decreasing T below T_N [4].

B. Parallel susceptibility of collinear z-axis antiferromagnets below T_N

In this section, we calculate $\chi_\parallel(T \leqslant T_N)$ in the presence of a uniaxial anisotropy field along the easy z axis as in Fig. 1. Here we follow the approach of Ref. [4] in which the influence of quantum DS_z^2 anisotropy was studied instead of the present generic classical anisotropy. In the collinear ordered state, we consider two sublattices. Sublattice $\vec{\mu}_i = \mu_i \hat{\mathbf{k}}$ is taken to point in the direction of the field H_z and sublattice $\vec{\mu}_j = -\mu_j \hat{\mathbf{k}}$ to point in the opposite direction in zero field.

The exchange field seen by a spin on sublattice i is [4]

$$\mathbf{H}_{\text{exch}i} = \frac{3k_B T_{NJ}}{2g^2\mu_B^2 S(S+1)}[\vec{\mu}_i(1+f_J) - \vec{\mu}_j(1-f_J)]. \quad (62a)$$

If $H_z = 0$, one has $\vec{\mu}_j = -\vec{\mu}_i$ and $\mu_i = \mu_0$ for all spins, yielding

$$\mathbf{H}_{\text{exch}i0} = \frac{3k_B T_{NJ} \bar{\mu}_0}{g\mu_B(S+1)} \quad (62b)$$

and

$$y_{\text{exch}0} \equiv \frac{g\mu_B H_{\text{exch}i}}{k_B T} = \frac{3}{(S+1)t}\bar{\mu}_0. \quad (62c)$$

The anisotropy field seen by $\vec{\mu}_i$ in the z direction is

$$H_{A0iz} = \frac{3H_{A1}}{g\mu_B S(S+1)}\mu_{iz} = \frac{3H_{A1}}{S+1}\bar{\mu}_0, \quad (63a)$$

yielding

$$y_{A0} \equiv \frac{g\mu_B H_{A0i}}{k_B T} = \frac{3h_{A1}}{(S+1)t}\bar{\mu}_0. \quad (63b)$$

Thus the parameter y_0 is

$$y_0 = y_{\text{exch}0} + y_{A0} = \frac{3}{(S+1)t}(1+h_{A1})\bar{\mu}_0 \quad (64)$$

However, $t_A = t/(1+h_{A1})$, so one can also write

$$y_0 = \frac{3}{(S+1)t_A}\bar{\mu}_0. \quad (65)$$

Then the reduced ordered moment in zero field $\bar{\mu}_0$ is obtained at each t or t_A by solving

$$\bar{\mu}_0 = B_S(y_0). \quad (66)$$

When a field H_z is present, one has

$$y_H \equiv \frac{g\mu_B H_z}{k_B T} = \frac{h_z}{t}. \quad (67)$$

If H_z is infinitesimal as needed to calculate $\chi_\parallel$, one must go back to Eq. (62a) to obtain the infinitesimal change in the

exchange field. In this case one has $d\vec{\mu}_j = d\vec{\mu}_i$, and Eq. (62a) then gives

$$dH_{\text{exch}iz} = \frac{3k_B T_{NJ} f_J}{g\mu_B(S+1)}d\bar{\mu}_{iz}. \quad (68)$$

Then one obtains

$$dy_{\text{exch}i} = \frac{3f_J}{(S+1)t}d\bar{\mu}_{iz}. \quad (69)$$

From Eqs. (63b) and (67), one also has

$$dy_{Ai} = \frac{3h_{A1}}{(S+1)t}d\bar{\mu}_{iz}, \quad dy_H = \frac{dh_z}{t}. \quad (70)$$

The sum of the three changes in dy_i is

$$dy_i = \frac{3}{(S+1)t}(f_J + h_{A1})d\bar{\mu}_{iz} + \frac{dh_z}{t}. \quad (71)$$

The change $d\bar{\mu}_{iz}$ in the reduced moment on sublattice i is governed by the Brillouin function, i.e.,

$$d\bar{\mu}_{iz} = B_S'(y_0)dy_i. \quad (72)$$

Substituting dy_i from Eq. (71) into (72) and solving for $d\bar{\mu}_{iz}$ gives the reduced z-axis susceptibility per spin according to Eq. (3b) as

$$\bar{\chi}_{\parallel \text{AFM}}(t) = \frac{1}{\tau^* - (f_J + h_{A1})}, \quad (73)$$

where

$$\tau^*(t) = \frac{(S+1)t}{3B_S'(y_0)}. \quad (74)$$

If $h_{A1} = 0$, one recovers the $\bar{\chi}_\parallel$ expression for the pure Heisenberg case given in Refs. [5,6].

Using Eq. (1j), one can also calculate $\bar{\chi}_{\parallel \text{AFM}}$ in Eq. (73) versus $t_A = T/T_N$ instead of versus $t = T/T_{NJ}$ from

$$\bar{\chi}_{\parallel \text{AFM}}(t_A) = \frac{1}{\tau_A^* - (f_J + h_{A1})}, \quad (75)$$

where

$$\tau_A^*(t_A) = \frac{(S+1)t_A(1+h_{A1})}{3B_S'(y_0)}. \quad (76)$$

We find

$$\bar{\chi}_\parallel(t_A = 1) = \frac{1}{1 - f_J}, \quad (77)$$

so from Eq. (75), one obtains

$$\frac{\bar{\chi}_{\parallel \text{AFM}}(t_A)}{\bar{\chi}_\parallel(t_A = 1)} = \frac{1 - f_J}{\tau_A^*(t_A) - (f_J + h_{A1})}, \quad (78)$$

where $\tau_A^*(t_A = 1) = 1 + h_{A1}$ and hence the ratio in Eq. (78) at $t_A = 1$ is equal to unity as required.

C. Summary: Anisotropic susceptibility of collinear z-axis antiferromagnets in reduced parameters

Using the definition of the reduced susceptibility in Eq. (3b), together with Eqs. (1), (48a), (51), and (75), the anisotropic reduced susceptibilities versus $t_A \equiv T/T_N$ for the
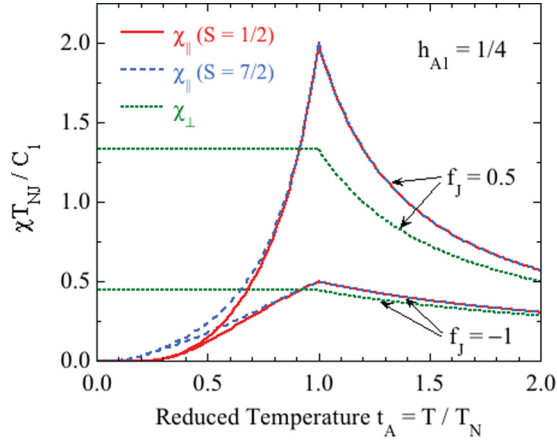
FIG. 9. Anisotropic reduced magnetic susceptibilities $\bar{\chi}_\parallel$ and $\bar{\chi}_\perp$ vs reduced temperature t_A for two different S values, two different f_J values and for a fixed anisotropy parameter $h_{A1} = 1/4$, according to Eqs. (79).

PM and AFM phases are summarized as

$$\bar{\chi}_\perp = \begin{cases} \frac{1}{1+h_{A1}-f_J} & (\text{AFM}, \quad t_A \leqslant 1) \\ \frac{1}{(1+h_{A1})t_A-f_J} & (\text{PM}, \quad t_A \geqslant 1), \end{cases} \tag{79a}$$

$$\bar{\chi}_\parallel = \begin{cases} \frac{1}{\tau_A^*-(f_J+h_{A1})} & (\text{AFM}, \quad t_A \leqslant 1) \\ \frac{1}{(1+h_{A1})t_A-(f_J+h_{A1})} & (\text{PM}, \quad t_A \geqslant 1), \end{cases} \tag{79b}$$

$$\frac{\chi_\parallel(T_N)}{\chi_\perp(T_N)} = 1 + \frac{h_{A1}}{1-f_J}, \tag{79c}$$

where

$$\tau_A^* = \frac{(S+1)(1+h_{A1})t_A}{3B_S'(y_0)}, \tag{79d}$$

$$y_0 = \frac{3\bar{\mu}_0}{(S+1)t_A}, \tag{79e}$$

$$\bar{\mu}_0 = B_S(y_0). \tag{79f}$$

In these reduced susceptibility units, $\bar{\chi}_\perp(t_A)$ is independent of S for all t_A, and $\bar{\chi}_{\parallel \text{AFM}}(t_A < 1)$ is dependent on S since τ_A^* depends on S. These features are illustrated in plots of $\bar{\chi}_\perp(t_A)$ and $\bar{\chi}_\parallel(t_A)$ in Fig. 9 for $S = 1/2$ and $7/2$ and for $f_J = -1$ and $f_J = 0.5$, all with a fixed value of the reduced anisotropy parameter $h_{A1} = 1/4$. An important feature of the temperature dependencies is that $\chi_{\parallel \text{PM}} > \chi_{\perp \text{PM}}$ at $t_A \geqslant 1$, but a crossover occurs where $\chi_{\parallel \text{AFM}} < \chi_{\perp \text{AFM}}$ at lower t_A. From Eq. (79c), as f_J increases algebraically towards its upper limit of unity at a fixed value of h_{A1}, the ratio $\chi_\parallel(T_N)/\chi_\perp(T_N)$ increases, as observed in Fig. 9.

VII. HIGH-FIELD PERPENDICULAR MAGNETIZATION OF THE ANTIFERROMAGNETIC AND PARAMAGNETIC PHASES

In this section, the "perpendicular" direction $\hat{\perp}$ of an applied field **H** refers to a direction perpendicular to the easy axis (for a collinear AFM) or plane (for a planar noncollinear AFM) of the anisotropy field **H**$_A$.
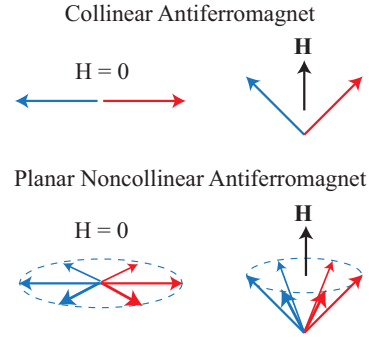

FIG. 10. Influence on the generic magnetic structure due to a high magnetic field applied perpendicular to the easy axis of a collinear antiferromagnet (AFM) (top panel) and to the easy plane of a planar noncollinear AFM (bottom panel). Hodographs of the zero-field magnetic moment vectors are shown on the left. In high fields as shown on the right, the AFM structures become canted towards the field. The ordered moments of the collinear AFM are now coplanar, whereas those of the noncollinear AFM now lie on the surface of a cone with the axis of the cone along the magnetic field axis as shown. At a sufficiently high field $H = H_{\text{c}\perp\text{AFM}}$ given by Eq. (83), the moments in either case become parallel to each other and a second-order transition from the canted AFM to the PM state occurs.

A. Antiferromagnetic phase

The $\chi_{\perp\text{AFM}}(T \leqslant T_N)$ for fields $H_\perp \to 0$ was calculated in Sec. VI A. Here we determine the magnetization in high perpendicular magnetic fields for both collinear and planar noncollinear AFMs at fields below the perpendicular critical field $H_{\text{c}\perp\text{AFM}} \equiv \mu_0(H = 0, T \leqslant T_N)/\chi_{\perp\text{AFM}}$. We find that $\mu_{\perp\text{AFM}}$ is proportional to $H_\perp$ up to $H_{\text{c}\perp\text{AFM}}$ with the same T-independent slope $\chi_{\perp\text{AFM}}$ as for $H_\perp \to 0$ in Eq. (48b), and that the ordered moment $\mu_0(T)$ is independent of $H_\perp$ in the AFM phase.

For collinear AFMs at high fields, the canted moments lie in a plane defined by the initial parallel axis and the applied field as shown in the top panel of Fig. 10. In contrast, for a planar noncollinear structure at $H = 0$, in large fields the moments in a hodograph lie on the surface of a cone with the tails of the moment vectors at the apex and the axis of the cone along the applied field axis as shown in the bottom panel of Fig. 10. We can therefore treat both the collinear and planar noncollinear cases simultaneously, where the anisotropy field is in the plane perpendicular to the applied field as shown in Fig. 2.

From Fig. 2, the torque on $\vec{\mu}_i$ due to a perpendicular field **H** in Eq. (59) is the same as that due to **H**$_{Ai}$ in Eq. (60) except for the scalar prefactor and the opposite direction. Therefore comparing Eqs. (59) and (60) one can include the influence of **H**$_{Ai}$ on the value of the induced moment $\mu_\perp$ by setting $H = H_\perp - H_{A0}\cos\theta$ in the expression setting the net torque equal to zero in the absence of H_{A0} [4]. Then using the definitions $\mu_\perp = \mu\cos\theta$, $\bar{\mu} = \mu/(gS\mu_B)$, and H_{A0} in terms of H_{A1} in Eq. (31a) gives

$$\mu_\perp = \frac{1}{T_{NJ}-\theta_{pJ}}\left[C_1 H_\perp - C_1 \frac{3H_{A1}\mu_\perp}{gS(S+1)\mu_B}\right], \tag{80}$$

where the single-spin Curie constant C_1 is given in Eq. (A1b). Solving for $\mu_\perp$ gives

$$\mu_\perp = \frac{C_1 H_\perp}{T_N - \theta_{pJ}},\qquad(81)$$

where to obtain this equation we used the expression for T_N in Eq. (36) and the definition of T_{A1} in Eq. (1d). Hence

$$\mu_\perp(T \leqslant T_N) = \chi_{\perp AFM} H_\perp \quad (\mu_\perp \leqslant \mu_0),$$
$$\chi_{\perp AFM} = \frac{C_1}{T_N - \theta_{pJ}},\qquad(82)$$

where $\chi_{\perp AFM}$ is seen to be the same as the zero-field perpendicular susceptibility already obtained in Eq. (61), which in turn is the same as $\chi_{\perp PM}(T_N)$ in Eq. (55b).

This independence of $\mu_\perp/H_\perp$ with respect to $H_\perp$ in the AFM phase indicates that the magnitude μ of the moments is independent $H_\perp$ and in particular is equal to the zero-field value, i.e., $\mu(T) = \mu_0(T)$. Thus the T-dependent critical field $H_{c\perp AFM}$ is given by the field at which $\mu_\perp = \mu_0(T)$, i.e.,

$$H_{c\perp AFM}(T \leqslant T_N) = \frac{\mu_0(T)}{\chi_{\perp AFM}}.\qquad(83)$$

Using Eq. (3b) together with the variable definitions in Eqs. (1), Eq. (82) gives

$$\bar{\chi}_{\perp AFM} = \frac{1}{1 + h_{A1} - f_J},\qquad(84)$$

which reproduces the first entry in Eqs. (79a). Using Eq. (3b), one obtains

$$\chi^*_{\perp AFM} = \frac{S+1}{3}\bar{\chi}_{\perp AFM} = \frac{S+1}{3(1 + h_{A1} - f_j)}.\qquad(85)$$

Then using the definition $\bar{\mu}_\perp = \chi^*_{\perp AFM} h_\perp$ from Eq. (3a) and setting $\bar{\mu}_\perp = \bar{\mu}_0$ yields the reduced critical field

$$h_{c\perp AFM}(t_A) = \left[\frac{3\bar{\mu}_0(t_A)}{S+1}\right](1 + h_{A1} - f_J),\qquad(86)$$

where $\bar{\mu}_0(t_A)$ is found by solving Eqs. (37) and $\bar{\mu}_0(t_A \geqslant 1) = 0$. The dependence of $h_{c\perp AFM}$ on t_A is thus the same as that of $\bar{\mu}_0$ on t_A shown above in Fig. 4. For given values of t_A, h_{A1}, and f_J, $h_{c\perp AFM}(t_A = 0)$ decreases with increasing spin S. At $t_A = 0$ one has $\bar{\mu}_0 = 1$. Then Eq. (86) gives

$$h_{c\perp AFM}(t_A = 0) = \frac{3(1 + h_{A1} - f_J)}{S+1}.\qquad(87)$$

B. Paramagnetic phase

The paramagnetic (PM) phase can be reached from the AFM phase by increasing the field to $H_\perp > H_{c\perp AFM}$ at $T < T_N$ or by increasing the temperature to $T > T_N$ at $H_\perp = 0$. In either case, the thermal-average moment induced by the applied magnetic field **H** is in the direction of **H** if **H** is in a principal axis direction as considered in this paper. In this section, both **H** and the field-induced PM moment $\mu_\perp$ are in the same $\hat{\perp}$ direction that is perpendicular to the easy axis of a collinear AFM or to the easy plane of a planar noncollinear AFM. Then according to Eq. (23a) and Fig. 1 or Eq. (27a) and Fig. 2, respectively, the anisotropy field H_A is zero in either

case. Therefore Eq. (A22) and the definitions of the reduced variables in Eq. (1) immediately give

$$\bar{\mu}_{\perp PM} = B_S\left[\frac{3f_J T_{NJ}\bar{\mu}_{\perp PM}}{(S+1)T} + \frac{g\mu_B H_\perp}{k_B T}\right]\qquad(88)$$

$$= B_S\left[\frac{3f_J\bar{\mu}_{\perp PM}}{(S+1)t} + \frac{h_\perp}{t}\right].\qquad(89)$$

Even though $H_A = 0$ for the perpendicular moment orientation, one still has $T_N > T_{NJ}$ if $h_{A1} > 0$. Therefore to compare with experimental data we reexpress the reduced temperature as $t \to (1 + h_{A1})t_A$ using Eq. (1j), yielding

$$\bar{\mu}_{\perp PM} = B_S\left\{\frac{1}{1 + h_{A1}}\left[\frac{3f_J\bar{\mu}_{\perp PM}}{(S+1)t_A} + \frac{h_\perp}{t_A}\right]\right\}.\qquad(90)$$

The $\bar{\mu}_{\perp PM}$ for given values of h_{A1}, f_J and t_A is determined by numerically solving Eq. (90).

The results for the two cases $h_\perp \leqslant h_{c\perp AFM}(t_A)$ and $h_\perp \geqslant h_{c\perp AFM}(t_A)$ are summarized respectively as

$$\bar{\mu}_\perp(h_\perp)$$
$$= \begin{cases} \frac{(S+1)h_\perp}{3(1 + h_{A1} - f_J)} & (\text{AFM},\ h_\perp \leqslant h_{c\perp AFM}) \\ B_S\left\{\frac{1}{1 + h_{A1}}\left[\frac{3f_J\bar{\mu}_\perp}{(S+1)t_A} + \frac{h_\perp}{t_A}\right]\right\} & (\text{PM},\ h_\perp \geqslant h_{c\perp AFM}) \end{cases},$$
$$(91)$$

where $h_{c\perp AFM}$ is given in Eq. (86). Using Eqs. (91), the $\bar{\mu}_\perp$ versus $h_\perp$ curves for spin $S = 1/2$ and $7/2$ with $f_J = -1$ at four reduced temperatures and $h_{A1} = 0$ and $1/2$ are plotted in Fig. 11. A discontinuity in the slope of $\bar{\mu}_\perp$ versus $h_\perp$ is seen at $h_\perp = h_{c\perp AFM}$ for each reduced temperature t_A, reflecting a second-order transition from the canted AFM to the PM phase.

VIII. HIGH-FIELD PARALLEL MAGNETIZATION OF z-AXIS COLLINEAR ANTIFERROMAGNETS: PARAMAGNETIC AND SPIN-FLOP PHASES

A. Introduction

When a collinear AFM is placed in a magnetic field parallel to the easy axis (defined to be the z axis here), different T-dependent behaviors can occur. A first-order spin flop (SF) transition may occur from the AFM phase to a SF phase as shown in the top panel of Fig. 12, where the orientations of the ordered moments aligned along the z-axis flop with increasing field to an approximately perpendicular canted perpendicular orientation [12]. It is common to use the term "spin flop" to denote both the magnetic phase and the magnetic phase transition. Upon further increasing the field, a second-order spin flop to paramagnetic (PM) phase transition occurs in which all moments then point in the direction of the field.

The PM phase is sometimes called a "ferromagnetic phase" in the literature because the magnetic structure of the field-induced PM phase has ferromagnetic (FM) alignment of the field-induced moments. However, we reserve the term "ferromagnetic phase" for a ferromagnetic structure that is caused by the interactions between the moments in zero applied magnetic field, not by the field. Indeed, a thermodynamic transition from
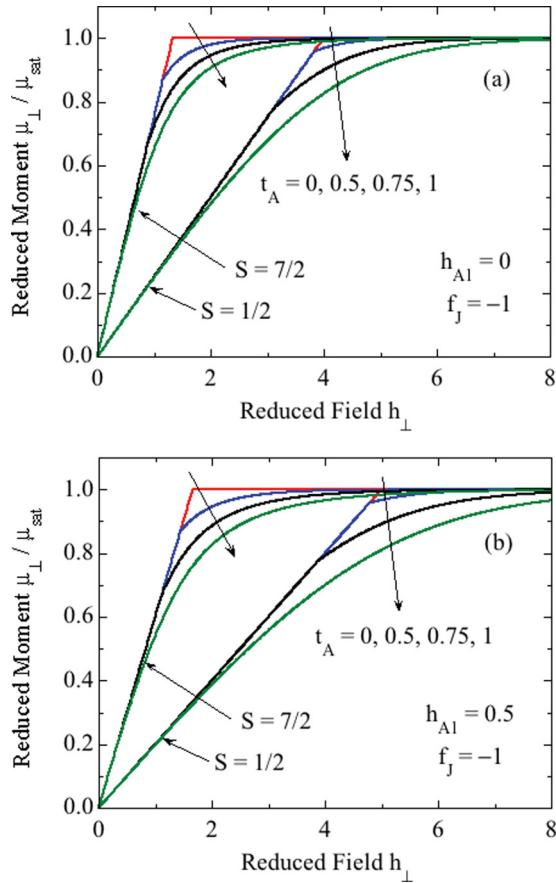
FIG. 11. Reduced perpendicular moment $\bar{\mu}_\perp \equiv \mu_\perp/\mu_{\rm sat}$ vs reduced perpendicular field $h_\perp$ for spins $S = 1/2$ and $S = 7/2$ at the reduced temperatures $t_{\rm A} = T/T_{\rm N}$ indicated for parameters $f_J = -1$ and reduced anisotropy fields (a) $h_{\rm A1} = 0$ and (b) $h_{\rm A1} = 1/2$, according to Eqs. (91). Discontinuities in slope at fields $h_{\rm c\perp}(T)$ are seen as the system undergoes second-order transitions from the canted AFM state to the PM state with increasing field. The reduced critical fields at $t_{\rm A} = 0$ for $h_{\rm A1} = 0$ are $h_{\rm c\perp AFM} = 4/3$ and 4 for $S = 7/2$ and $1/2$, respectively, and for $h_{\rm A1} = 1/2$ are $h_{\rm c\perp AFM} = 5/3$ and 5 for $S = 7/2$ and $1/2$, respectively. Both are in agreement with Eq. (86).

a PM phase to a FM phase cannot occur versus T in finite H because the FM order parameter (the net magnetization) is never nonzero in a finite H at a finite T.

A first-order spin-flip transition may occur with increasing field directly from the AFM phase to the PM phase if the anisotropy field along the z axis is sufficiently strong, as shown in the middle panel of Fig. 12. Within MFT, the magnitude and direction of the initially antiparallel moment can also vary smoothly with field, resulting eventually in a second-order AFM to PM transition as shown in the bottom panel of Fig. 12.

B. z-axis induced moment and free energy of the paramagnetic (PM) phase

In this section, we change notation for the PM phase from $\mu_\parallel$ to $\mu_{z{\rm PM}}$. The general high-field expression for the PM phase was already obtained in Eq. (50). Utilizing Eqs. (1), Eq. (50)
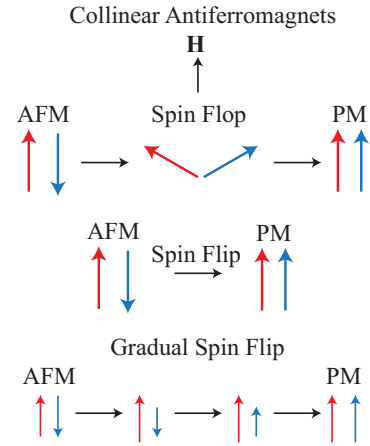

FIG. 12. Phase transitions that can potentially occur in collinear antiferromagnets (AFM) when a magnetic field **H** is applied along the easy axis. The magnitude H of the field increases from left to right. The top panel shows a first-order spin-flop (SF) transition that occurs from a collinear AFM structure to a SF phase at a SF field $H_{\rm SF}$, which is a canted AFM structure. At higher fields, the angle between the two sublattice magnetic moments goes continuously to zero, corresponding to a second-order transition from the SF phase to a paramagnetic (PM) phase at a critical field $H_{\rm cSF}$. Alternative scenarios with increasing H include either a first-order spin-flip transition directly from the AFM to the PM phase as shown in the middle panel, or a continuous evolution ("gradual spin flip") of the AFM phase into the PM phase via a second-order phase transition as illustrated in the bottom panel.

can be written in reduced variables as

$$\bar{\mu}_{z{\rm PM}} = B_S(y_{\rm PM}),$$
$$y_{\rm PM} = \frac{3(f_J + h_{\rm A1})}{(S+1)t}\bar{\mu}_{z{\rm PM}} + \frac{h_z}{t}$$
$$= \frac{1}{(1+h_{\rm A1})t_{\rm A}}\left[\frac{3(f_J + h_{\rm A1})}{S+1}\bar{\mu}_{z{\rm PM}} + h_z\right]. \quad (92)$$

When the reduced temperature is taken to be t, one can write

$$y_{\rm PM} = \frac{b_z}{t}, \quad (93)$$

where the reduced magnetic induction b_z seen by a representative spin is

$$b_z = \frac{3(f_J + h_{\rm A1})}{S+1}\bar{\mu}_{z{\rm PM}} + h_z. \quad (94)$$

Shown in Fig. 13(a) are plots of $\bar{\mu}_{z{\rm PM}}$ versus reduced field h_z obtained from Eqs. (92) for parameters $f_J = -1$ and $h_{\rm A1} = 1/2$, each for spins $S = 1/2$ and $7/2$, at reduced temperatures $t = T/T_{\rm NJ}$ as indicated. Perhaps unexpectedly, $\bar{\mu}_{z{\rm PM}}$ for $t \to 0$ is seen to be proportional to h_z from $h_z = 0$ to a critical field $h_{\rm cPM}$ at which $\bar{\mu}_{z{\rm PM}}$ saturates to the value of unity and continues to have that value at higher fields. The scale of the abscissa is reduced by about a factor of 3 for $S = 7/2$ compared to that for $S = 1/2$. However, the shapes of the plots for the two spin values are very similar for the same reduced temperature.
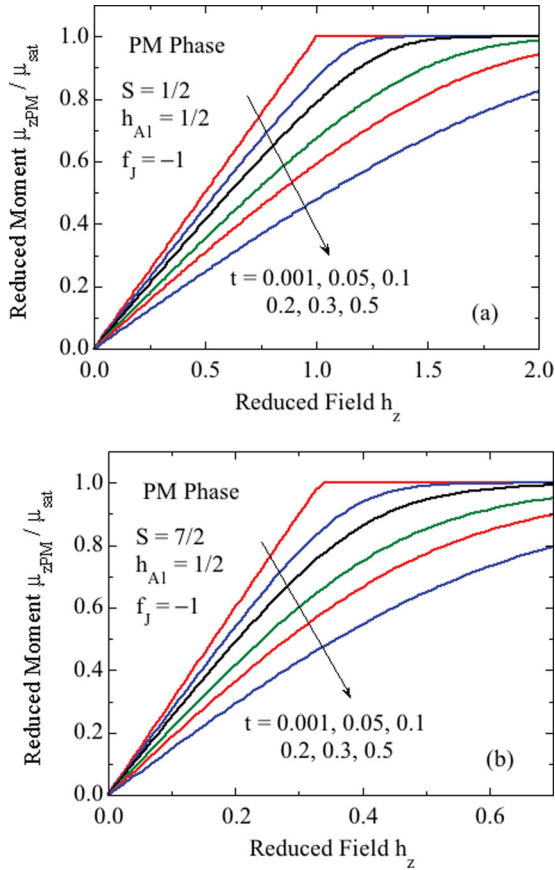
FIG. 13. Reduced z-axis moment $\mu_{z\mathrm{PM}}/\mu_{\mathrm{sat}}$ of the paramagnetic (PM) phase vs reduced field $h_z = g\mu_{\mathrm{B}}H_z/k_{\mathrm{B}}T_{\mathrm{N}J}$ for spins (a) $S = 1/2$ and (b) $S = 7/2$ at the indicated reduced temperatures $t = T/T_{\mathrm{N}J}$ and for $f_J = -1$ and $h_{\mathrm{A}1} = 1/2$, according to Eqs. (92).

In $h_z = 0$, one sees from Fig. 13 that $\bar{\mu}_{z\mathrm{PM}} = 0$, so Eq. (20a) gives the internal energy per spin as

$$\frac{U_{\mathrm{mag}}(h_z = 0, t)}{k_{\mathrm{B}}T_{\mathrm{N}J}} = 0. \tag{95}$$

Also, the PM phase in $h_z = 0$ is completely disordered at all temperatures, so the entropy per spin is

$$\frac{S_{\mathrm{mag}}(h_z = 0, t)}{k_{\mathrm{B}}} = \ln(2S + 1). \tag{96}$$

Thus the free energy in $h_z = 0$ is given by Eq. (20d) as

$$\frac{F_{\mathrm{mag}}(h_z = 0, t)}{k_{\mathrm{B}}T_{\mathrm{N}J}} = -t \ln(2S + 1). \tag{97}$$

Now including the field dependence using Eq. (20e) gives

$$\frac{F_{\mathrm{mag}}(h_z, t)}{k_{\mathrm{B}}T_{\mathrm{N}J}} = -t \ln(2S + 1) - S \int_0^{h_z} \bar{\mu}_z(h_z, t)dh_z. \tag{98}$$

The reduced free energy is plotted versus h_z for spins $S = 1/2$ and $S = 7/2$ in Fig. 14 with the same parameters as in Fig. 13, obtained using Eq. (98).
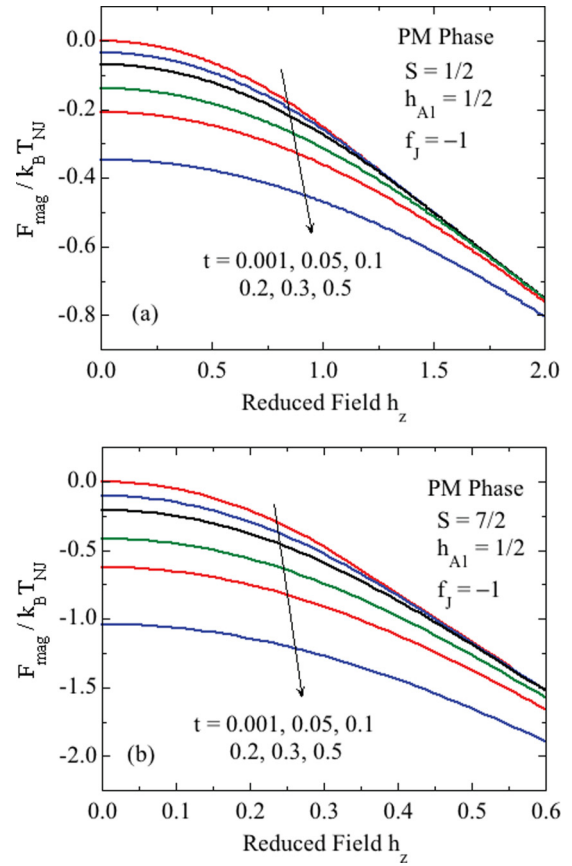

FIG. 14. Reduced free energy $F_{\mathrm{mag}}/k_{\mathrm{B}}T_{\mathrm{N}J}$ of the paramagnetic (PM) phase vs reduced field h_z for spins (a) $S = 1/2$ and (b) $S = 7/2$ at the indicated reduced temperatures t and for $f_J = -1$ and $h_{\mathrm{A}1} = 1/2$, obtained using Eq. (98) and the data in Fig. 13.

C. Spin-flop phase of collinear antiferromagnets

1. Ordered moment in zero field

The magnetic structure and magnetic field orientation in the spin-flop (SF) phase in the top panel of Fig. 12 with nonzero anisotropy field $\mathbf{H}_{\mathrm{A}}$ along the easy axis are the same as those used for calculation of the high-field perpendicular magnetization in the Appendix for the case of zero anisotropy field $H_{\mathrm{A}} = 0$. In that case we obtained Eq. (A38) in which the reduced ordered moment $\bar{\mu} \equiv \mu/\mu_{\mathrm{sat}}$ depends only on $t \equiv T/T_{\mathrm{N}J}$ and not on the applied field $H_\perp$ if $H_\perp \leqslant H_{\mathrm{c}\perp}$. Equation (A38) is identical to Eq. (A14) for determining $\bar{\mu}_0(t)$ for $H = H_{\mathrm{A}} = 0$. Similarly, in the spin-flop phase, $\mathbf{H}$ and $\mathbf{H}_{\mathrm{A}}$ are in the same direction perpendicular to the $H = 0$ AFM ordering plane and hence the ordered moment again cannot depend on H_z or H_{A} and is therefore given by the same Eqs. (A38) and (A14). We have confirmed this conclusion from detailed numerical exact-diagonalization calculations in Sec. VIII C 2b below. Thus Eq. (A38) in the case of the SF phase reads

$$\bar{\mu}_{\mathrm{SF}} = B_S\left[\frac{3\bar{\mu}_{\mathrm{SF}}}{(S+1)t}\right] \tag{99a}$$

$$= B_S\left[\frac{3\bar{\mu}_{\mathrm{SF}}}{(S+1)(1 + h_{\mathrm{A}1})t_{\mathrm{A}}}\right], \tag{99b}$$
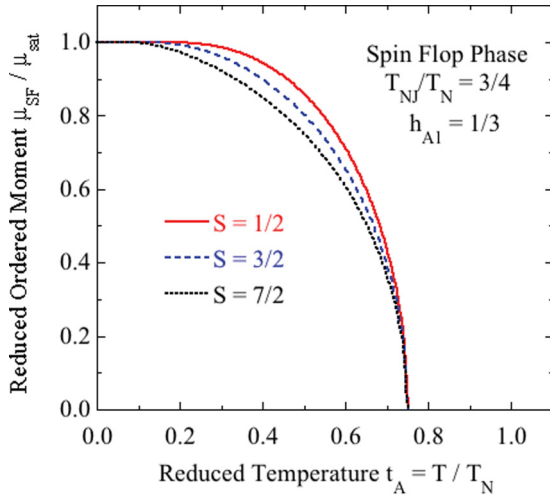
FIG. 15. Reduced ordered moment $\bar{\mu}_{\text{SF}} = \mu_{\text{SF}}/\mu_{\text{sat}}$ of the spin-flop phase vs reduced temperature t_A for spins $S = 1/2$, 3/2, and 7/2 with $h_{\text{A1}} = 1/3$, calculated from Eq. (99b). The ordered moment of the SF phase does not depend on f_J or on applied field for $h_z \leqslant h_{\text{cSF}}$.

where to obtain the second equality we used Eq. (1j). The ordered moment in the SF phase goes to zero at a temperature $T_{\text{N}J}$ below the Néel temperature T_{N}, as shown in Fig. 15 for spins $S = 1/2$, 3/2, and 7/2 with $h_{\text{A1}} = 1/3$ for which $T_{\text{N}J}/T_{\text{N}} = 3/4$ according to Eq. (1i). This feature is critically important to the construction of the phase diagrams in the h_z-t_A plane that are presented in Fig. 32 below.

The total derivative of $\bar{\mu}_{\text{SF}}$ with respect to reduced temperature t_A is obtained by substituting $t \to (1 + h_{\text{A1}})t_A$ from Eq. (1j) into Eq. (A15), yielding

$$\frac{d\bar{\mu}_{\text{SF}}}{dt_A} = -\frac{\bar{\mu}_{\text{SF}}}{t_A\left[\frac{(S+1)(1+h_{\text{A1}})t_A}{3B'_S(y_A)} - 1\right]}, \tag{100a}$$

where

$$y_A = \frac{3\bar{\mu}_{\text{SF}}}{(S+1)(1+h_{\text{A1}})t_A}, \tag{100b}$$

$\bar{\mu}_{\text{SF}}(t_A)$ is obtained by numerically solving Eq. (99b) and the $B_S(y_A)$ and $B'_S(y_A)$ functions are given in Eqs. (A11). For $h_{\text{A1}} = 0$, Eq. (100a) reduces to Eq. (A15) (with $t_A = t$), as required.

2. Magnetization versus z-axis field

The magnetic susceptibility $\chi_{z\text{SF}}$ along the easy z axis of the SF phase shown in the top panel of Fig. 12 is not the same as $\chi_{\perp}$ of the AFM phase in Eq. (61) obtained when the applied field is perpendicular to the easy axis or plane as in Fig. 10. The reason for this difference is that when the applied field is along the z axis in the SF phase, this field and the anisotropy field are in the same direction for all magnetic moments, whereas in the AFM case the anisotropy field lies within the xy plane and hence these two fields are perpendicular to each other. Thus the reduced critical field for the spin flop phase h_{cSF}, at which the ordered moments become parallel to the field with increasing field, is smaller than $h_{\text{c}\perp\text{AFM}}$ of the AFM phase in a perpendicular field in the presence of an anisotropy field.

a. Torque calculation. To calculate the z-axis susceptibility of the SF phase, we use a similar calculation as in Sec. VII A, but with the replacement

$$H_{\perp} \to H_z + H_A = H_z + \frac{3H_{\text{A1}}\bar{\mu}_{\text{SF}}\cos\theta}{S+1}, \tag{101}$$

where we have used Eqs. (23a) and (31a) to express H_A in terms of H_{A1} and have set $\theta_i \to \theta$ and $\bar{\mu}_i, \bar{\mu} \to \bar{\mu}_{\text{SF}}$. Inserting this expression into Eq. (A30) gives

$$\frac{3k_{\text{B}}}{S+1}(T_{\text{N}J} - \theta_{\text{p}J})\bar{\mu}_{\text{SF}}\cos\theta = g\mu_{\text{B}}H_z + \frac{3g\mu_{\text{B}}H_{\text{A1}}\bar{\mu}_{\text{SF}}\cos\theta}{S+1}. \tag{102}$$

Then solving for $\bar{\mu}_{z\text{SF}} = \bar{\mu}_{\text{SF}}\cos\theta$ gives

$$\bar{\mu}_{z\text{SF}} = \frac{(S+1)h_z}{3(1 - f_J - h_{\text{A1}})}, \tag{103a}$$

$$\text{or } h_z = \frac{3(1 - f_J - h_{\text{A1}})}{S+1}\bar{\mu}_{z\text{SF}}, \tag{103b}$$

where we used $T_{\text{N}J} - \theta_{\text{p}J} = T_{\text{N}J}(1 - f_J)$, the reduced anisotropy field h_{A1} was defined in Eq. (1i), and similarly for the reduced applied field h_z. Thus $\bar{\mu}_z \propto h_z$ in the SF phase. Since $\bar{\mu}_z \geqslant 0$, the maximum physical range of h_{A1} is

$$0 \leqslant h_{\text{A1}} < 1 - f_J. \tag{104}$$

The reduced susceptibilities defined in Eqs. (3a) and (3b) are then

$$\chi_{z\text{SF}}* = \frac{S+1}{3(1 - f_J - h_{\text{A1}})}, \tag{105}$$

$$\bar{\chi}_{z\text{SF}} = \frac{1}{1 - f_J - h_{\text{A1}}}. \tag{106}$$

One sees by comparison with Eq. (84) that $\bar{\chi}_{z\text{SF}} > \bar{\chi}_{\perp\text{AFM}}$. This inequality was qualitatively explained previously by Buschow and de Boer [13].

b. Alternate Hamiltonian diagonalization calculation. In this section, we give an alternative derivation of the field-induced moment of the SF phase. The energy E_i of a representative spin i in a magnetic induction $\mathbf{B}_i$ is

$$E_i = -\vec{\mu}_i \cdot \mathbf{B}_i = g\mu_{\text{B}}\mathbf{S} \cdot \mathbf{B}_i, \tag{107}$$

where in the second equality we used the expression for the magnetic moment operator

$$\vec{\mu} = -g\mu_{\text{B}}\mathbf{S}, \tag{108}$$

the negative sign comes from the negative charge on the electron, and $\mathbf{S}$ is the spin operator. As usual, we normalize all energies by $k_{\text{B}}T_{\text{N}J}$, so Eq. (107) becomes

$$\epsilon \equiv \frac{E_i}{k_{\text{B}}T_{\text{N}J}} = \mathbf{S} \cdot \mathbf{b}_i, \tag{109}$$

where the reduced induction $\mathbf{b}_i$ is defined as in Eq. (1c), and $\mathbf{b}_i$ is the sum of the reduced applied, anisotropy, and exchange fields.

Using Eqs. (A3), (A6), (A27), and (107), the exchange part of the reduced Hamiltonian for $\mathbf{S}_i$, assumed without loss of

generality to lie in the xz plane, is

$$\frac{\mathcal{H}_{\mathrm{exch}i}}{k_{\mathrm{B}}T_{\mathrm{N}J}} = \frac{3\bar{\mu}_{\mathrm{SF}}}{S+1}(S_x \sin\theta + f_J S_z \cos\theta)$$

$$= \frac{3}{S+1}(S_x \bar{\mu}_{x\mathrm{SF}} + f_J S_z \bar{\mu}_{z\mathrm{SF}}), \qquad (110\mathrm{a})$$

where we used the relations $\bar{\mu}_{\mathrm{SF}} = \mu_{\mathrm{SF}}/g\mu_{\mathrm{B}}S$, $\bar{\mu}_{x\mathrm{SF}} = \bar{\mu}_{\mathrm{SF}}\sin\theta$, and $\bar{\mu}_{z\mathrm{SF}} = \bar{\mu}_{\mathrm{SF}}\cos\theta$, and μ_{SF} is the magnitude of the ordered moment of each spin. Here, S_x is the usual combination of raising and lowering operators $S_x = (S_+ + S_-)/2$ and S_z is diagonal in the $|S, S_z\rangle$ Hilbert space. Similarly, the parts of the Hamiltonian for the anisotropy and applied fields are

$$\frac{\mathcal{H}_{\mathrm{A}i}}{k_{\mathrm{B}}T_{\mathrm{N}J}} = \frac{3h_{\mathrm{A}1}}{S+1}\bar{\mu}_z S_z, \qquad (110\mathrm{b})$$

$$\frac{\mathcal{H}_{\mathrm{H}i}}{k_{\mathrm{B}}T_{\mathrm{N}J}} = S_z h_z. \qquad (110\mathrm{c})$$

We thereby obtain the total reduced Hamiltonian

$$\frac{\mathcal{H}}{k_{\mathrm{B}}T_{\mathrm{N}J}} = \left(\frac{3\bar{\mu}_{x\mathrm{SF}}}{S+1}\right)S_x + \left[\left(\frac{3\bar{\mu}_{z\mathrm{SF}}}{S+1}\right)(f_J + h_{\mathrm{A}1}) + h_z\right]S_z$$

$$\equiv b_x S_x + b_z S_z, \qquad (111\mathrm{a})$$

where

$$b_x = \frac{3\bar{\mu}_{x\mathrm{SF}}}{S+1}, \quad b_z = \left(\frac{3\bar{\mu}_{z\mathrm{SF}}}{S+1}\right)(f_J + h_{\mathrm{A}1}) + h_z. \ (111\mathrm{b})$$

The reduced magnetic moment operators for reduced eigenenergies $\epsilon_n = E_n/k_{\mathrm{B}}T_{\mathrm{N}J}$ with $n = 1$ to $2S + 1$ are [4]

$$\bar{\mu}_x^{\mathrm{op}} = -\frac{1}{S}\frac{\partial\epsilon_n}{\partial b_x}\bigg|_{b_x=3\bar{\mu}_x/(S+1)}, \qquad (112\mathrm{a})$$

$$\bar{\mu}_z^{\mathrm{op}} = -\frac{1}{S}\frac{\partial\epsilon_n}{\partial b_z}\bigg|_{b_z=[3\bar{\mu}_z/(S+1)](f_J+h_{\mathrm{A}1})+h_z}. \qquad (112\mathrm{b})$$

Then the thermal-average reduced moments $\bar{\mu}_{x\mathrm{SF}}$ and $\bar{\mu}_{z\mathrm{SF}}$ for the SF phase are calculated by solving the simultaneous equations

$$\bar{\mu}_{x\mathrm{SF}} = \frac{1}{Z_S}\sum_{n=1}^{2S+1}\bar{\mu}_x^{\mathrm{op}}e^{-\epsilon_n/t},$$
$$\qquad (113\mathrm{a})$$
$$\bar{\mu}_{z\mathrm{SF}} = \frac{1}{Z_S}\sum_{n=1}^{2S+1}\bar{\mu}_z^{\mathrm{op}}e^{-\epsilon_n/t},$$

where the partition function is

$$Z_S = \sum_{n=1}^{2S+1}e^{-\epsilon_n/t}, \qquad (113\mathrm{b})$$

the reduced magnitude of the ordered moment is

$$\bar{\mu}_{\mathrm{SF}} = \sqrt{\bar{\mu}_{x\mathrm{SF}}^2 + \bar{\mu}_{z\mathrm{SF}}^2}, \qquad (113\mathrm{c})$$

and in this section we use the reduced temperature $t \equiv T/T_{\mathrm{N}J}$. The two Eqs. (113a) are solved iteratively for $\bar{\mu}_{x\mathrm{SF}}$ and $\bar{\mu}_{z\mathrm{SF}}$ for each desired combination of f_J, $h_{\mathrm{A}1}$, h_z, and t for a fixed spin S [4].
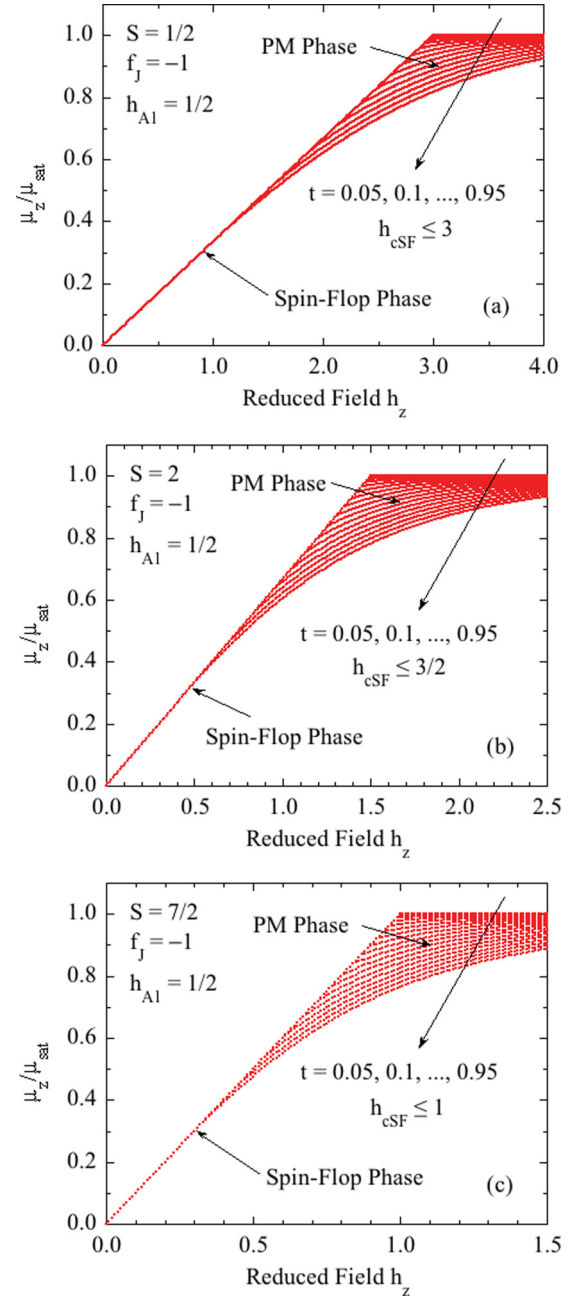

FIG. 16. Reduced induced moment per spin $\bar{\mu}_z \equiv \mu_z/\mu_{\mathrm{sat}}$ for the low-field spin-flop (SF) and high-field paramagnetic (PM) phases of a collinear or planar noncollinear antiferromagnet vs reduced field h_z for reduced anisotropy field $h_{\mathrm{A}1} = 1/2$ and $f_J = -1$ at reduced temperatures $t = T/T_{\mathrm{N}J}$ from 0.05 to 0.95 for spins (a) $S = 1/2$, (b) 2, and (c) 7/2 calculated using Eqs. (113). The SF and PM field ranges are separated by a break in slope in $\bar{\mu}_z$ versus h_z at the reduced critical field $h_z = h_{\mathrm{cSF}}(t)$ in Eq. (114). Note the different abscissa scales in (a)–(c).

Calculations of $\bar{\mu}_{z\mathrm{SF}}$ versus h_z isotherms at many t values obtained using Eqs. (113) are shown in Fig. 16 for spins $S = 1/2$, 2, and 7/2 with $f_J = -1$ and $h_{\mathrm{A}1} = 1/2$, where the data for the PM phase at $h_z \gtrsim h_{\mathrm{cSF}}$ (below) are obtained automatically. These results agree with what would have been obtained from the results in the previous section based on

torque calculations. We also find that the magnitude of the reduced ordered moment $\bar{\mu}_{SF}$ is independent of h_z for the SF phase (over the proportional part of the $\bar{\mu}_z$ versus h_z isotherm) at each temperature.

3. Critical field

The critical field H_{cSF} of the spin flop phase is defined as the value of the applied field H_z at which all the magnetic moments become aligned with the field, as in the right-hand side of the top panel of Fig. 12. Since μ_{zSF}/H_z is independent of H_z within the SF phase, this criterion and Eq. (103a) gives the reduced critical field

$$h_{cSF} = \frac{3(1 - f_J - h_{A1})}{S + 1} \bar{\mu}_{SF},\qquad(114)$$

where $\bar{\mu}_{SF}$ versus t or t_A is obtained by solving the first or second of Eqs. (99), respectively. The h_{cSF} is dependent on temperature because $\bar{\mu}_{SF}$ is. Since $0 \leqslant \bar{\mu}_{SF} \leqslant 1$, the physically relevant range for positive h_{cSF} is

$$0 \leqslant h_{cSF} \leqslant \frac{3(1 - f_J - h_{A1})}{S + 1}.\qquad(115)$$

For $h_z \geqslant h_{cSF}$, the system is in the PM phase with all induced moments having the same magnitude $\bar{\mu}_{zPM}$ and pointing in the direction of **H**.

Shown in Fig. 17 are plots of h_{cSF} versus t_A for $f_J = -1$ and spins $S = 1/2$ and $7/2$, each with anisotropy parameters $h_{A1} = 0$ to 1. The shapes of the curves are noticeably different for the two spin values. One also sees that the critical fields are much smaller for $S = 7/2$ than for $S = 1/2$, consistent with Eq. (114).

4. Spin-flop and paramagnetic phase magnetization summary

To summarize, the field dependencies of the magnetization for the low-field SF and high-field PM phases are given by Eqs. (103a) and (92), respectively, as

$$\bar{\mu}_{zSF} = \bar{\mu}_z = \frac{(S + 1)h_z}{3(1 - f_J - h_{A1})} \quad (h_z \leqslant h_{cSF}),\qquad(116a)$$

$$\bar{\mu}_{zPM} = B_S(y_{PM}),\qquad(116b)$$

$$y_{PM} = \frac{1}{(1 + h_{A1})t_A}\left[\frac{3(f_J + h_{A1})}{S + 1}\bar{\mu}_{zPM} + h_z\right]$$
$$(h \geqslant h_{cSF}),$$

where h_{cSF} is given in Eq. (114) and $\bar{\mu}_{SF}$ is obtained by solving Eq. (99b). Note that the slope of $\bar{\mu}_{zSF}$ versus h_z for the SF phase in Eq. (116a) depends on S, f_J, and h_{A1}, and not on the temperature. The temperature only determines the maximum field at which the proportionality occurs.

The reduced z-axis moment of the SF phase $\bar{\mu}_{zSF}$ is plotted versus the reduced field h_z in Fig. 18 for $t_A = 1/2$ and for $S = 1/2$ and $7/2$ with $h_{A1} = 0$ to 1. The low-field SF portion is proportional to h_z but then undergoes a second-order phase transition via a slope reduction to the PM state for which $\bar{\mu}_{zSF}$ exhibits negative curvature. For $h_{A1} = 1$, only the PM phase occurs for both spin values, as seen in Fig. 18, because one can show that $h_{cSF} = 0$ for any S if $f_J = -1$, $t_A = 0.5$, and $h_{A1} = 0.5$, as illustrated in Fig. 17 for $S = 1/2$ and $7/2$. It is important to note here that t_A is not proportional to the absolute
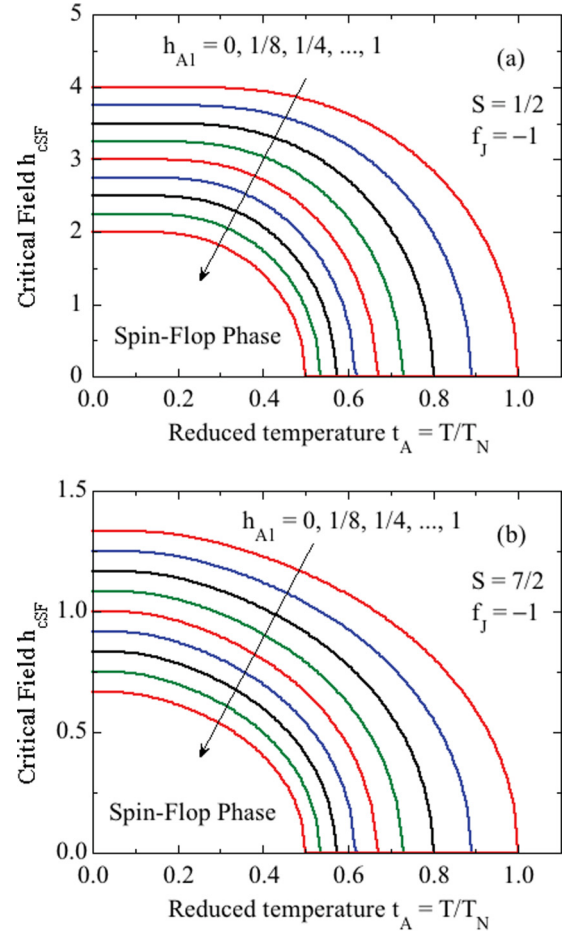

FIG. 17. Reduced critical field h_{cSF} for the spin-flop phase of a collinear antiferromagnet vs reduced temperature t_A with $f_J = -1$ and $h_{A1} = 0$ to 1 for spins (a) $S = 1/2$ and (b) $7/2$, calculated using Eq. (114).

temperature, since it depends on h_{A1} according to the formula in the figures. Therefore, in Fig. 19, the same quantities are plotted as in Fig. 18, but where the reduced temperature $t = T/T_{NJ}$, proportional to the absolute temperature T, is fixed to the same value of $1/2$. Qualitative differences are seen between the two figures.

5. Internal energy versus temperature

We established in Sec. VIII C 2 that the ordered moment $\bar{\mu}_{SF}$ is independent of field within the SF phase, i.e., for $0 \leqslant h_z \leqslant h_{cSF}(t)$. For $h_z = 0$, the ordered moments are oriented in the xy plane for which the anisotropy field is zero as inferred from Eq. (23) and Fig. 3(b). Hence the magnetic induction seen by a spin is identical to that of a spin in an AFM in zero applied and anisotropy fields, and therefore the internal energy per spin is given by Eq. (A17) or by Eq. (40c) with $h_{A1} = 0$, i.e.,

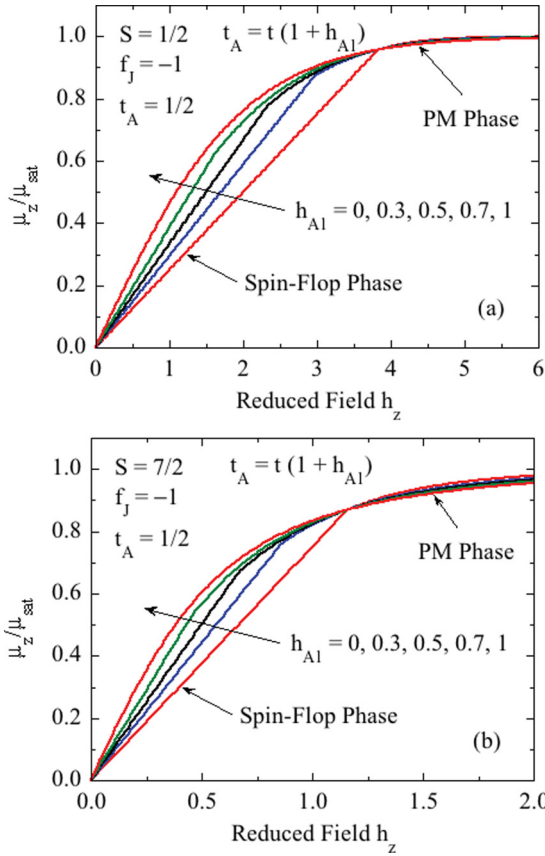$$\frac{U_{mag}}{k_B T_{NJ}} = -\frac{3S}{2(S + 1)}\bar{\mu}_0^2,\qquad(117)$$

FIG. 18. Reduced ordered moment $\bar{\mu}_z \equiv \mu_z/\mu_{\rm sat}$ vs reduced field h_z for the spin-flop (SF) and subsequent paramagnetic (PM) phases of a collinear or planar noncollinear antiferromagnet at reduced temperature $t_{\rm A} = T/T_{\rm N} = t(1+h_{\rm A1}) = 1/2$ with $f_J = -1$ and $h_{\rm A1} = 0$ to 1 for spins (a) $S = 1/2$ and (b) 7/2, calculated using Eqs. (114) and (116). The SF and PM ranges are separated by a break in slope in $\mu_z/\mu_{\rm sat}$ vs h_z at $h_z = h_{\rm cSF}$. However, the curve in each of (a) and (b) with $h_{\rm A1} = 1$ is paramagnetic over the full field ranges shown.
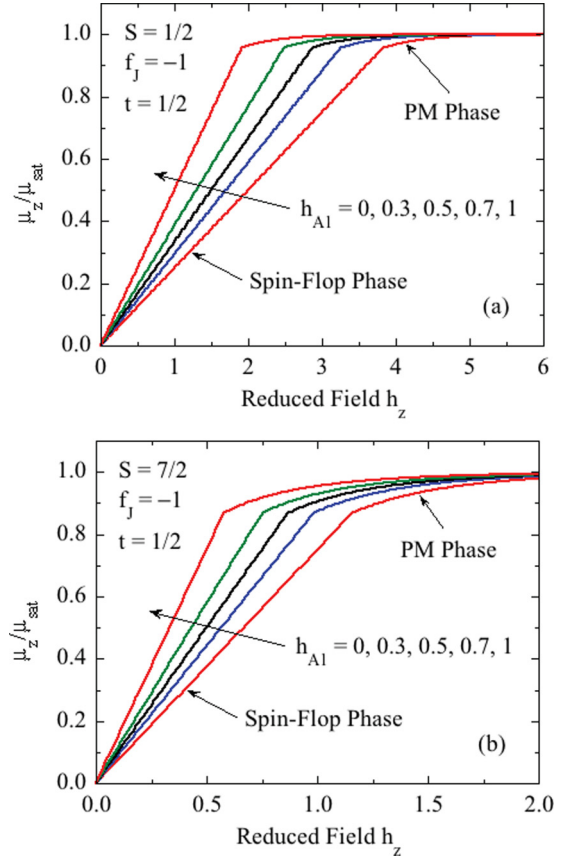
FIG. 19. Same as Fig. 18, except that the reduced temperature $t = T/T_{NJ}$ is fixed at the value of 1/2 instead of $t_{\rm A} = T/T_{\rm N} = 1/2$. The plots are different than in Fig. 18 because $T_{\rm N}$ depends on $h_{\rm A1}$.

states at $h_z = h_{\rm cSF}$ are not obvious from the figure. The value of $h_{\rm cSF}(t=0)$ for each spin value is given in the respective panel.

where $\bar{\mu}_0(t)$ is obtained by solving Eq. (A14). At $t = 0$, one has $\bar{\mu}_0 = 1$, yielding

$$\frac{U_{\rm mag}(h_z \leqslant h_{\rm cSF}, t=0)}{k_B T_{NJ}} = -\frac{3S}{2(S+1)}. \quad (118)$$

Shown in Fig. 20 are plots of $U_{\rm mag}/k_B T_{NJ}$ versus t for spins $S = 1/2$ to 7/2 in half-integer increments. The internal energy for all spin values goes to zero at the same temperature $T = T_{NJ}$ because $\bar{\mu}_0$ does. One also sees that Eq. (118) is satisfied for all spin values.

6. Free energy

The free energy $F_{\rm mag}$ is calculated from Eqs. (20) using Eq. (117) and $U_{\rm mag}$ data such as in Fig. 20 and $\bar{\mu}_z(h_z,t)$ data such as illustrated in Figs. 16 and 19. Plots of $F_{\rm mag}/k_B T_{NJ}$ versus h_z at fixed values of $t = T/T_{NJ}$ from 0.05 to 1 for spins $S = 1/2$ and 7/2 are shown in Fig. 21. Because the free energy in Eq. (20e) is derived from an integral of $\bar{\mu}_z(h_z,t)$ over h_z, the second-order transitions between the SF and PM
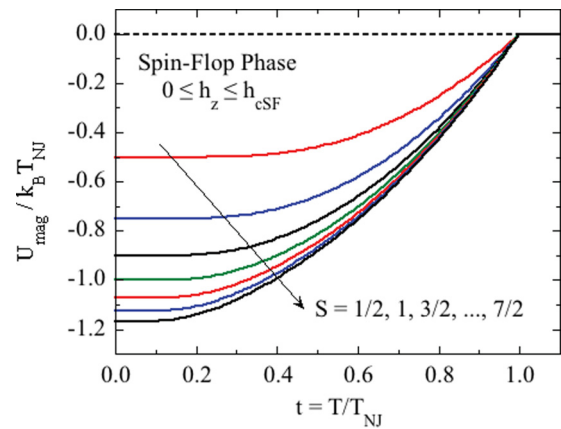

FIG. 20. Internal energy per spin $U_{\rm mag}$ normalized by $k_B T_{NJ}$ vs reduced temperature t for the spin-flop phase with spins $S = 1/2$ to 7/2, obtained from Eq. (117). $U_{\rm mag}$ is independent of field in the field range of stability of the SF phase with respect to the PM phase, given by $0 \leqslant h_z \leqslant h_{\rm cSF}$, where $h_{\rm cSF}$ is given in Eq. (114).
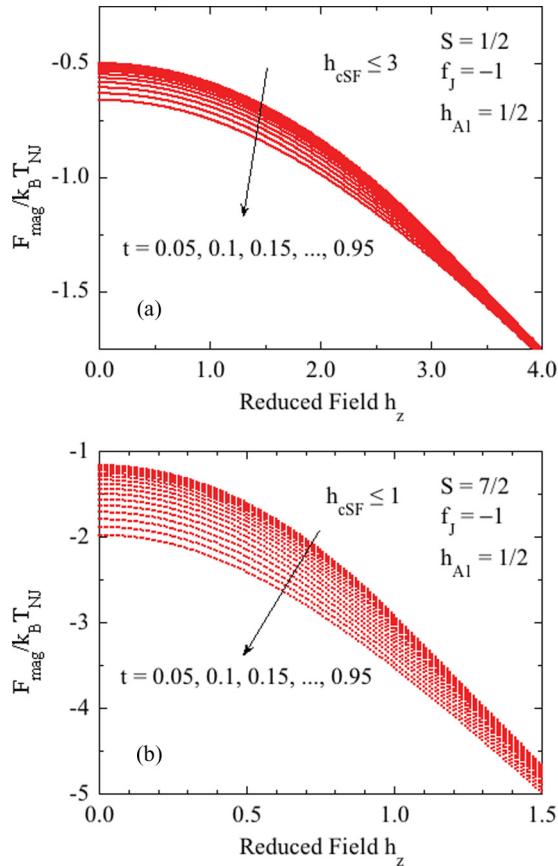
FIG. 21. Reduced magnetic free energy per spin $F_{\mathrm{mag}}/k_{\mathrm{B}} T_{\mathrm{N}J}$ for the low-field spin-flop (SF) and high-field paramagnetic (PM) phases of a collinear or planar noncollinear antiferromagnet vs reduced field h_z for reduced anisotropy parameter $h_{\mathrm{A}1} = 1/2$ and $f_J = -1$ at reduced temperatures $t = T/T_{\mathrm{N}J}$ from 0.05 to 0.95 for spins (a) $S = 1/2$ and (b) 7/2, calculated using Eqs. (20e), (116), and (117) together with $\bar{\mu}_z(h_z, t)$ data such as in Figs. 16 and 19. Note the different axis scales for the two panels. The second-order phase transitions from the SF to the PM phase occur at $h_z = h_{\mathrm{cSF}}(t)$ in Eq. (114) and Fig. 17 and are not obvious in either panel. The respective value of $h_{\mathrm{cSF}}(t = 0)$ [the upper limit of $h_{\mathrm{cSF}}(t)$] is shown in each panel.

IX. HIGH-FIELD PARALLEL MAGNETIZATION OF z-AXIS COLLINEAR ANTIFERROMAGNETS: ANTIFERROMAGNETIC PHASE

Here we consider the general behavior of a collinear AFM where the field is applied along the easy z axis of the AFM structure at finite temperatures. By definition, in the collinear AFM phase the ordered moments are always aligned along the z axis.

A. Preliminaries

When the magnetization along the easy axis of a collinear AFM becomes nonlinear in finite fields, one must define two different sublattices 1 and 2 because in general the magnitudes of the ordered moments parallel and antiparallel to the applied field $\mathbf{H}$ are different by amounts greater than infinitesimal. Sublattice 1 is defined to consist of all moments that are

parallel to $\mathbf{H}$ and sublattice 2 consists of the moments that are antiparallel to $\mathbf{H}$ when $H_z = 0$. When H_z increases, the magnitudes of the z-components μ_{1z} and μ_{2z} are in general not the same, which gives a net uniform magnetization in the direction of the field. However, within the unified MFT we do not require the two sublattices to be bipartite, where the exchange interactions only connect spins of one sublattice with those on the other. The exchange interactions can connect further neighbors and can be nonfrustrating and/or frustrating for AFM order. An anisotropy field along the uniaxial z axis is present, as shown in Fig. 1.

For moments $\vec{\mu}_i$ and $\vec{\mu}_j$ on the same ("s") sublattice of a collinear AFM structure, as defined above, the angle between the moments is $\phi_{ji} = 0$ in Eq. (A3) and for a pair of moments on different ("d") sublattices, the angle between them in $H_z = 0$ is $\phi_{ji} = 180°$. We then write the expressions (A6a) and (A6b) for $T_{\mathrm{N}J}$ and $\theta_{\mathrm{p}J}$ at $H_z = 0$ for the two-sublattice collinear AFM, respectively, as

$$T_{\mathrm{N}J} = -\frac{S(S+1)}{3k_{\mathrm{B}}} \left(\sum_j^{\mathrm{s}} J_{ij} - \sum_j^{\mathrm{d}} J_{ij} \right), \quad (119a)$$

$$\theta_{\mathrm{p}J} = -\frac{S(S+1)}{3k_{\mathrm{B}}} \left(\sum_j^{\mathrm{s}} J_{ij} + \sum_j^{\mathrm{d}} J_{ij} \right). \quad (119b)$$

Solving these simultaneous equations for the two sums gives

$$
\begin{aligned}
\sum_j^{\mathrm{s}} J_{ij} &= -\frac{3k_{\mathrm{B}}(T_{\mathrm{N}J} + \theta_{\mathrm{p}J})}{2S(S+1)} = -\frac{3k_{\mathrm{B}} T_{\mathrm{N}J}(1 + f_J)}{2S(S+1)}, \\
\sum_j^{\mathrm{d}} J_{ij} &= \frac{3k_{\mathrm{B}}(T_{\mathrm{N}J} - \theta_{\mathrm{p}J})}{2S(S+1)} = \frac{3k_{\mathrm{B}} T_{\mathrm{N}J}(1 - f_J)}{2S(S+1)},
\end{aligned}
\quad (120)
$$

where $f_J \equiv \theta_{\mathrm{p}J}/T_{\mathrm{N}J}$ is defined in Eq. (A7). We emphasize that $T_{\mathrm{N}J}$, $\theta_{\mathrm{p}J}$, and f_J are defined, even in the presence of the anisotropy field, only in terms of the exchange constants and magnetic structure by the above equations, whereas T_{N} and θ_{p} are the actual Néel and Weiss temperatures in the presence of a uniaxial anisotropy field and zero or infinitesimal magnetic field that are both aligned along the easy z axis.

In the following, we parametrize the high-field magnetization using the variables f_J, which only depends on the exchange constants and AFM structure, and the reduced anisotropy field $h_{\mathrm{A}1}$ defined in Eq. (1e). This choice of variables allows one to separate the effects on the magnetization due to the anisotropy field from those due to the exchange interactions and AFM structure.

B. Exchange, anisotropy, and applied fields

For a collinear AFM in a parallel applied field H_z along the easy z axis, only the z components of the moments and the exchange fields are relevant. Using the definition $\bar{\mu}_{iz} \equiv \mu_{iz}/\mu_{\mathrm{sat}} = \mu_{iz}/(gS\mu_{\mathrm{B}})$ for the two sublattices $i = 1, 2$, and Eqs. (A3) and (120), the z component of the exchange field

seen by each moment on sublattice 1 is

$$
H_{\text{exch}\,1z} = -\frac{1}{g^2\mu_{\text{B}}^2}\left(\mu_{1z}\sum_j^{\text{s}} J_{ij} + \mu_{2z}\sum_j^{\text{d}} J_{ij}\right)
$$

$$
= \frac{3k_{\text{B}}T_{\text{N}J}}{2g\mu_{\text{B}}(S+1)}[\bar{\mu}_{1z}(1+f_J) - \bar{\mu}_{2z}(1-f_J)].
$$

(121a)

We express the magnetic fields in reduced form using Eq. (1c). For the local exchange field seen by a spin in sublattice 1 in Eq. (121a), the reduced field is

$$
h_{\text{exch}\,1z} \equiv \frac{g\mu_{\text{B}}H_{\text{exch}\,1z}}{k_{\text{B}}T_{\text{N}J}} = \frac{3[\bar{\mu}_{1z}(1+f_J) - \bar{\mu}_{2z}(1-f_J)]}{2(S+1)}.
$$

(121b)

Similarly, the exchange field for a spin in sublattice 2 is

$$
H_{\text{exch}\,2z} = -\frac{1}{g^2\mu_{\text{B}}^2}\left(\mu_{1z}\sum_j^{\text{d}} J_{ij} + \mu_{2z}\sum_j^{\text{s}} J_{ij}\right)
$$

$$
= \frac{3k_{\text{B}}T_{\text{N}J}}{2g\mu_{\text{B}}(S+1)}[-\bar{\mu}_{1z}(1-f_J) + \bar{\mu}_{2z}(1+f_J)],
$$

(122a)

yielding the reduced exchange field

$$
h_{\text{exch}\,2z} \equiv \frac{g\mu_{\text{B}}H_{\text{exch}\,2z}}{k_{\text{B}}T_{\text{N}J}} = \frac{3[-\bar{\mu}_{1z}(1-f_J) + \bar{\mu}_{2z}(1+f_J)]}{2(S+1)}.
$$

(122b)

Using Eqs. (23b), (31a), (A20), and the expression $\bar{\mu}_i\cos\theta = \bar{\mu}_{iz}$, one obtains the anisotropy field

$$
H_{\text{A}iz} = \frac{3H_{\text{A}1}}{S+1}\bar{\mu}_{iz},
$$

(123a)

yielding the reduced anisotropy field

$$
h_{\text{A}iz} \equiv \frac{g\mu_{\text{B}}H_{\text{A}iz}}{k_{\text{B}}T_{\text{N}J}} = \frac{3h_{\text{A}1}}{S+1}\bar{\mu}_{iz}.
$$

(123b)

One also has the reduced applied field

$$
h_z \equiv \frac{g\mu_{\text{B}}H_z}{k_{\text{B}}T_{\text{N}J}}.
$$

(123c)

The total reduced local magnetic inductions seen by spins in sublattices $i = 1$, 2 are then

$$
b_{iz} \equiv \frac{g\mu_{\text{B}}B_{iz}}{k_{\text{B}}T_{\text{N}J}} = h_{\text{exch}\,iz} + h_{\text{A}iz} + h_z.
$$

(124)

Inserting the above expressions for the components on the right-hand side gives

$$
b_{1z} = \frac{3[\bar{\mu}_{1z}(1+f_J+2h_{\text{A}1}) - \bar{\mu}_{2z}(1-f_J)]}{2(S+1)} + h_z, \quad (125a)
$$

$$
b_{2z} = \frac{3[-\bar{\mu}_{1z}(1-f_J) + \bar{\mu}_{2z}(1+f_J+2h_{\text{A}1})]}{2(S+1)} + h_z.
$$

(125b)

C. Coupled equations for the two sublattice magnetizations

The values of $\bar{\mu}_{iz}$ ($i = 1$, 2) versus H and T are governed by separate Brillouin functions for the two sublattices as in Eqs. (A10). One thus has two simultaneous consistency relations

$$
\bar{\mu}_{iz} = B_S\left(\frac{b_{iz}}{t}\right) \quad (i = 1, 2).
$$

(126)

Substituting Eqs. (125) into (126) gives

$$
\bar{\mu}_{1z} = B_S\left\{\frac{3[\bar{\mu}_{1z}(1+f_J+2h_{\text{A}1}) - \bar{\mu}_{2z}(1-f_J)]}{2(S+1)t} + \frac{h_z}{t}\right\},
$$

(127a)

$$
\bar{\mu}_{2z} = B_S\left\{\frac{3[-\bar{\mu}_{1z}(1-f_J) + \bar{\mu}_{2z}(1+f_J+2h_{\text{A}1})]}{2(S+1)t} + \frac{h_z}{t}\right\}.
$$

(127b)

When $H_z = 0$ and $T \leqslant T_{\text{N}}$, one has $\bar{\mu}_{2z} = -\bar{\mu}_{1z}$ and Eqs. (127a) and (127b) each reduce to the same general expression (37) for the ordered moment versus temperature, as required. For the PM regime $T \geqslant T_{\text{N}}$, $\bar{\mu}_{1z} = \bar{\mu}_{2z}$ and Eqs. (127a) and (127b) each reduce to the z-axis magnetic moment of the PM state of the AFM given by Eqs. (92), as also required.

D. Sublattice, average and staggered moments, and free energy versus magnetic field, temperature, and anisotropy parameter

Two important quantities can be obtained from Eqs. (127) from which the thermal-average sublattice magnetic moments $\bar{\mu}_{1z}$ and $\bar{\mu}_{2z}$ versus temperature, magnetic field and anisotropy parameter are calculated. The first is the net average magnetic moment, normalized by the saturation moment, which is

$$
\bar{\mu}_{z\,\text{ave}} = \frac{\bar{\mu}_{1z} + \bar{\mu}_{2z}}{2}.
$$

(128a)

This is the uniform magnetization along the easy axis measured in a conventional magnetometer. The second important quantity is the AFM order parameter $\bar{\mu}_z^\dagger$, which is the average z-axis staggered moment in the z direction normalized by the saturation moment, given by

$$
\bar{\mu}_z^\dagger = \frac{\bar{\mu}_{1z} - \bar{\mu}_{2z}}{2}.
$$

(128b)

By assumption $\bar{\mu}_{1z} \geqslant \bar{\mu}_{2z}$, so $\bar{\mu}_z^\dagger \geqslant 0$. The spin system is in the AFM phase when $\bar{\mu}_z^\dagger > 0$ and is in the associated high-field PM phase when $\bar{\mu}_z^\dagger = 0$.

The potential phase transitions between collinear AFM and PM states discussed below will be preempted if the free energy of the AFM phase for some combination of t, h_z, and $h_{\text{A}1}$ is higher than that of the SF phase, and conversely. Therefore in this section we eventually determine the free energy of the AFM phase versus temperature from the values of the thermal-average moments $\bar{\mu}_{1z}$ and $\bar{\mu}_{2z}$ in the presence of the anisotropy and applied fields for comparison with the free energy of the SF phase found previously in Sec. VIII C 6.

Equations (127) were solved for $\bar{\mu}_{1z}$ and $\bar{\mu}_{2z}$ versus h_z for given values of S, t, f_J, and $h_{\text{A}1}$ using an iterative
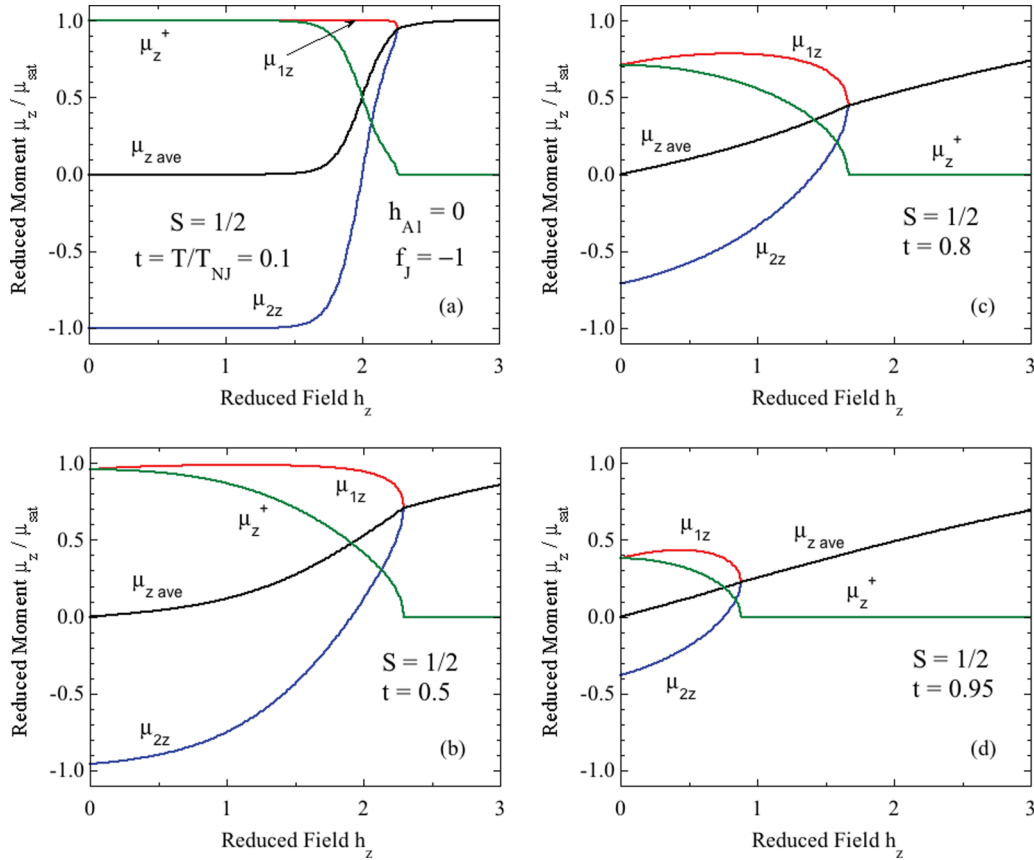
FIG. 22. Ordered moments $\bar{\mu}_{iz} \equiv \mu_{iz}/\mu_{\rm sat}$ ($i = 1, 2$) of the two magnetic sublattices along with the AFM order parameter $\bar{\mu}_z^\dagger \equiv (\bar{\mu}_{1z} - \bar{\mu}_{2z})/2$ and the average ordered moment $\bar{\mu}_{z\,\rm ave} \equiv (\bar{\mu}_{1z} + \bar{\mu}_{2z})/2$ for spin $S = 1/2$, $f_J = -1$, and $h_{\rm A1} = 0$, all vs the reduced applied magnetic field h_z along the easy z axis for reduced temperatures $t \equiv T/T_{\rm NJ}$ of (a) 0.1, (b) 0.5, (c) 0.8, and (d) 0.95. The AFM regime is defined by the region where $\bar{\mu}_z^\dagger > 0$, and the PM regime is defined by $\bar{\mu}_z^\dagger = 0$. The transition field between these two regimes is defined as the criticial field $h_{\rm cAFM}$. Only second-order transitions are observed for $0 < t_{\rm A} < 1$ with $f_J = -1$ and $h_{\rm A1} = 0$.

procedure [4]. Starting with $h_z = 0$, the initial value of $\bar{\mu}_{1z}$ was set to 1 and $\bar{\mu}_{2z}$ solved for. Then for that value of $\bar{\mu}_{2z}$, $\bar{\mu}_{1z}$ was solved for. These steps were iterated until the differences in $\bar{\mu}_{1z,2z}$ between subsequent iterations were each less than 10^{-10}. Typically, the number of iterations needed was less than 10, but occasionally up to $\sim 10^4$ iterations were needed when approaching a phase transition. Once $\bar{\mu}_{1z}$ and $\bar{\mu}_{2z}$ were determined, $\bar{\mu}_{z\rm ave} = (\bar{\mu}_{1z} + \bar{\mu}_{2z})/2$ and $\bar{\mu}_z^\dagger = (\bar{\mu}_{1z} - \bar{\mu}_{2z})/2$ were determined. This sequence was repeated for the next value of h_z, where the starting value of $\bar{\mu}_{1z}$ was the final value from the previous value of h_z.

Shown in Figs. 22 and 23 are plots of $\bar{\mu}_{1z}$, $\bar{\mu}_{2z}$, $\bar{\mu}_{z\rm ave}$, and $\bar{\mu}_z^\dagger$ versus h_z for $f_J = -1$, $h_{\rm A1} = 0$, $t = 0.1, 0.5, 0.8$, and 0.95 for spins $S = 1/2$ and 7/2, respectively. The data versus h_z for $S = 1/2$ and $S = 7/2$ have similar evolutions of the shapes on decreasing temperature, but the abscissa ranges for $S = 7/2$ are a factor of three smaller than for $S = 1/2$. Qualitative plots of $\bar{\mu}_{iz}(i = 1, 2)$ similar to those in Figs. 22 and 23 were shown in Fig. 11 of Ref. [14]. The boundary between the AFM and PM states occurs with increasing field when $\bar{\mu}_z^\dagger \to 0^+$. We denote this reduced critical field by $h_{\rm c\,AFM}$. Thus for $h_z \geqslant h_{\rm c\,AFM}$, one has $\bar{\mu}_{1z} = \bar{\mu}_{2z}$ and $\bar{\mu}_z^\dagger = 0$. Second-order transitions at $h_{\rm c\,AFM}$ are observed for the full temperature range $0 < t_{\rm A} \leqslant 1$ for $f_J = -1$ and $h_{\rm A1} = 0$.

First-order transitions between the AFM and PM phases can occur over a range of low temperatures ending at a tricritical point temperature above which the transitions are second-order. For example, we changed f_J from -1 to the value of $-1/4$ while leaving $h_{\rm A1} = 0$ as in Fig. 22. Numerical solutions for $\bar{\mu}_{iz}$ ($i = 1, 2$), $\bar{\mu}_z^\dagger$ and $\bar{\mu}_{z\rm ave}$ are plotted versus h_z in Fig. 24 for reduced temperatures $t_{\rm A} = 0.1, 0.5, 0.8$, and 0.95. At high T, the AFM to PM transitions are seen to be second order. However, at $t = 0.5$ and 0.1, the transitions are strongly and weakly first order, respectively, where a discontinuous change in the AFM order parameter $\bar{\mu}_z^\dagger$ occurs at the transition.

We carried out additional calculations of $\bar{\mu}_z^\dagger$ and $\bar{\mu}_{z\rm ave}$ versus h_z and reduced temperature $t = T/T_{\rm NJ}$. Plots of $\bar{\mu}_{z\rm ave}$ versus h_z for spin $S = 1/2$ and $f_J = -1$ for $t = 0.05$ to 0.95 for reduced anisotropy fields $h_{\rm A1} = 1/4, 1/2, 3/4$, and 1 calculated using Eqs. (127) are shown in Fig. 25. One sees a clear evolution from first-order to second-order transitions with increasing temperature. The values of the AFM critical field $h_{\rm cAFM}$ were determined from Fig. 25 as the value of h_z at which $\bar{\mu}^\dagger \to 0$ with increasing h_z. Second-order transitions are characterized by a continuous change for $\bar{\mu}^\dagger \to 0$, whereas a first-order transition shows a discontinuous change as noted above. After converting t to $t_{\rm A}$ using Eq. (1j), plots of the resulting $h_{\rm cAFM}$ versus $t_{\rm A}$ are shown in Fig. 26 for $S =$

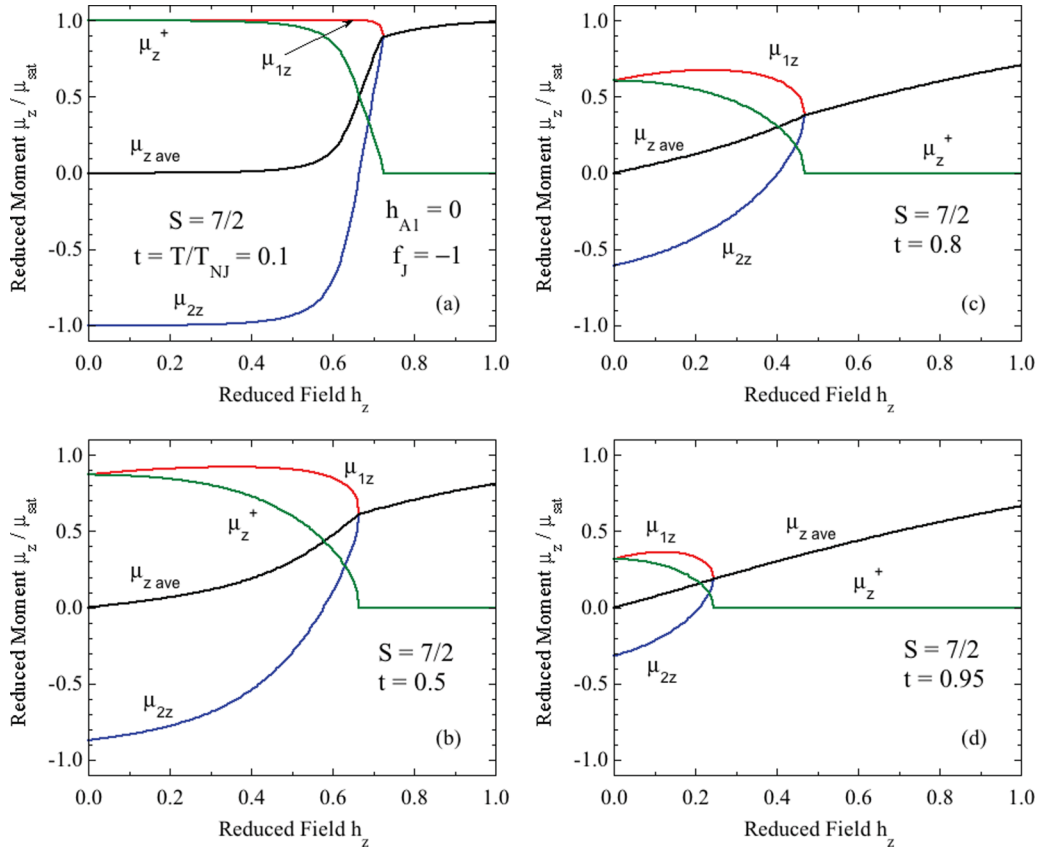FIG. 23. Same as Fig. 22 except for spin $S = 7/2$. Note the factor of three difference in the abscissa scale between this figure and that one.

$1/2$, $f_J = -1$, and h_{A1} values from 0 to 1. The first-order transition data are represented by solid red curves, and the second-order data by solid curves connecting data points of different colors. These plots are not phase diagrams, which are given in Fig. 32 below for the same values of h_{A1} as in Fig. 25 and also for $h_{A1} = 0$ and $1/8$.

E. Magnetic free energy

Once $\bar{\mu}_{z\text{ave}}$ is determined as described above, the reduced magnetic free energy of the AFM phase $F_{\text{magAFM}}/k_B T_{NJ}$ is calculated versus t, h_z, and h_{A1} using Eqs. (20). Plots of $F_{\text{magAFM}}/k_B T_{NJ}$ versus h_z for $f_J = -1$, $S = 1/2$ and reduced temperatures t from 0.05 to 0.95 are shown for reduced anisotropy fields $h_{A1} = 1/4$ to 1 in Fig. 27. One sees that at low temperatures for each value of h_{A1}, $F_{\text{magAFM}}/k_B T_{NJ}$ shows a discontinuity in slope at the respective h_{cAFM} corresponding to the first-order discontinuity in $\bar{\mu}_z$ in Fig. 25, whereas at the higher temperatures $F_{\text{magAFM}}/k_B T_{NJ}$ varies smoothly through h_{cAFM}, corresponding to a second-order transition in $\bar{\mu}_z$, as quantified in Fig. 26.

X. PHASE DIAGRAMS

The phase diagrams discussed here are those with the anisotropy field oriented along the z axis as in Fig. 1, for which the ground state in $h_z = 0$ is a collinear AFM aligned along that axis, and with a reduced external field h_z in the $+z$ direction. We first discuss the zero-temperature properties and phase diagrams of Heisenberg systems with classical anisotropy

fields and then extend the discussion to finite-temperature phase diagrams. Because phase diagrams for $S = 1/2$ are not relevant when uniaxial quantum DS_z^2 anisotropy is present in Heisenberg spin systems [4], here we emphasize phase diagrams for this spin value.

A. Zero-temperature phase diagrams and magnetizations versus field

The zero-temperature properties and phase diagrams are determined from the relative free energies of SF and AFM phases and their dependencies on the parameters S, f_J, h_{A1}, and h_z. The PM phase appears at and above the critical field of the phase with the lower free energy.

1. Spin-flop phase

For $t \to 0$, the entropy of the SF phase in $H_z = 0$ is zero due to the nondegenerate ground state arising from the nonzero exchange field, so Eqs. (20) yield

$$\frac{F_{\text{magSF}}(h_z = 0, t \to 0)}{k_B T_{NJ}} = \frac{U_{\text{magSF}}(h_z = 0, t \to 0)}{k_B T_{NJ}}$$

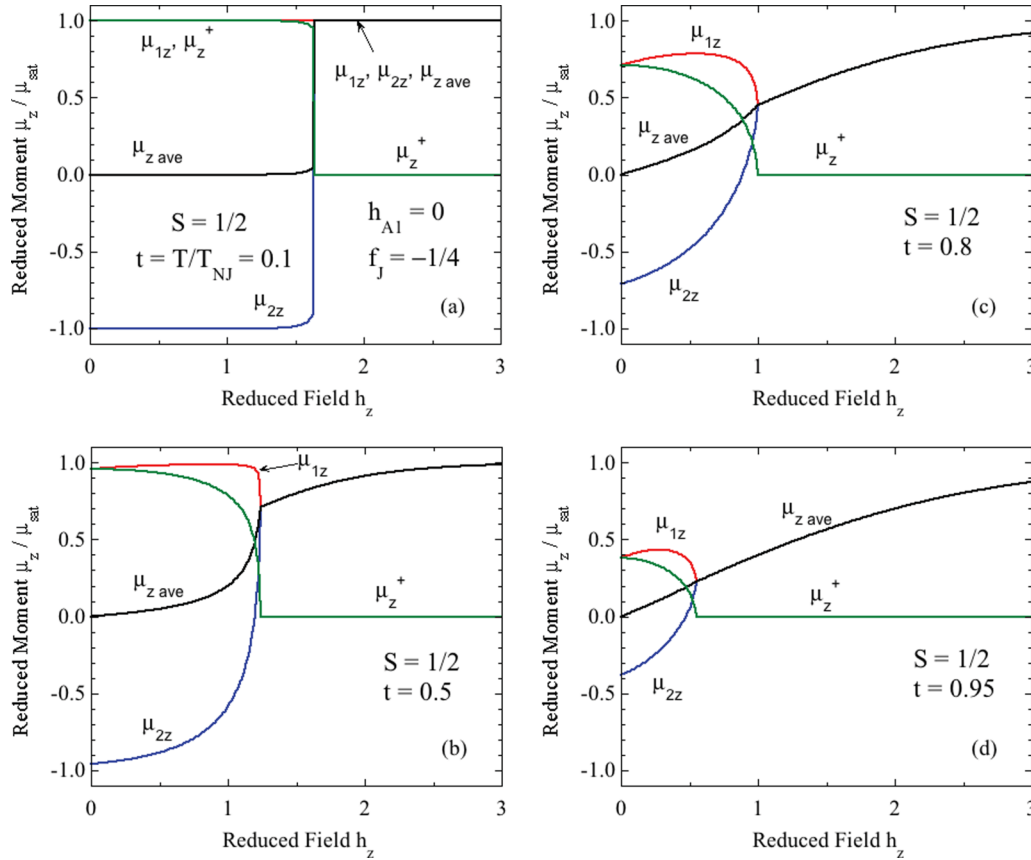$$- S \int_0^{h_z} \bar{\mu}_{z\text{SF}}(h_z, t \to 0) dh_z.$$

(129a)

FIG. 24. Same as Fig. 22 except that here $f_J = -1/4$. The data for $t = 0.1$ show strongly first-order transitions, for $t = 0.5$ weakly first-order transitions, and second-order transitions for $t = 0.8$ and 0.95.

Equation (118) gives the first term as

$$\frac{U_{\text{magSF}}(h_z = 0, t \to 0)}{k_B T_{NJ}} = -\frac{3S}{2(S+1)}, \qquad (129b)$$

and Eqs. (116) give

$$\bar{\mu}_{zSF}(h_z, t \to 0) = \begin{cases} h_z/h_{cSF} & (h_z \leqslant h_{cSF}) \\ 1 & (h_z \geqslant h_{cSF}) \end{cases}, \qquad (129c)$$

where Eq. (114) gives the SF critical field as

$$h_{cSF}(t \to 0) = \frac{3(1 - f_J - h_{A1})}{S + 1} \qquad (129d)$$

using $\bar{\mu}_{SF} = 1$ for $t \to 0$. Thus Eq. (20e) gives the normalized free energy of the SF phase versus h_z for $t \to 0$ as

$$\frac{F_{\text{magSF}}(h_z, t \to 0)}{k_B T_{NJ}}$$

$$= \begin{cases} -\frac{3S}{2(S+1)} - S\frac{h_z^2}{2h_{cSF}} & (h_z \leqslant h_{cSF}) \\ -\frac{3S}{2(S+1)} - S\left[\frac{h_{cSF}}{2} + (h_z - h_{cSF})\right] & (h_z \geqslant h_{cSF}). \end{cases}$$

$$(130)$$

2. Antiferromagnetic phase

For the AFM phase at $t \to 0$, the moments cannot respond to the field without a spin-flip transition to the PM phase. Also, the entropy is zero at $t \to 0$ because the ground state is nondegenerate on account of the presence of the exchange

and anisotropy fields. Thus using Eq. (40c) with $\bar{\mu}_0 = 1$, the reduced free energy per spin is

$$\frac{F_{\text{magAFM}}(h_z, t \to 0)}{k_B T_{NJ}}$$

$$= \frac{U_{\text{magAFM}}(h_z, t \to 0)}{k_B T_{NJ}}$$

$$= -\frac{3S(1 + h_{A1})}{2(S+1)} \quad (h_z \leqslant h_{cAFM}). \qquad (131)$$

Thus if $h_{A1} = h_z = 0$, the free energies of the SF and AFM phases in Eqs. (130) and (131), respectively, are the same, as required. The AFM critical field h_{cAFM}, at which $\bar{\mu}_{2z} = -1$ flips to the PM state with $\bar{\mu}_{2z} = \bar{\mu}_{1z} = +1$ with increasing h_z, is determined next.

The spin-flip field to the PM state (the $t = 0$ AFM critical field h_{cAFM}) is determined by the conditions under which $\bar{\mu}^\dagger$ in Eq. (128b) goes to zero with increasing h_z. This was carried out by solving Eqs. (127b) at $t = 0.01$ for various values of S, $h_{A1} > 0$ and $-1 \leqslant f_J < 1$. In this way, we obtain

$$h_{cAFM} = \frac{3(1 + h_{A1})}{S + 1} \quad (t \to 0, \ -1 \leqslant f_J < 1), \qquad (132)$$

which is independent of f_J in the given f_J range. This expression is in agreement with our numerical data for the AFM to PM spin-flip transition field at $t \to 0$ obtained from numerical calculations such as the extrapolations to $t = 0$ in Fig. 26 above for $S = 1/2$, $f_J = -1$, and various values
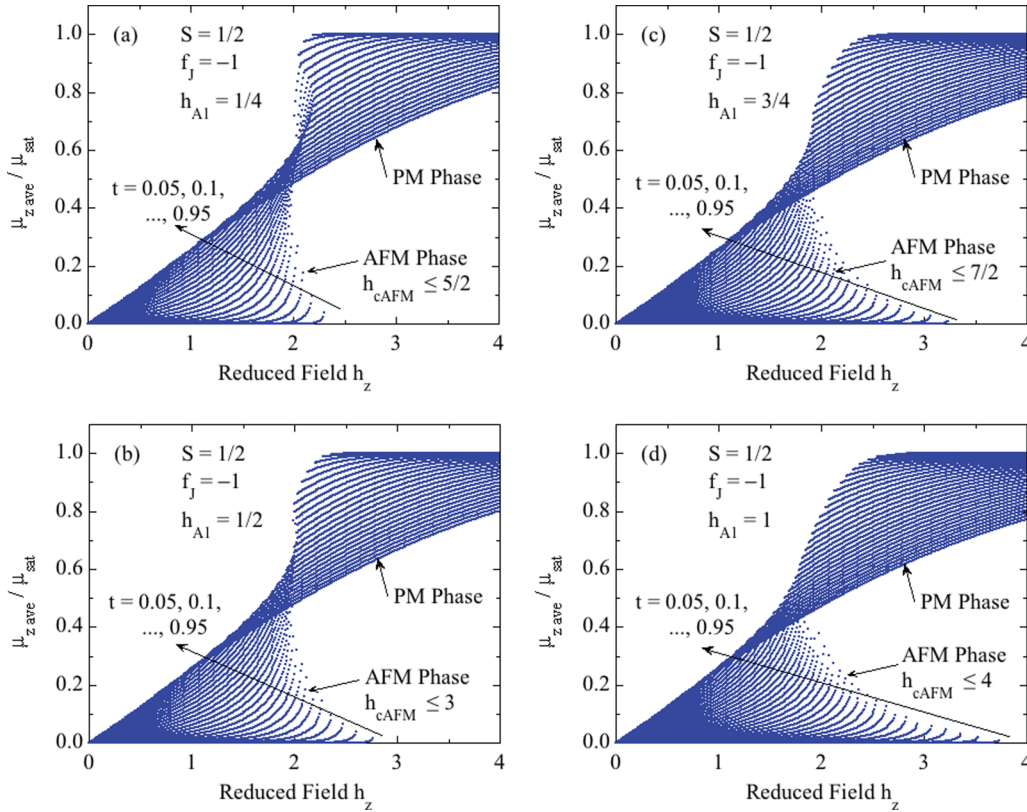
FIG. 25. Reduced average z-axis moment per spin $\bar{\mu}_{z\text{ave}} \equiv \mu_{z\text{ave}}/\mu_{\text{sat}}$ for the low-field AFM and high-field PM phases of a collinear antiferromagnet versus reduced field h_z for spin $S = 1/2$ and $f_J = -1$ at reduced temperatures $t = T/T_{NJ}$ as shown for reduced anisotropy fields (a) $h_{A1} = 1/4$, (b) 1/2, (c) 3/4, and (d) 1 calculated using Eqs. (127) and (128a).

of h_{A1}, and in the phase diagram in Fig. 32(f) below for $S = 1/2$, $f_J = -1$, and $h_{A1} = 1$.

Using Eqs. (20) and (131), we obtain the field dependence of the free energy per spin of the AFM phase (and high-field

FIG. 26. AFM critical field h_{cAFM} vs reduced temperature t_A for $S = 1/2$ with $f_J = -1$ and h_{A1} from 0 to 1 as indicated. First-order transition lines are in red without data points and second-order transitions are in other colors with data points. A tricritical point separates the first- and second-order transitions on the transition line for each $h_{A1} \geqslant 1/8$.

PM phase) as

$$\frac{F_{\text{magAFM}}(t \to 0)}{k_B T_{NJ}} = -\frac{3S(1 + h_{A1})}{2(S + 1)} \quad (h_z \leqslant h_{\text{cAFM}}), \quad (133)$$

$$\frac{F_{\text{magAFM}}(t \to 0)}{k_B T_{NJ}} = -\frac{3S(1 + h_{A1})}{2(S + 1)} - S(h_z - h_{\text{cAFM}})$$

$$(h_z \geqslant h_{\text{cAFM}}).$$

3. Comparison of the free energies of the spin-flop and antiferromagnetic phases

Figure 28 illustrates the free energies F_{mag} per spin versus reduced field h_z of the SF and AFM phases (and their high-field PM phases) for $t \to 0$, given in Eqs. (130) and (133), respectively, for $f_J = -1$ and anisotropy parameters $h_{A1} = 0$ to 1.5. For $h_{A1} = 0$, the lowest-energy phase for $h_z > 0$ is the SF phase. Upon increasing h_{A1}, one sees an evolution where the AFM phase is more stable at low fields, but transforms to the SF phase at increasing values of h_z, where the AFM to SF phase transition is first order due to the discontinuity in slope of F_{mag} versus h_z at the transition point, which corresponds to a discontinuity in the magnetization there.

Shown in Fig. 29 are zero-temperature phase diagrams in the h_z-h_{A1} plane for collinear z-axis AFMs with $f_J = -1$ and for spins $S = 1/2$ and $S = 7/2$, obtained by determining which of the AFM and SF phases (and associated high-field PM phases) has the lower free energy using Eqs. (130) and (133). One sees that the phase diagrams are the same
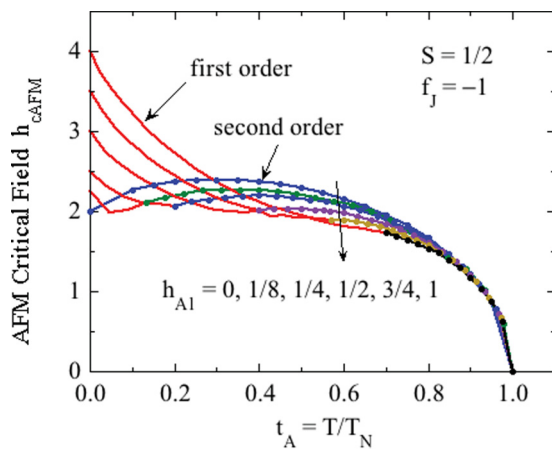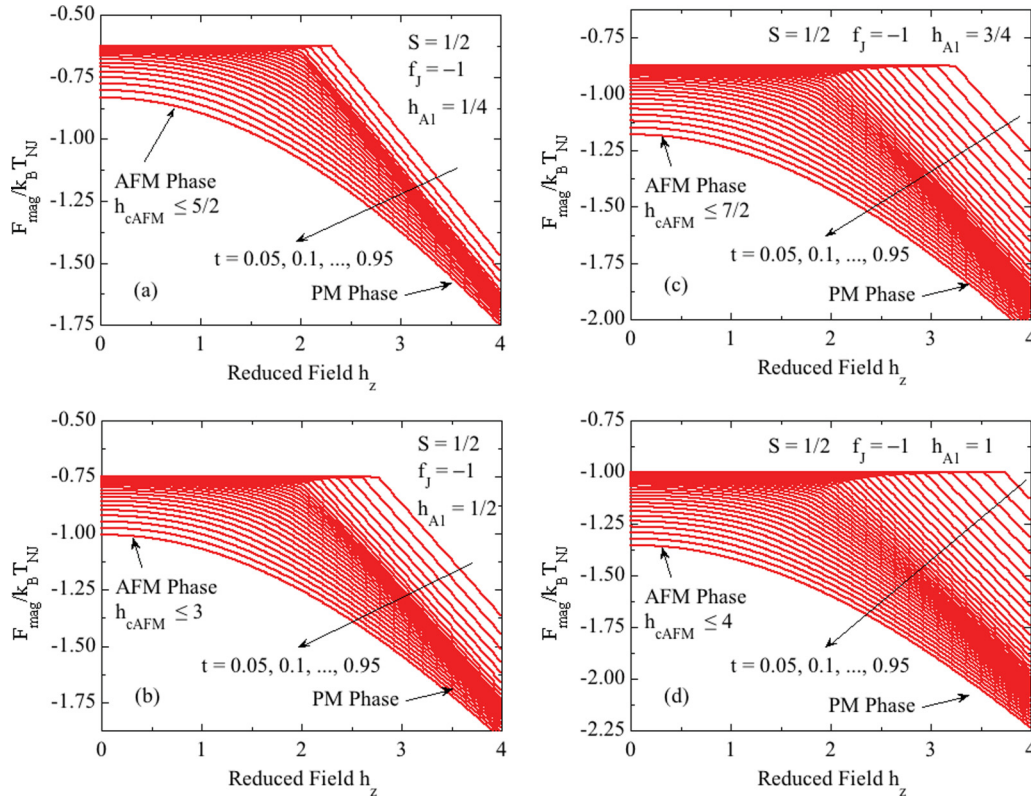
FIG. 27. Reduced magnetic free energy per spin $F_{\mathrm{mag}}/k_{\mathrm{B}}T_{\mathrm{NJ}}$ for the low-field AFM and high-field PM phases of a collinear antiferromagnet vs reduced field h_z for spin $S = 1/2$ and $f_J = -1$ at reduced temperatures $t = T/T_{\mathrm{NJ}}$ as shown for reduced anisotropy fields (a) $h_{\mathrm{A1}} = 1/4$, (b) 1/2, (c) 3/4, and (d) 1 calculated using Eqs. (20) and data such as in Fig. 25.

for $S = 1/2$ and 7/2, apart from a reduction in ordinate scale by a factor of three for $S = 7/2$ compared to that for $S = 1/2$. For $h_{\mathrm{A1}} > 1$, the AFM phase undergoes a spin-flip transition directly to the PM phase with increasing h_z, sidestepping the intermediate SF phase.

The anisotropy parameter $h_{\mathrm{A1}} = 1$ at which the h_{SF} and h_{cSF} lines meet in Fig. 29 is a point where the SF and PM phases are degenerate and hence PM, which occurs at the lower end of a vertical line in the figure. The upper end of a vertical line also corresponds to the PM phase. We thus infer that all points along a vertical line correspond to a transition line between the PM and AFM phases. Consistent with this, the region to the immediate left of a vertical line is PM and to the right is AFM. A first-order transition from the PM to the AFM phase thus occurs on crossing a vertical line with increasing h_{A1}.

The analytic behavior of the AFM-SF transition field h_{SF} for $f_J = -1$ such as in Fig. 29 in the region $0 \leqslant h_{\mathrm{A1}} \leqslant 1$ is found to be

$$h_{\mathrm{SF}} = \frac{3}{S+1}\sqrt{2h_{\mathrm{A1}} - h_{\mathrm{A1}}^2}. \tag{134}$$

However, this expression is only valid for $f_J = -1$, which corresponds to a bipartite AFM with only nearest-neighbor exchange interactions of equal value. If $f_J \neq -1$, we find

$$h_{\mathrm{SF}} = \frac{3}{S+1}\sqrt{h_{\mathrm{A1}}(1 - f_J) - h_{\mathrm{A1}}^2}, \tag{135}$$

$$0 < h_{\mathrm{A1}} < (1 - f_J)/2, \quad -3 \lesssim f_J < 1,$$

where the upper h_{A1} limit is the maximum value for which $h_{\mathrm{SF}} < h_{\mathrm{cSF}}$, the lower limit on f_J is obtained by requiring $h_{\mathrm{SF}} < h_{\mathrm{cAFM}}$ for the given h_{A1} range, and the upper limit on f_J is required for any AFM, where the value $f_J = 1$ corresponds to a FM rather than an AFM.

Thus the deviation of $f_J \equiv \theta_{\mathrm{p}J}/T_{\mathrm{NJ}}$ from the value of -1 usually assumed can have a very significant influence on the variation of h_{SF} with h_{A1} according to Eq. (135), a situation not investigated previously to our knowledge. This is important in view of the fact that within MFT one can have $-\infty < f_J < 1$ for AFMs. Indeed, most real AFMs are not bipartite with more than nearest-neighbor interactions.

The reduced fundamental exchange parameter h_{A1} is expressed in terms of the reduced exchange field h_{A0} at $T = 0$ using Eq. (31a), the $t = 0$ value $\bar{\mu}_i = 1$, and the definition in Eq. (1c) as

$$h_{\mathrm{A1}} = \frac{S+1}{3}h_{\mathrm{A0}}. \tag{136}$$

Inserting this into Eq. (134) gives

$$h_{\mathrm{SF}} = \sqrt{2\left(\frac{S+1}{3}\right)h_{\mathrm{A0}} - h_{\mathrm{A0}}^2}. \tag{137}$$

Now using Eq. (A13) for the exchange field together with Eq. (1c) gives the reduced exchange field at $T = 0$ as
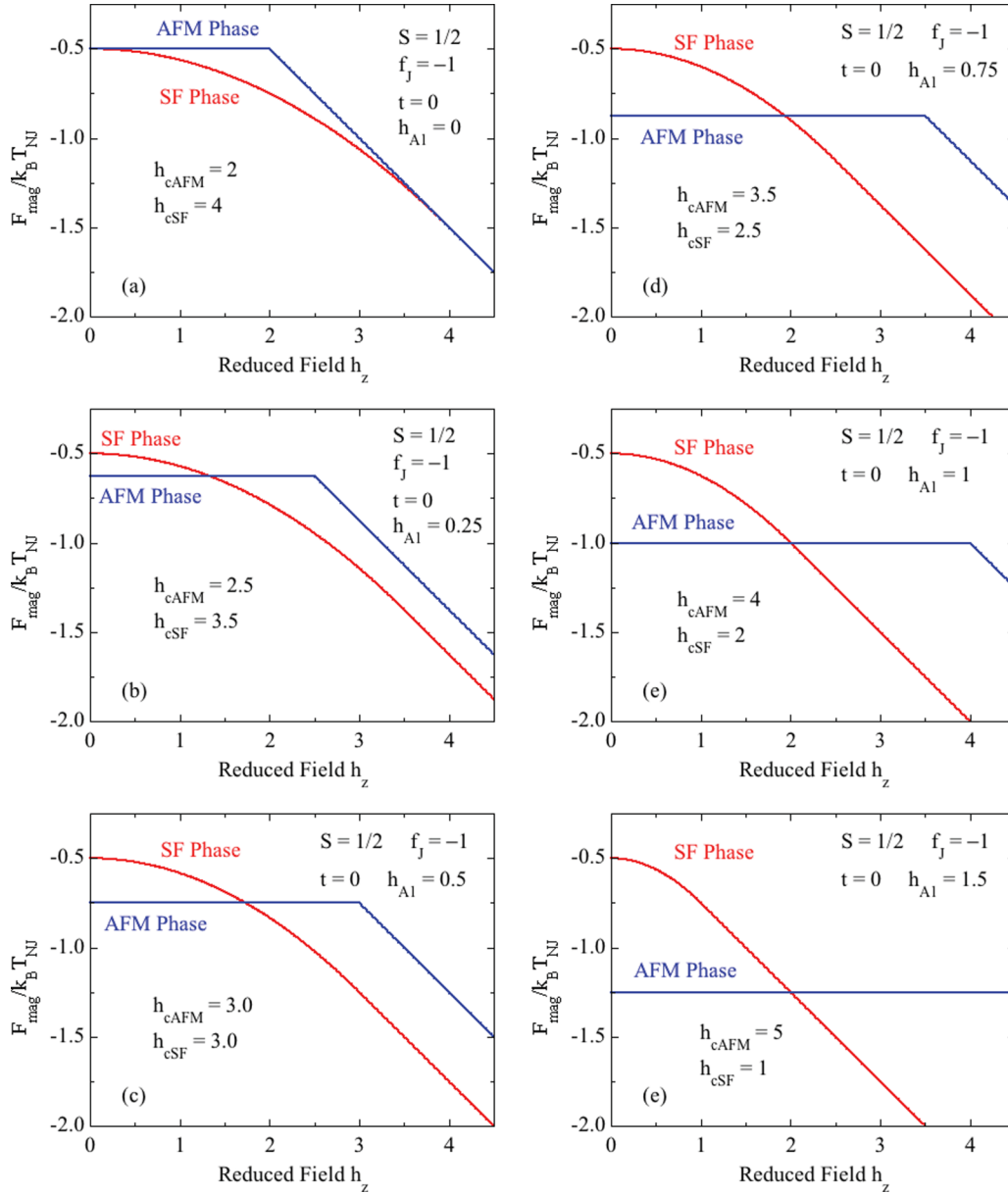
$$h_{\mathrm{exch0}} = \frac{S+1}{3}. \tag{138}$$

FIG. 28. Reduced free energy $F_{\rm mag}/k_B T_{NJ}$ at reduced temperature $t \to 0$ vs reduced magnetic field h_z for collinear z-axis AFMs with spin $S = 1/2$ and reduced anisotropy fields h_{A1} of (a) 0, (b) 1/4, (c) 1/2, (d) 3/4, (e) 1, and (f) 3/2. The phases in competition are the collinear antiferromagnetic (AFM) and spin-flop (SF) phases. The PM phases occur above the respective critical fields of the AFM and SF phases as listed. The data were calculated from Eqs. (130) and (133).

Substituting this into Eq. (137) gives

$$h_{\rm SF} = \sqrt{2h_{\rm exch0}h_{A0} - h_{A0}^2} . \tag{139}$$

In terms of the unreduced fields, one has

$$H_{\rm SF} = \sqrt{2H_{\rm exch0}H_{A0} - H_{A0}^2} . \tag{140}$$

This expression is identical to the standard equation for $H_{\rm SF}$ obtained using spin-wave theory assuming $f_J = -1$ [9]. A more accurate expression obtained from Eq. (135) is

$$H_{\rm SF} = \sqrt{H_{\rm exch0}H_{A0}(1 - f_J) - H_{A0}^2} . \tag{141}$$

As noted previously, $f_J < 1$ for an AFM.

4. Magnetization versus field

The magnetization of the SF phase is proportional to field according to Eq. (103a), which at $T = 0$ reads

$$\bar{\mu}_z = \frac{h_z}{h_{\rm cSF}} \quad (h_z \leqslant h_{\rm cSF}), \tag{142}$$

where the spin-flop critical field is given by Eq. (114) with $\bar{\mu}_{\rm SF} = 1$ at $T = 0$ as

$$h_{\rm cSF} = \frac{3(1 - f_J - h_{A1})}{S + 1} . \tag{143}$$

According to Eqs. (135), if $h_{A1} > (1 - f_J)/2$ the AFM phase undergoes a first-order transition with $\bar{\mu}_{z\rm ave} = 0$ to the fully saturated PM state with $\bar{\mu}_{z\rm ave} = 1$ at the $T = 0$ transition field

FIG. 30. Reduced z-axis moment $\bar{\mu}_z \equiv \mu_z/\mu_{\text{sat}}$ per spin vs reduced field $h_z = g\mu_B H_z/k_B T_{NJ}$ for spins $S = 1/2$ at zero temperature for anisotropy parameters h_{A1} as listed and $f_J \equiv \theta_{pJ}/T_{NJ} = -1$.
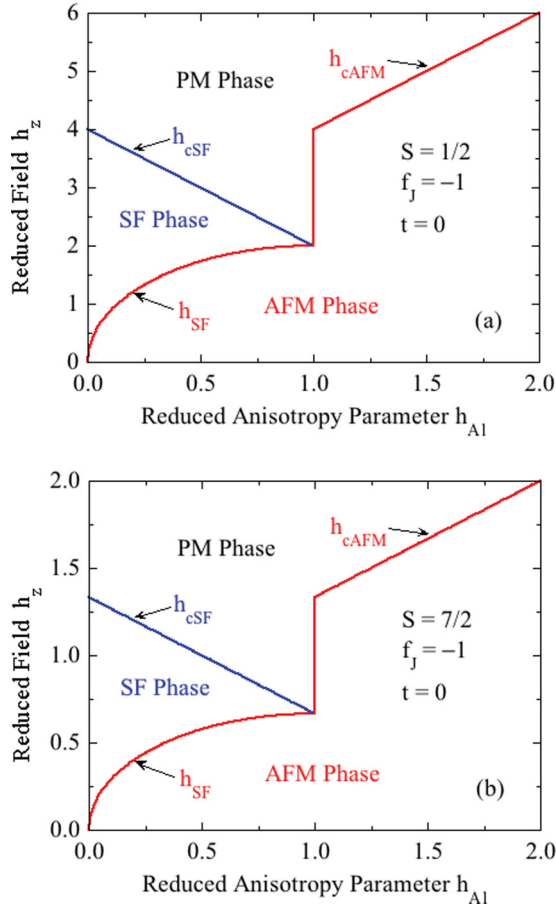

FIG. 29. Zero-temperature phase diagrams in the h_z-h_{A1} plane for collinear z-axis AFMs with $f_J = -1$ and for spins (a) $S = 1/2$ and (b) 7/2. The phases in competition are the collinear z-axis antiferromagnetic (AFM) and canted spin-flop (SF) phases, with the paramagnetic (PM) phase in each case above the respective critical field h_{cAFM} and h_{cSF}. Note that the ordinate axes are different for the two spin values. The transitions from AFM to PM and AFM to SF are first order, and from SF to PM are second order. The vertical transition lines separate the PM phase from the AFM phase, with a first-order transition occurring upon traversing the lines horizontally.

$h_z = h_{cAFM}$ in Eq. (132), whereas if $h_{A1} < (1 - f_J)/2$, the AFM state instead has a first-order transition to the SF phase at h_{SF} until the SF phase saturates at $h_z = h_{cSF}$ to $\bar{\mu}_z = 1$ after which it remains constant at $\bar{\mu}_z(h_z) = 1$. With these criteria, the $\bar{\mu}_z(h_z)$ behaviors were determined as shown in Fig. 30 for $S = 1/2$, $f_J = -1$ and a range of h_{A1} values from 0.02 to 0.9 as shown. Changing the value of f_J results in no qualitative change in the $\bar{\mu}_z$ versus h_z plots, but where the corresponding ranges of h_{A1} values and ordinate scales giving similar-looking plots as in Fig. 30 are changed appropriately.

5. *Perpendicular magnetic fields*

When the applied field is perpendicular to the easy axis or easy plane of a collinear or noncollinear AFM as shown in Fig. 10, only one transition versus field occurs which is a second-order transition from the canted AFM phase to the PM phase at the perpendicular critical field $h_{c\perp AFM}$ given by
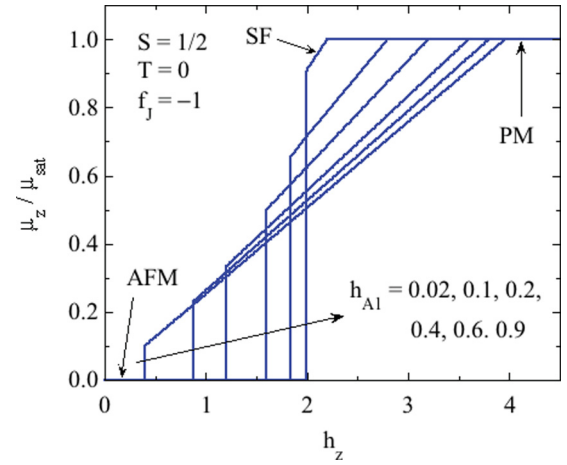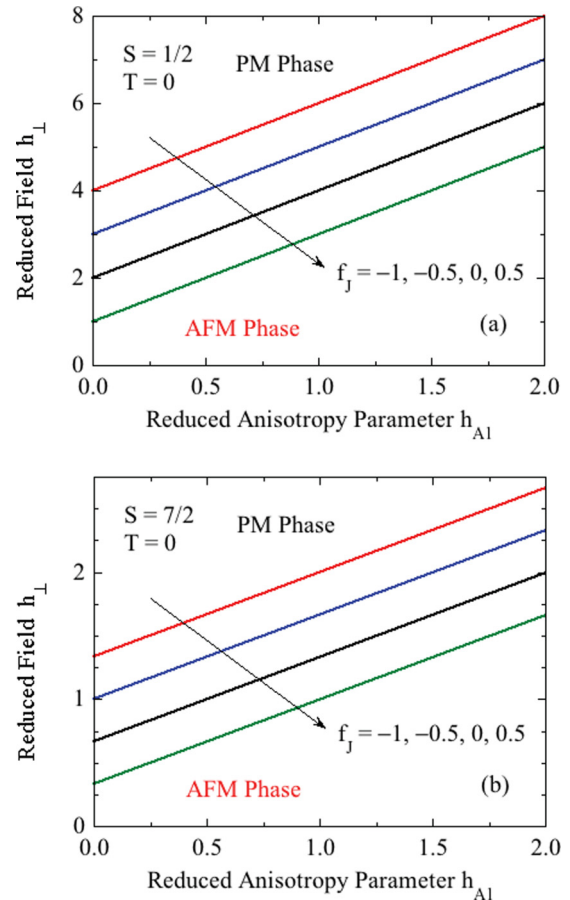

FIG. 31. Zero-temperature phase diagrams in the $h_\perp$-h_{A1} plane for collinear z-axis AFMs with $f_J = -1$ to 0.5 and for spins (a) $S = 1/2$ and (b) 7/2. The phases in competition are the canted antiferromagnetic (AFM) and the paramagnetic (PM) phase that occurs above the respective critical field $h_{c\perp}$. The plots are drawn according to Eq. (144). The ordinate axes are different for the two spin values. The transitions from canted AFM to PM are second order.
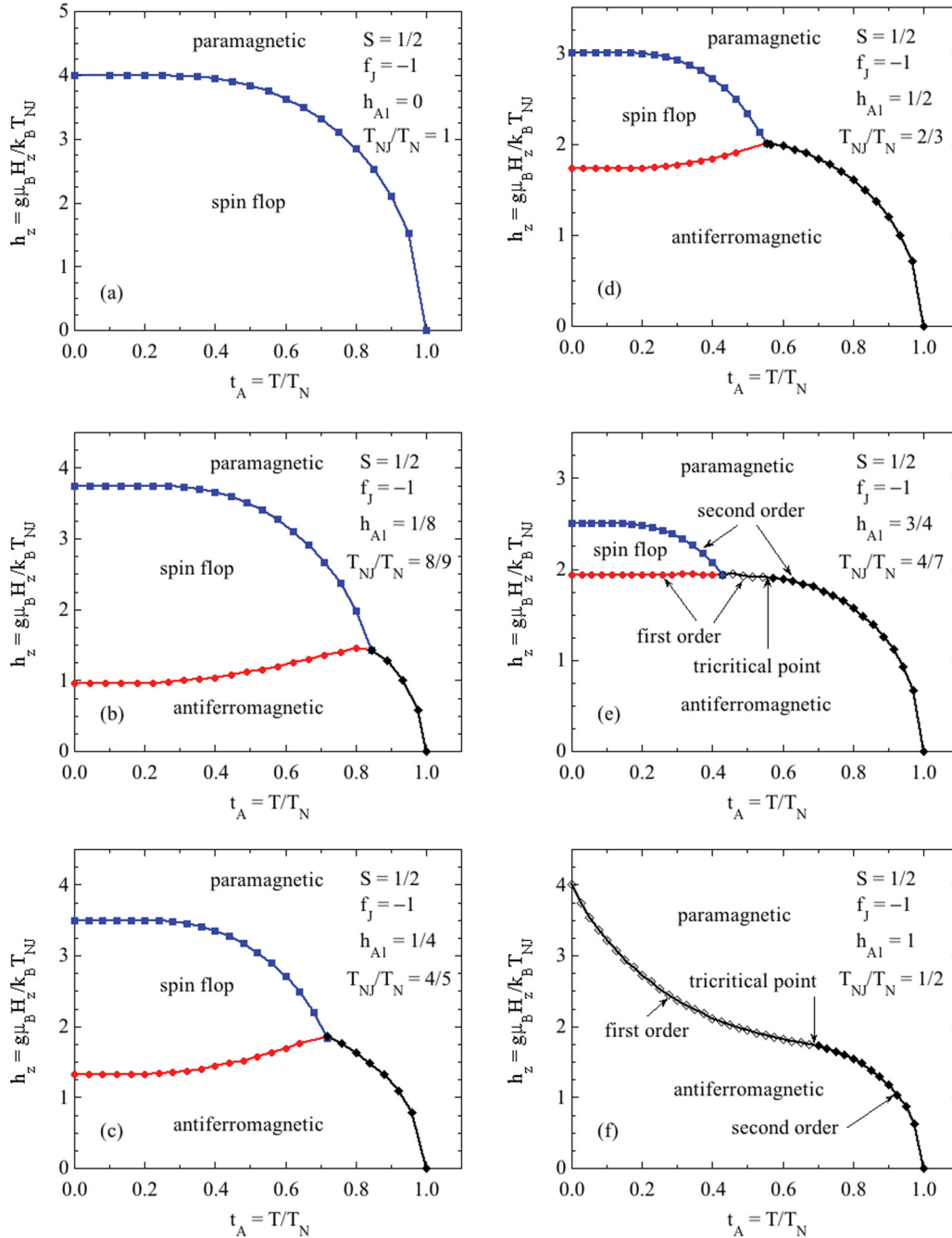
FIG. 32. Reduced parallel magnetic field h_z vs reduced temperature t_A phase diagrams for spin $S = 1/2$ and reduced anisotropy fields h_{A1} equal to (a) 0, (b) 1/8, (c) 1/4, (d) 1/2, (e) 3/4, and (f) 1 obtained from numerical calculations. The SF to PM transitions are second order and the AFM to SF transitions are first order. The AFM to PM transitions can be second order [(a)–(d)], or both first and second orders in different field ranges separated by a tricritical point [(e) and (f)]. The lines are guides to the eye.

Eq. (86) at $T = 0$ as

$$h_{c \perp AFM0} = \left(\frac{3}{S + 1} \right) (1 + h_{A1} - f_J). \qquad (144)$$

The phase diagrams in the $h_\perp$-h_{A1} plane for spins $S = 1/2$ and $7/2$ are shown in Fig. 31, where the AFM-PM transition lines vary linearly with h_{A1} for each value of S and f_J.

B. Field versus temperature phase diagrams for fields along the easy axis of collinear antiferromagnets

In order to determine the phase diagrams in the field versus temperature plane for given values of S, f_J, and h_{A1}, one must determine which of the AFM or SF phases and associated PM phases have the lowest free energy at each temperature and field for given values of S, h_{A1}, and f_J using information such as illustrated above in Figs. 21 and 27. The transitions from the AFM to the SF phase are always first order. For transitions

of the SF or AFM phase to the associated PM phase, the transition field is determined as the field at which the angle $\theta \to 0$ or $\mu_z^\dagger \to 0$, respectively. First-order transitions have discontinuities in these quantities on crossing a transition line.

Shown in Fig. 32 are the h_z versus t_A phase diagrams for $S = 1/2$, $f_J = -1$, and six values of the reduced anisotropy parameter h_{A1} from 0 to 1. The phase diagrams were initially constructed versus $t = T/T_{NJ}$ but the abscissa was then converted to $t_A = T/T_N$ using Eq. (1j). The $t = 0$ transition fields obtained from Fig. 29 are included in Fig. 32. For $h_{A1} = 0$, the phase diagram contains no z-axis-aligned AFM phase because for any finite field the ordered moments flop to form a canted AFM phase, the spin-flop phase. Even a rather small value $h_{A1} = 1/8$ gives rise to a SF phase in a large area of the phase diagram in Fig. 32(b) and a bicritical point appears where the AFM, SF, and PM phase lines meet. With further increase of h_{A1}, the SF phase region shrinks, as shown for $h_{A1} = 1/4$, $1/2$, and $3/4$ in Figs. 32(c)–32(e). In addition, for $h_{A1} = 3/4$, a tricritical point occurs at $t_A \approx 0.56$ separating second- and first-order AFM to PM transitions, as shown. Finally, for $h_{A1} = 1$ in Fig. 32(f), the spin-flop region disappears and the tricritical point moves to higher temperature with respect to T_N compared to that for $h_{A1} = 3/4$. We note that in Fig. 32(e) for $h_{A1} = 1$, the $T = 0$ value of the AFM to PM transition field is larger than for lower h_{A1} values at higher temperatures, and is the same as the $T = 0$ value of the SF to PM transition field for $h_{A1} = 0$ in Fig. 32(a).

In a spin-flop transition of an otherwise collinear antiferromagnet, the spins flop from alignment along the z axis to what is generally thought to be an approximately perpendicular orientation. An interesting question is how close to a $\theta = 90°$ angle the moments in the SF phase make with the z axis (θ_{SF}) on the (first-order) transition line between the AFM and SF phases. Shown in Fig. 33 are plots of θ_{SF} versus reduced temperature t_A for the parameters in the phase diagrams in Figs. 32(b)–32(e). These data were obtained as part of the calculations required to construct the phase diagrams in Fig. 32. One sees rather strong dependencies of θ_{SF} on both t_A and the anisotropy parameter h_{A1}. Futhermore, the maximum angle of the moments from the z axis on the transition line versus temperature depends strongly on h_{A1}, varying from only about $40°$ for $h_{A1} = 3/4$ to about $77°$ for $h_{A1} = 1/8$. Thus when a spin-flop transition occurs, the angle that the moments make with the z axis is generally not close to $90°$. According to Fig. 33, this discrepancy increases with increasing h_{A1}.

C. Magnetization versus field isotherms for fields along the easy axis of collinear antiferromagnets

High-field magnetization versus field $M(H)$ isotherm measurements are basic to characterizing the magnetic properties of AFMs. Here we utilize the above information specifying the conditions for phase transitions between the AFM, SF, and PM phases with fields along the easy z axis to calculate magnetization versus field data at particular temperatures below the respective T_N. These calculations allow direct comparisons to experimental $M_z(H)$ data on single crystals.

For anisotropy parameter $h_{A1} = 0$, for the spin-flop phase plots of $\bar{\mu}_{zSF}$ versus h_z for a fixed temperature $t_A \equiv T/T_N = 1/2$ and a selection of anisotropy parameters $h_{A1} = 0$ to 1
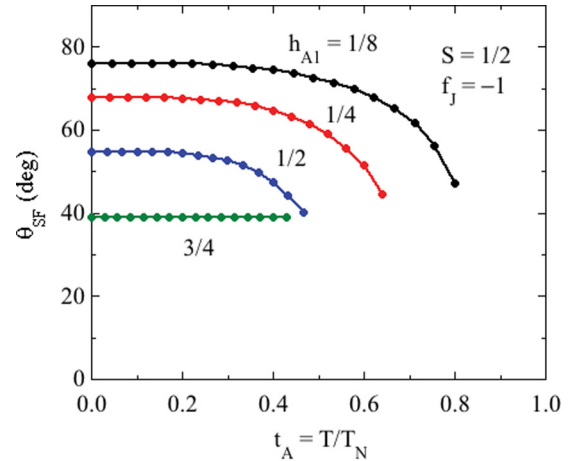

FIG. 33. The angle θ_{SF} that the ordered moments in the spin-flop phase make with the applied field along the z axis on the first-order transition line between the AFM and SF phases in Fig. 32 vs reduced temperature t_A for the same reduced anisotropy parameters h_{A1} for which the phase diagrams in Figs. 32(b)–32(e) were constructed.

were presented in Fig. 18 for spins $S = 1/2$ and $7/2$, which included both the SF and PM regimes. Plots of $\bar{\mu}_{zSF}$ versus h_z for fixed $h_{A1} = 1/2$ with different values of $t = T/T_{NJ}$ were presented in Fig. 16 for $S = 1/2$, 2, and $7/2$.

The behaviors of $\bar{\mu}_z$ versus h_z for $S = 1/2$ and $f_J = -1$ were calculated for values of t_A from ~ 0.1 to 0.9 and h_{A1} values in the range $1/4 \leqslant h_{A1} \leqslant 1$, including the influence of phase transitions as applicable. The calculations are shown in Fig. 34, where the first or second-order nature of the phase transitions are reflected in the field dependence of the magnetization.

D. Phase diagrams for fields perpendicular to the easy axis or plane of collinear or planar noncollinear antiferromagnets

The critical field $h_{c\perp AFM}$ dividing the canted AFM from the PM state of collinear or planar noncollinear AFMs versus reduced anisotropy h_{A1} and f_J parameters for fields perpendicular to the easy axis or plane of collinear or planar noncollinear AFMs is given in Eq. (86). Plots of $h_{c\perp AFM}$ versus t_A are shown in Fig. 35 for the same values of h_{A1} for which the phase diagrams in Fig. 32 were constructed. From a comparison of the two figures, one sees that for each value of $h_{A1} > 0$, the $h_{c\perp AFM}(t_A)$ value in Fig. 35 lies at a higher field than the maximum transition field in Fig. 32 at the same temperature.

XI. SUMMARY

The main purpose of this work is to enable an estimate of the amount of uniaxial or planar anisotropy that exists in an otherwise isotropic Heisenberg spin system to be made from experimental magnetic susceptibility and/or high-field magnetization data. The systems described contain identical crystallographically equivalent spins. Another important goal was to provide a classical description of magnetic anisotropy of quantum $S = 1/2$ systems for which quantum uniaxial DS_z^2 single-ion anisotropy is not applicable. In this paper, the
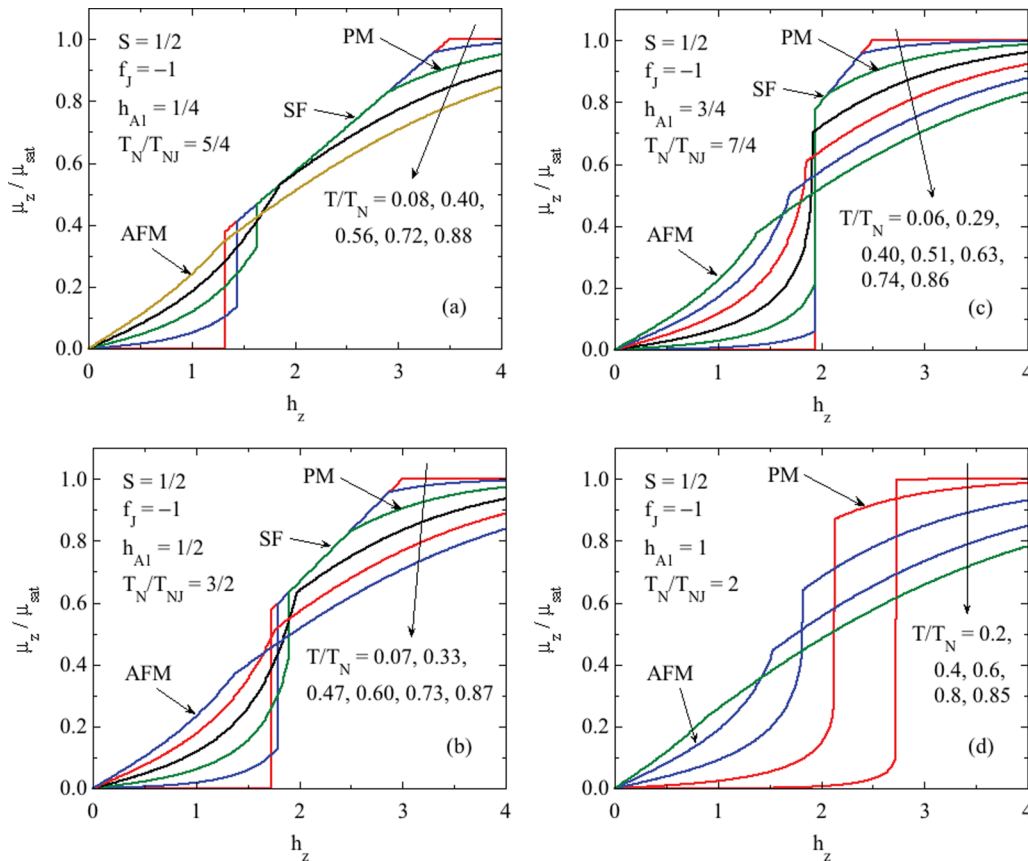
FIG. 34. Reduced z-axis magnetic moment $\bar{\mu}_z \equiv \mu_z/\mu_{sat}$ vs reduced magnetic field $h_z = g\mu_B H_z/k_B T_{NJ}$ at the listed reduced temperatures $t_A = T/T_N$ for spins $S = 1/2$, $f_J = -1$ and with reduced anisotropy parameters h_{A1} equal to (a) 1/4, (b) 1/2, (c) 3/4, and (d) 1. The SF to PM transitions are second order and the AFM to SF transitions are first order. The AFM to PM transitions can be second order [(a) and (b)], or either first or second order in different field ranges separated by a tricritical point [(c) and (d)] (see the phase diagram in Fig. 32).

anisotropy is quantified by the fundamental reduced anisotropy parameter h_{A1} in Eq. (1e), which depends on S and the unreduced anisotropy field H_{A1}, normalized by the Néel temperature in the absence of anisotropy T_{NJ}, but not on the
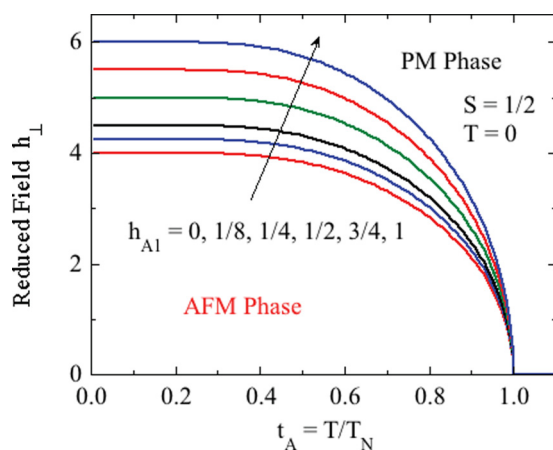

FIG. 35. Phase diagram in the reduced perpendicular field $h_\perp$ vs reduced temperature t_A plane for easy-axis or easy-plane collinear or planar noncollinear AFMs. Plots of data obtained using Eq. (86) are shown for the same values of reduced anisotropy parameter h_{A1} for which the phase diagrams in Fig. 32 were constructed.

temperature T. The T dependence of the anisotropy field is included via the T dependence of the reduced ordered and/or field-induced moment $\bar{\mu}$ in Eq. (31a). The present treatment is strictly valid for local-moment antiferromagnets but not for itinerant ones.

There are several ways to extract h_{A1} from experimental data for single crystals of local-moment collinear antiferromagnets with uniaxial or planar anisotropy. Indeed, if one has single-crystal low-field magnetic susceptibility versus temperature data as well as high-field magnetization isotherm data, this parameter is overdetermined and one can compare the values obtained from analyses of the respective data sets. Since g anisotropy is not included in the present treatment, the single-spin Curie constant C_1 in the Curie-Weiss law (A1) is the same for fields parallel and perpendicular to the easy axis or easy plane for the known value of S. However, g anisotropy for the AFM and PM phases is easily accomplished by substituting the appropriate values of g_α for g in the expression for the Curie constant if the values of g_α are known from independent measurements such as electron spin resonance.

A. Analysis of single-crystal magnetic susceptibility data

An easy way to determine h_{A1} is to measure the anisotropy of the Weiss temperature θ_p in the Curie-Weiss law (A1) for the paramagnetic susceptibility at $T \geqslant T_N$ of single crystals.

Here we only consider uniaxial z-axis anisotropy, since xy-plane anisotropy gives the same expression for h_{A1}. From Eqs. (48) and (51), respectively, the Weiss temperatures in the Curie-Weiss law for the xy plane and z-axis field directions at temperatures $T \geqslant T_N$ are

$$\theta_{pxy} = \theta_{pJ}, \tag{145a}$$

$$\theta_{pz} = \theta_{pJ} + h_{A1}T_{NJ}, \tag{145b}$$

so

$$\theta_{pz} - \theta_{pxy} = h_{A1}T_{NJ}. \tag{146}$$

Then using Eq. (1i), one obtains

$$\theta_{pz} - \theta_{pxy} = \frac{h_{A1}T_N}{1 + h_{A1}}, \tag{147}$$

which allows one to easily solve for h_{A1} from the two measured Weiss temperatures and the measured Néel temperature T_N.

Another parameter of the theory is $f_J \equiv \theta_{pJ}/T_{NJ}$, the ratio of the Weiss and Néel temperatures due to exchange interactions alone. This is not measurable directly but can be derived as follows. Using Eqs. (1i) and (145a), one obtains

$$\frac{\theta_{pxy}}{T_N} = \frac{\theta_{pJ}}{T_{NJ}(1 + h_{A1})} = \frac{f_J}{1 + h_{A1}}, \tag{148}$$

from which f_J can be obtained using h_{A1} from above.

Another expression useful for determining the values of h_{A1} and f_J for collinear z-axis AFMs is Eq. (79c), which gives

$$\frac{\chi_z(T_N)}{\chi_{xy}(T_N)} = 1 + \frac{h_{A1}}{1 - f_J}. \tag{149}$$

Thus any of the combinations of two of Eqs. (146), (148), and (149) can be used to solve for h_{A1} and f_J. Self-consistency can be checked by comparing the derived sets with each other, and/or with values derived from high-field magnetization data for collinear AFMs as described in the following section.

B. Analysis of high-field z-axis magnetization data

According to Figs. 4 and 15 for AFM and SF phases, respectively, for $T \lesssim 0.2\,T_N$ the zero-field reduced ordered moment is nearly saturated at the value of unity, irrespective of the spin value. It is this low-temperature range of collinear antiferromagnets aligned along the z axis for which the high-field behavior is examined in this section.

For $h_{A1} > 0$, according to Eq. (135) and Figs. 30 and 34(a)–34(c), a spin-flop (SF) transition from the AFM phase to the SF phase occurs at the reduced SF field

$$h_{SF} = \frac{3}{S + 1}\sqrt{h_{A1}(1 - f_J - h_{A1})}. \tag{150}$$

This transition is easy to see in $M_z(H)$ isotherm measurements because it is first order. In the SF phase, the magnetization is proportional to field according to Eq. (129c), which we reproduce here:

$$\bar{\mu}_z(h_z, t \to 0) = \begin{cases} h_z/h_{cSF} & (h_z \leqslant h_{cSF}) \\ 1 & (h_z \geqslant h_{cSF}), \end{cases} \tag{151a}$$

where the SF critical field at which the SF phase undergoes a second-order transition to its PM phase is

$$h_{cSF} = \frac{3(1 - f_J - h_{A1})}{S + 1}. \tag{151b}$$

From Eqs. (150) and (151b), one has the ratio

$$\frac{h_{cSF}}{h_{SF}} = \sqrt{\frac{1 - f_J - h_{A1}}{h_{A1}}}. \tag{152}$$

Thus if both h_{cSF} and h_{SF} can be measured at low temperatures, an additional equation that does not involve the spin S is available to solve for f_J and h_{A1}.

For $h_z < h_{cSF}$, the reduced single-spin susceptibility $\bar{\chi}_{zSF}$ for the spin-flop phase is given by Eq. (106) as

$$\bar{\chi}_{zSF} \equiv \frac{\chi_{zSF}T_{NJ}}{C_1} = \frac{1}{1 - f_J - h_{A1}}, \tag{153}$$

where the single-spin Curie constant given in Eq. (A1b) is assumed to be known from the fit of the high-temperature susceptibility by the Curie-Weiss law, $T_{NJ} = T_N/(1 + h_{A1})$ from Eq. (1i) and χ_{zSF} is often measurable at fields above h_{SF} if the SF transition is observed.

C. Analysis of high-field perpendicular magnetization data

The present section discusses the magnetic response to high fields applied perpendicular to the easy axis or plane of a collinear or planar noncollinear antiferromagnet. The reduced perpendicular susceptibility per spin $\bar{\chi}_{\perp AFM}$ is given by Eq. (84) as

$$\frac{\chi_{\perp AFM}T_{NJ}}{C_1} = \frac{1}{1 - f_J + h_{A1}}. \tag{154}$$

Comparing this equation with Eq. (153) shows that $\chi_{\perp AFM} < \chi_{zSF}$, with

$$\frac{\chi_{\perp AFM}}{\chi_{zSF}} = \frac{1 - f_J - h_{A1}}{1 - f_J + h_{A1}}. \tag{155}$$

Finally, the critical field for the AFM to PM transition, if it occurs instead of a transition to a SF phase, is given by Eq. (87) as

$$h_{c\perp AFM} = \frac{3(1 - f_J + h_{A1})}{S + 1}. \tag{156}$$

This field is somewhat larger than h_{cSF} in Eq. (151b), the difference being

$$h_{c\perp AFM} - h_{cSF} = \frac{3h_{A1}}{S + 1}. \tag{157}$$

This expression is very useful because it does not contain f_J. The drawback is that these two critical fields are often too large to measure except for materials with low T_N. Alternatively, the ratio of the two critical fields is

$$\frac{h_{cSF}}{h_{c\perp AFM}} = \frac{H_{cSF}}{H_{c\perp AFM}} = \frac{1 - f_J - h_{A1}}{1 - f_J + h_{A1}}. \tag{158}$$

The right side is the inverse of the respective ratio of the susceptibilities obtained from Eq. (155).

D. Comparison of classical anisotropy with quantum DS_z^2 anisotropy predictions

Finally, we compare the predictions of the present work for T_N and θ_p with those for quantum DS_z^2 anisotropy [4]. In the present case, the Néel temperature is simply described by Eq. (1i) as

$$T_N = T_{NJ}(1 + h_{A1}), \qquad (159)$$

which is a linear function of h_{A1} irrespective of its value. However, for $-DS_z^2$ anisotropy, where a positive sign of D is defined such that z-axis collinear AFM ordering is favored over xy-plane ordering, and with $d \equiv D/k_B T_{NJ}$, one obtains a nonlinear dependence of T_N on d. On the other hand, for small d one obtains [4]

$$T_N = T_{NJ}\left[1 + \frac{d(2S-1)(2S+3)}{15}\right]. \qquad (160)$$

In contrast to Eq. (159), this linear dependence on d also depends explicitly on S for $S \geqslant 1$. Comparison of Eqs. (159) and (160) indicates that for weak anisotropy one can relate the anisotropy parameters in the present classical anisotropy model to that in the quantum $-DS_z^2$ model for $S \geqslant 1$ by

$$h_{A1} = \frac{d(2S-1)(2S+3)}{15}. \qquad (161)$$

Similarly, the Weiss temperature in the Curie-Weiss law with the field applied along the easy axis of a uniaxial antiferromagnet is given by Eq. (51d) as

$$\theta_p = \theta_{pJ} + T_{NJ}h_{A1}. \qquad (162)$$

In the case of uniaxial DS_z^2 anisotropy, one also obtains a linear dependence on d given by [4]

$$\theta_p = \theta_{pJ} + T_{NJ}\frac{d(2S-1)(2S+3)}{15}, \qquad (163)$$

where here again the second term depends on S, is zero for $S = 1/2$, and gives the same correspondence as in Eq. (161).

ACKNOWLEDGMENTS

APPENDIX: UNIFIED MOLECULAR-FIELD THEORY IN THE ABSENCE OF ANISOTROPY

Here we review the properties of Heisenberg AFMs within the context of the unified MFT [4–6] in the absence of any type of anisotropy that are needed for the theoretical development in the presence of classical anisotropy fields. All spins are assumed to be identical and crystallographically equivalent.

1. Curie-Weiss law

The Curie-Weiss law for the magnetic susceptibility χ_α in the paramagnetic (PM) state in the α principal-axis direction

at temperatures $T \geqslant T_N$, where T_N is Néel temperature resulting from the combined influences of the anisotropy and Heisenberg exhange interactions, is written for a representative spin by

$$\chi_\alpha = \frac{C_1}{T - \theta_{p\alpha}}, \qquad (A1a)$$

where the Weiss temperature $\theta_{p\alpha}$ depends in general on α,

$$C_1 = \frac{g^2 S(S+1)\mu_B^2}{3k_B} \qquad (A1b)$$

is the single-spin Curie constant, g is the spectroscopic splitting factor (g factor), μ_B is the Bohr magneton and k_B is Boltzmann's constant. For simplicity it is assumed in this paper that the g factor is isotropic. For moments that are aligned along a principal axis α, g can be replaced by a variable g_α in the respective equations. Here we consider isotropic Weiss temperatures arising from exchange interactions only, denoted as θ_{pJ}.

2. Exchange field

In MFT, one replaces the sum of the Heisenberg exchange interactions acting on a representative central spin i by an effective magnetic field called the Weiss molecular field or "exchange field" $\mathbf{H}_{\text{exch}i}$ and treats it as an applied field where the exchange energy $E_{\text{exch}i}$ for spin i is

$$E_{\text{exch}i} = -\vec{\mu}_i \cdot \mathbf{H}_{\text{exch}i}. \qquad (A2)$$

Taking into account the exchange interactions of $\vec{\mu}_i$ with all neighbors $\vec{\mu}_j$ with which it interacts, the exchange field is given in general by

$$\mathbf{H}_{\text{exch}i} = -\frac{1}{g^2\mu_B^2}\sum_j J_{ij}\vec{\mu}_j, \qquad (A3)$$

where J_{ij} is the Heisenberg exchange interaction between spins i and j and a positive (negative) value corresponds to an AFM (ferromagnetic FM) interaction. Since all magnetic moments are assumed to be identical and in crystallographically equivalent positions in the lattice, each spin has the same local exchange field in $\mathbf{H} = 0$, irrespective of the orientation of the spin with respect to those of the other spins in the system. The component of $\mathbf{H}_{\text{exch}i}$ in the direction of $\vec{\mu}_i$ is

$$H_{\text{exch}i} = \hat{\mu}_i \cdot \mathbf{H}_{\text{exch}i} = -\frac{1}{g^2\mu_B^2}\sum_j J_{ij}\mu_j\cos\alpha_{ji}, \qquad (A4)$$

where α_{ji} is the angle between $\vec{\mu}_j$ and $\vec{\mu}_i$ when $H \neq 0$. If $H = 0$ we denote these angles instead by ϕ_{ji}.

In the ordered magnetic state in $\mathbf{H} = 0$, the component of the local $\mathbf{H}_{\text{exch}i0}$ in the direction of $\vec{\mu}_i$, and also its magnitude, is

$$H_{\text{exch}0} = -\frac{\mu_0}{g^2\mu_B^2}\sum_j J_{ij}\cos\phi_{ji}, \qquad (A5)$$

where we dropped the subscript i because of the equivalence of each moment in $H = 0$ and μ_0 is the magnitude of the T-dependent ordered moment in $\mathbf{H} = 0$, which is the same for all spins because of their crystallographic equivalence.

3. Antiferromagnetic ordering

For $H \to 0$, the AFM ordering temperature $T_{\mathrm{N}J}$ and the Weiss temperature $\theta_{\mathrm{p}J}$ in the Curie-Weiss law (A1) due to exchange interactions alone are respectively given by

$$T_{\mathrm{N}J} = -\frac{S(S+1)}{3k_{\mathrm{B}}} \sum_j J_{ij} \cos\phi_{ji}, \tag{A6a}$$

$$\theta_{\mathrm{p}J} = -\frac{S(S+1)}{3k_{\mathrm{B}}} \sum_j J_{ij}, \tag{A6b}$$

where the sums are over all neighbors j of a given central spin i, the subscript J on the left sides signifies that these quantities arise from exchange interactions only, and ϕ_{ji} is the angle between moments j and i in the AFM structure at $T < T_{\mathrm{N}J}$ with $H = 0$. The ratio f_J is defined as

$$f_J \equiv \frac{\theta_{\mathrm{p}J}}{T_{\mathrm{N}J}} = \frac{\sum_j J_{ij}}{\sum_j J_{ij} \cos\phi_{ji}}, \tag{A7}$$

where to obtain the second equality Eqs. (A6) were used. For a FM, $\phi_{ji} = 0$ for all j, and hence $f_J = 1$. For AFMs, at least one of the J_{ij} must be positive (AFM interaction) and at least one of the $\phi_{ji} \neq 0$, leading to $f_J < 1$. Thus within MFT, for AFM ordering one has

$$-\infty < f_J < 1. \tag{A8}$$

By comparing Eqs. (A5) and (A6a), one can write the zero-field exchange field $\mathbf{H}_{\mathrm{exch0}}$ seen by each magnetic moment $\vec{\mu}_{i0}$ as

$$\mathbf{H}_{\mathrm{exch}\,i0} = \frac{3k_{\mathrm{B}}T_{\mathrm{N}J}\vec{\mu}_{i0}}{g^2\mu_{\mathrm{B}}^2 S(S+1)} = \frac{T_{\mathrm{N}J}}{C_1}\vec{\mu}_{i0},$$

$$H_{\mathrm{exch0}} = \frac{3k_{\mathrm{B}}T_{\mathrm{N}J}\mu_0}{g^2\mu_{\mathrm{B}}^2 S(S+1)} = \frac{T_{\mathrm{N}J}}{C_1}\mu_0, \tag{A9}$$

where the single-spin Curie constant C_1 is defined in Eq. (A1b).

Within MFT the thermal-average ordered and/or field-induced magnetic moment $\vec{\mu}_i$ is in the direction of its local magnetic induction $\mathbf{B}_i = \mathbf{H}_{\mathrm{exch}i} + \mathbf{H}$. When a classical anisotropy field is present, one adds $\mathbf{H}_{\mathrm{A}i}$ to this. The magnitude μ_i of $\vec{\mu}_i$ in that direction is determined using the Brillouin function $B_S(y)$ according to the self-consistency requirement

$$\mu_i = \mu_{\mathrm{sat}} B_S(y_i), \tag{A10a}$$

where

$$y_i = \frac{g\mu_{\mathrm{B}}B_i}{k_{\mathrm{B}}T} \tag{A10b}$$

and B_i is the component of $\mathbf{B}_i$ in the direction of $\vec{\mu}_i$. Our unconventional definition of the Brillouin function is [15]

$$B_S(y) = \frac{1}{2S}\left\{(2S+1)\coth\left[(2S+1)\frac{y}{2}\right] - \coth\left(\frac{y}{2}\right)\right\}, \tag{A11a}$$

for which the lowest-order Taylor-series expansion about $y = 0$ is

$$B_S(y) = \frac{(S+1)y}{3} + \mathcal{O}(y^3). \tag{A11b}$$

The derivative of $B_S(y)$ is

$$B_S'(y) \equiv \frac{dB_S(y)}{dy}$$

$$= \frac{1}{4S}\left\{\mathrm{csch}^2\left(\frac{y}{2}\right) - (2S+1)^2\mathrm{csch}^2\left[(2S+1)\frac{y}{2}\right]\right\}. \tag{A11c}$$

From Eq. (A11b), the lowest-order term of a Taylor-series expansion of $B_S'(y)$ about $y = 0$ is

$$B_S'(y) = \frac{S+1}{3} + \mathcal{O}(y^2). \tag{A11d}$$

We define the reduced temperature t and reduced zero-field ordered moment $\bar{\mu}_0(t)$ in $H = 0$ as

$$t = \frac{T}{T_{\mathrm{N}J}}, \tag{A12a}$$

$$\bar{\mu}_0 = \frac{\mu_0}{gS\mu_{\mathrm{B}}}, \tag{A12b}$$

where the saturation moment μ_{sat} of each spin is

$$\mu_{\mathrm{sat}} = gS\mu_{\mathrm{B}}. \tag{A12c}$$

Using Eq. (A12b), one can write the magnitude of the zero-field exchange field in Eq. (A9) as

$$H_{\mathrm{exch0}} = \frac{3k_{\mathrm{B}}T_{\mathrm{N}J}\bar{\mu}_0}{g\mu_{\mathrm{B}}(S+1)}. \tag{A13}$$

For $H = 0$, with $B_i = H_{\mathrm{exch0}}$ in Eq. (A13), Eq. (A10a) for calculating the ordered moment versus T in $H = 0$ becomes

$$\bar{\mu}_0 = B_S(y_0), \quad \text{with } y_0 = \frac{3\bar{\mu}_0}{(S+1)t}. \tag{A14}$$

This zero-field expression is valid within MFT for a FM and any type of AFM containing identical crystallographically equivalent spins. The total derivative $d\bar{\mu}_0/dt$ is obtained from Eq. (A14) as

$$\frac{d\bar{\mu}_0}{dt} = -\frac{\bar{\mu}_0}{t\left[\frac{(S+1)t}{3B_S'(y_0)} - 1\right]}, \tag{A15}$$

where $\bar{\mu}_0(t)$ is obtained by numerically solving Eq. (A14) and the $B_S(y)$ and $B_S'(y)$ functions are given in Eqs. (A11).

4. Internal energy and heat capacity for AFM ordering in zero field

The internal energy per spin U_{mag} in zero field is given for any AFM containing identical crystallographically equivalent spins by

$$U_{\mathrm{exch0}} = -\tfrac{1}{2}\mu_0 H_{\mathrm{exch0}}, \tag{A16}$$

where the factor of $1/2$ compensates for the fact that H_{exch0} arises from exchange interactions between a central spin and each of its interacting neighbors, and hence arises from pairs of spins, whereas U_{exch0} is per spin. Writing U_{exch0} in reduced parameters using Eqs. (A12) and using Eq. (A13) gives

$$\frac{U_{\mathrm{exch0}}}{k_{\mathrm{B}}T_{\mathrm{N}J}} = -\frac{3S\bar{\mu}_0^2}{2(S+1)}. \tag{A17}$$

The magnetic heat capacity per spin is given in reduced units by

$$\frac{C_{\text{mag}}}{k_B} = \frac{d(U_{\text{exch0}}/k_B T_{NJ})}{dt} = -\left[\frac{3S\bar{\mu}_0}{(S+1)}\right]\frac{d\bar{\mu}_0}{dt}, \quad (A18)$$

where $\bar{\mu}_0(t)$ is obtained by solving Eq. (A14) and $d\bar{\mu}_0/dt$ is given by Eq. (A15).

5. Magnetization in the paramagnetic state

Let the applied field be in the α principle-axis direction. In the paramagnetic state above T_{NJ}, the thermal average of each magnetic moment is in the direction of the applied field. Hence $\alpha_{ji} = 0$ in Eq. (A4) and one obtains

$$H_{\text{exch}\alpha} = -\frac{\mu_\alpha}{g^2\mu_B^2}\sum_j J_{ij} = -\frac{\bar{\mu}_\alpha S}{g\mu_B}\sum_j J_{ij}, \quad (A19)$$

where we dropped the subscript i because all induced moments are equivalent in the PM state. As in Eq. (A12b), we define the reduced moment in the α direction as

$$\bar{\mu}_\alpha \equiv \frac{\mu_\alpha}{gS\mu_B}. \quad (A20)$$

Then using Eq. (A6b), Eq. (A19) becomes

$$H_{\text{exch}\alpha} = \frac{3\bar{\mu}_\alpha k_B \theta_{pJ}}{g\mu_B(S+1)}, \quad (A21a)$$

so

$$\frac{g\mu_B H_{\text{exch}\alpha}}{k_B T} = \frac{3\bar{\mu}_\alpha \theta_{pJ}}{(S+1)T}. \quad (A21b)$$

Including the applied field H_α in B_i, Eqs. (A10) give

$$\bar{\mu}_\alpha = B_S\left[\frac{3\bar{\mu}_\alpha \theta_{pJ}}{(S+1)T} + \frac{g\mu_B H_\alpha}{k_B T}\right]. \quad (A22)$$

For $H_\alpha \to 0$, using Eq. (A6b) and the first-order Taylor series expansion in Eq. (A11b), Eq. (A22) becomes

$$\mu_\alpha = \frac{C_1 H_\alpha}{T - \theta_{pJ}}, \quad (A23a)$$

where C_1 is the single-spin Curie constant in Eq. (A1b), which yields an isotropic Curie-Weiss law (A1) given by

$$\chi_{\text{PM}\alpha}(T) = \frac{\mu_\alpha}{H_\alpha} = \frac{C_1}{T - \theta_{pJ}}, \quad (A23b)$$

yielding

$$\chi_{\text{PM}\alpha}(T_{NJ}) = \frac{C_1}{T_{NJ} - \theta_{pJ}}. \quad (A23c)$$

We define the reduced magnetic field h_α in the α principal-axis direction as

$$h_\alpha \equiv \frac{g\mu_B H_\alpha}{k_B T_{NJ}}. \quad (A24)$$

Then in reduced variables Eq. (A22) becomes

$$\bar{\mu}_\alpha = B_S\left[\frac{3\bar{\mu}_\alpha f_J}{(S+1)t} + \frac{h_\alpha}{t}\right], \quad (t \geqslant 1) \quad (A25)$$

where the ratio $f_J = \theta_{pJ}/T_{NJ}$ is given in terms of the exchange constants and the magnetic structure in Eq. (A7).

Equation (A25) must be solved numerically for $\bar{\mu}_\alpha$ for given values of S, f_J, h_α and t.

6. Magnetization of a planar AFM in a perpendicular field

To determine the perpendicular component $\mu_\perp$ of a magnetic moment in a collinear or planar noncollinear AFM oriented in the xy plane, the net torque $\vec{\tau}$ on a representative mmoment $\vec{\mu}_i$ is set to zero according to

$$\vec{\tau} = \vec{\mu}_i \times \mathbf{H}_{\text{exch}\,i} + \vec{\mu}_i \times \mathbf{H} = 0. \quad (A26)$$

The magnetic moment vectors are written in spherical coordinates as

$$\vec{\mu}_i = \mu[\sin\theta(\cos\phi_i\,\hat{\mathbf{i}} + \sin\phi_i\,\hat{\mathbf{j}}) + \cos\theta\,\hat{\mathbf{k}}],$$
$$\vec{\mu}_j = \mu[\sin\theta(\cos\phi_j\,\hat{\mathbf{i}} + \sin\phi_j\,\hat{\mathbf{j}}) + \cos\theta\,\hat{\mathbf{k}}]$$
$$= \mu\{\sin\theta[(\cos\phi_i\cos\phi_{ji} - \sin\phi_i\sin\phi_{ji})\,\hat{\mathbf{i}}$$
$$+ (\sin\phi_i\cos\phi_{ji} + \cos\phi_i\sin\phi_{ji})\,\hat{\mathbf{j}}] + \cos\theta\,\hat{\mathbf{k}}\}, \quad (A27a)$$

where in the last equality we used trig identities with

$$\phi_{ji} = \phi_j - \phi_i. \quad (A27b)$$

Using the definition of the exchange field in Eq. (A3) and the requirement that $\sum_j J_{ij}\sin\phi_{ji} = 0$ for stability of an AFM structure [6], the first term in Eq. (A26) is found to be

$$\vec{\mu}_i \times \mathbf{H}_{\text{exch}\,i} = -\frac{3\bar{\mu}^2 S k_B}{S+1}\sin\theta\cos\theta(T_{NJ} - \theta_{pJ})$$
$$\times (\sin\phi_i\,\hat{\mathbf{i}} - \cos\phi_i\,\hat{\mathbf{j}}). \quad (A28)$$

Taking $\mathbf{H} = H_\perp\hat{\mathbf{k}}$, the second term in Eq. (A26) is

$$\vec{\mu}_i \times \mathbf{H} = \bar{\mu}g\mu_B S H_\perp\sin\theta(\sin\phi_i\,\hat{\mathbf{i}} - \cos\phi_i\,\hat{\mathbf{j}}). \quad (A29)$$

Substituting Eqs. (A28) and (A29) into (A26) gives

$$\frac{3\bar{\mu}k_B}{S+1}\cos\theta(T_{NJ} - \theta_{pJ}) = g\mu_B H_\perp. \quad (A30)$$

Using $\bar{\mu} \equiv \mu/(gS\mu_B)$, one obtains

$$\frac{3k_B}{g\mu_B S(S+1)}\mu\cos\theta(T_{NJ} - \theta_{pJ}) = g\mu_B H_\perp. \quad (A31)$$

Referring to Fig. 2, the perpendicular component $\mu_\perp$ of the induced magnetic moment of each spin is

$$\mu_\perp = \mu\cos\theta, \quad (A32)$$

where $\mu(T)$ is the magnitude of the ordered moment. Then Eq. (A31) gives

$$\mu_\perp = \frac{C_1 H_\perp}{T_{NJ} - \theta_{pJ}} \equiv \chi_{\perp J} H_\perp, \quad (A33a)$$

$$\chi_{\perp J} \equiv \frac{\mu_\perp}{H_\perp} = \frac{C_1}{T_{NJ} - \theta_{pJ}}. \quad (A33b)$$

This applies for fields $H_\perp$ less than the critical field $H_{c\perp J}(T)$ at which the moments become parallel and the system exhibits a second-order transition into the PM state. From Eq. (A33a), the critical field is given by

$$H_{c\perp J}(T) = \frac{\mu(T)}{\chi_{\perp J}}, \tag{A34}$$

where $\mu(T)$ is the ordered moment in the AFM state versus T.

Comparing Eqs. (A33b) and (A23c) one sees that

$$\chi_{\perp J}(T \leqslant T_{NJ}) = \chi_{PMJ}(T_{NJ}). \tag{A35}$$

Thus $\chi_{\perp J}$ in the AFM state at $T \leqslant T_{NJ}$ is independent of T with the value χ_{PMJ} of the PM state at $T = T_{NJ}$.

Dividing each side of Eq. (A30) by $k_B T_{NJ}$ gives

$$\frac{3\bar{\mu}\cos\theta}{S+1}(1 - f_J) = h_\perp,$$

$$\frac{3\bar{\mu}\cos^2\theta}{(S+1)t}(1 - f_J) = \frac{h_\perp \cos\theta}{t}. \tag{A36}$$

The magnitude of the induced moment is obtained by solving

$$\bar{\mu} = B_S\left[\left(\frac{g\mu_B}{k_B T}\right)(H_{\mathrm{exch}\,i} + H_\perp \cos\theta)\right]$$

$$= B_S\left\{\frac{3\bar{\mu}}{(S+1)t}\left[1 - (1 - f_J)\cos^2\theta\right] + \frac{h_\perp \cos\theta}{t}\right\}, \tag{A37}$$

where $H_\perp \cos\theta$ is the component of **H** in the direction of each of the magnetic moments, the reduced field is $h_\perp \equiv g\mu_B H_\perp/k_B T_{NJ}$ from Eq. (A24) and the reduced temperature is $t \equiv T/T_{NJ}$ according to Eq. (A7).

Substituting the left-hand side of Eq. (A36) for $h_\perp \cos(\theta)/t$ into Eq. (A37) and simplifying yields

$$\bar{\mu} = B_S\left[\frac{3\bar{\mu}}{(S+1)t}\right]. \tag{A38}$$

This is identical to Eq. (A14) for determining $\bar{\mu}_0(t)$ with $H = 0$. Hence the ordered moment magnitude is independent of field for $h_\perp$ less than the reduced perpendicular critical field $h_{c\perp}$, which is given by the first of Eqs. (A36) with $\theta = 0$ as

$$h_{c\perp} = \frac{3\bar{\mu}(1 - f_J)}{S+1}, \tag{A39}$$

where the ordered reduced moment $\bar{\mu}$ is temperature dependent and hence so is $h_{c\perp}$.

[1] K. Yosida, On the antiferromagnetism of single crystals, Prog. Theor. Phys. **6**, 691 (1951).

[2] J. Kanamori, Anisotropy and Magnetostriction of Ferromagnetic and Antiferromagnetic Materials, in *Magnetism*, Vol. 1, edited by G. T. Rado and H. Suhl (Academic Press, New York, 1963), Chap. 4, pp. 127–203.

[3] D. C. Johnston, Magnetic dipole interactions in crystals, Phys. Rev. B **93**, 014421 (2016).

[4] D. C. Johnston, Influence of uniaxial single-ion anisotropy on the magnetic and thermal properties of Heisenberg antiferromagnets within unified molecular field theory, Phys. Rev. B **95**, 094421 (2017).

[5] D. C. Johnston, Magnetic Susceptibility of Collinear and Noncollinear Heisenberg Antiferromagnets, Phys. Rev. Lett. **109**, 077201 (2012).

[6] D. C. Johnston, Unified molecular field theory for collinear and noncollinear Heisenberg antiferromagnets, Phys. Rev. B **91**, 064427 (2015); arXiv:1407.6353v1.

[7] N. S. Sangeetha, E. Cuervo-Reyes, A. Pandey, and D. C. Johnston, EuCo$_2$P$_2$: A model molecular-field helical Heisenberg antiferromagnet, Phys. Rev. B **94**, 014422 (2016).

[8] For a review of antiferromagnetism and spin wave theory, see F. Keffer, Spin Waves, in *Handbuch der Physik*, Vol. XVIII/2, ed. H. P. J. Wijn (Springer-Verlag, Berlin, 1966), pp. 1–273.

[9] R. L. Carlin and A. J. van Duyneveldt, Field-dependent magnetic phenomena, Acc. Chem. Res. **13**, 231 (1980).

[10] T. Oguchi, Anisotropy energy in MnF$_2$ at low temperatures, Phys. Rev. **111**, 1063 (1958).

[11] D. C. Johnston, R. J. McQueeney, B. Lake, A. Honecker, M. E. Zhitomirsky, R. Nath, Y. Furukawa, V. P. Antropov, and Y. Singh, Magnetic exchange interactions in BaMn$_2$As$_2$: A case study of the J_1-J_2-J_c Heisenberg model, Phys. Rev. B **84**, 094445 (2011).

[12] E. Stryjewski and N. Giordano, Metamagnetism, Adv. Phys. **26**, 487 (1977).

[13] K. H. J. Buschow and F. R. de Boer, *Physics of Magnetism and Magnetic Materials* (Kluwer, New York, 2004), Chap. 4, pp. 19–42.

[14] Y. Shapira and S. Foner, Magnetic phase diagram of MnF$_2$ from ultrasonic and differential magnetization measurements, Phys. Rev. B **1**, 3083 (1970).

[15] F. Reif, *Fundamentals of Statistical and Thermal Physics* (McGraw-Hill, New York, 1965).